FLOW FAILURE OF SATURATED BAUXITE UNDER UNDRAINED MONOTONIC LOADING

飽和したボーキサイトの非排水単調載荷条件下での流動破壊

A Thesis submitted in partial fulfillment of the requirements for the degree of

MASTER OF CIVIL ENGINEERING

Prepared by

Brahian Román Cabrera

ブライアン ロマン カブレラ

Signature	Date	Seal
Advisor:		
Co-Advisor:		

The University of Tokyo

Graduate School of Engineering

Department of Civil Engineering

Tokyo, Japan

July 2018

TABLE OF CONTENTS

LIST OF FIGURES

LIST OF TABLES

ACKNOWLEDGEMENT

I am indebted to many persons for their support during my time in Japan. First, I would like to express my utmost gratitude to Professor Junichi Koseki for kindly accepting supervising my research, even though we did not get in touch before I came to Japan. I am very grateful to Professor Koseki for his patience, kindness, guidance and all the knowledge he shared with me. He is the model of person I dream to be one day.

Many thanks as well to Kuwano sensei and Kyokawa sensei for their valuable contributions to my research project.

Also, I would like to thank the members of the Geotechnical Engineering Laboratory for all the support, understanding and constructive criticism. Especially thanks to Mr. Le Nguyen for being very willing to teach me how to conduct experiments in the triaxial equipment, Mr. Takeshi Sato for his help in technical matters, Mr. Jimbo Satoshi for guiding me when I arrived at Japan, Mr. Chuang Zhao for teaching me how to achieve fully saturation, Mr Yudai Aoyagi and Mr. Zain Maqsood for their advice and help when I faced technical difficulties, and to Mr. Jaylord Tan Tian for his kindness in sharing information regarding Bauxite.

In addition, many thanks to all my friends from The University of Tokyo. Especially to Mr. Javier Tello, Mr. Charlie Ruiz, Miss Quynh Trang, Mr. Anton Kerezov, Mr. Lucas Bispo, Mr. Victor Shinkin, Miss Nandita Saha and Miss Saho “Helen” Wang for spending wonderful times together.

I would also like to thank the financial support provided by the Ministry of Education, Culture, Sports Science and Technology of Japan (MEXT). Thank you very much for giving me this opportunity.

Finally, I gratefully acknowledge the support of my family in this two years. They were there every time I needed them.

ABSTRACT

Mining industry plays an important role in the global economy as it enhances economic growth. Only in the past decade about 9 trillion US dollars was invested globally in mining. The process of Bauxite Mining involves the design, construction and maintenance of several geotechnical structures such as rock slopes, waste rock dumps, ore heaps (bulk cargoes) and tailings dams. It is important to ensure the safety and serviceability of the structures mentioned above to avoid economic and human life losses as well as environmental damage. However, there have been many cases of failure of bulk cargoes leading to great material and human losses in the last 2 decades due to liquefaction.

Liquefaction can be divided in two different phenomena: Flow Liquefaction and Cyclic Mobility depending whether the static shear stress required for equilibrium is greater or not than the residual (post-liquefaction) shear strength. If the static shear stress is greater than the liquefied shear strength, then a sudden, catastrophic failure will occur (Flow Failure).

Hence, it is of paramount importance to study the susceptibility of Bauxite to flow-type failure mechanisms. To do so, there are two approaches at the level of element tests in laboratory equipment. One based on undrained cyclic tests and another based undrained monotonic tests using the Steady State Theory. This thesis used the latter approach.

Bauxite has different mineralogy and particle shape than most "academic" soils normally used in research (e.g. Toyoura, Ottawa and Silica Sands among others). To study the effects of these differences a mixture of several Silica Sands resembling Bauxite's gradation and content of fines was prepared (Simulated Bauxite).

A set of 20 undrained monotonic tests with pore water pressure measurement in a high-pressure triaxial equipment under several conditions of density and effective confining stress were conducted in both Bauxite and Simulated Bauxite. 16 were done in Bauxite covering a wide range of void ratios (e_{min}=0.727 to e_{max}=1.329) and effective confining stress (25kPa to 1000 kPa). Only 4 were conducted on Simulated Bauxite focusing on loose samples (e_{min}=0.718 to e_{max}=0.781) at effective confining stress ranging from 200kPa to 800kPa. Moist-tamping method of sample preparation was preferred since it

allows covering a wide range of densities and the level of fabric anisotropy is smaller than in other methods.

Results showed that, Bauxite presents only two types of undrained monotonic response: flow with limited deformation (Quasi Steady State) and dilation. Even for the loosest density condition achieved by using moist-tamping and a very small effective confining pressure (e=1.322 and 25 kPa) flow type behavior was not achieved.

For contractive samples of Bauxite, the excess pore water pressure for all tests on Bauxite showing Quasi Steady State behavior reaches 73% of the initial confining stress. However, none of the tests fulfills the criteria to define initial liquefaction which requires the water pressure excess to build up to a value of 100%. Then, the predominant mechanism occurring at the peak deviator stress was regarded as Collapse of granular soils, not as liquefaction.

Dilative responses of Bauxite also showed a considerable contractive behavior which induces a reduction in the effective confining pressure until the Point of Phase Transformation. The excess pore water pressure in dilative samples increases up to an average of 81% of the effective confining stress, being even higher than for the contractive soils at the peak state where collapse starts. At this point the effective confining pressure is reduced to an average of 40% of its initial value, so despite not undergoing collapse (peak deviator stress and strain-softening) the stiffness of the soil is greatly reduced.

By plotting the final states of all the aforementioned tests, an area separating dilative than contractive responses was narrow down which probes the applicability of the Steady State Theory for Bauxite, although only 3 tests reach the Steady State Line.

The undrained shear strength mobilized at the Quasi Steady State was obtained for 11 tests showing values ranging from 3.7 kPa to 167.9 kPa. These values were established as post-liquefaction shear strength for stability analysis. The average ratio $\frac{S_{qss}}{\sigma'_o}$ was defined as 0.16 which lies within the database of ratios obtained from laboratory tests (0.02-0.22) although it is a bit higher than ratios obtained from back analysis of failures (0.05-0.12)

In the case of Simulated Bauxite, flow type behavior and flow with limited deformation (Quasi Steady State) were achieved and it was possible to draw the Steady State Line.

Two samples of similar void ratio and subjected to the same effective confining stress in actual Bauxite (BX) and Simulated Bauxite (Simulated BX) were compared. Actual BX has a higher peak deviator stress (250 kPa against 208 kPa) than Simulated BX. The strain-softening in BX is more pronounced and the Quasi Steady State occurs at a lower level of axial strain than in Simulated BX (2.5% against 3.8% of axial strain). However, at the residual level both display very similar deviator stress. The effective stress path that both tests follow until the critical state is very similar reaching an almost identical minimum value of effective confining stress (162kPa of Simulated BX against 167kPa of BX). Nevertheless, actual BX required a higher excess pore water pressure to reach such value (780kPa approximately), whereas Simulated BX only required 500 kPa of excess pore water pressure indicating that negative dilatancy developed by BX is lower than Simulated BX under similar conditions. This fact was interpreted as BX presenting greater resistance to liquefaction than simulated BX. Actual BX has also greater post-liquefaction shear strength than Simulated Bauxite when the two similar tests are compared (105.6 kPa against 90.8 kPa).

The SSL of Simulated BX is below the SSL of actual BX. Therefore, there are states of density and confining pressure for which actual BX is not susceptible to Flow Failure (dilative response), but at which Simulated BX is susceptible (contractive response). This also implies that actual BX possess greater resistance to liquefaction than simulated BX. In terms of Collapse Surface, actual BX has a steeper collapse surface (M_L = 1.089) than Simulated BX (M_L = 1.040) which allows to conclude that actual BX requires greater reduction in effective confining stress to undergo Flow Failure. Therefore, it is possible to conclude that actual BX shows more resistance to the development of excess pore water pressure and therefore it is more resistant to liquefaction than Simulated BX. This is probably due to the higher level of plasticity and clay content (IP = 10.9) of BX.

1. INTRODUCTION AND OVERVIEW

1.1 BACKGROUND

1.1.1 Applications of Geotechnical Engineering to Mining

Mining is defined as the extraction of valuable minerals (e.g. Iron, Aluminum) from the earth. This industry plays an important role in the global economy as it enhances economic growth. Only in the past decade about 9 trillion US dollars was invested globally in mining (World Bank Mining Group Department, 2015).

Mining involve design, construction and maintenance of several geotechnical structures. The following scheme illustrates the 4 main steps of the Bauxite mining process.

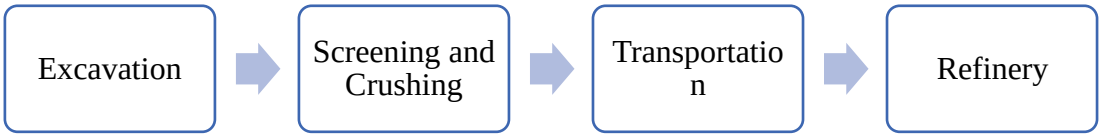

Figure 1.1 Bauxite Mining Process

- ✓ Excavation:

After establishing an area with abundant mineral resources, excavation is carried out. The hardness of the rock forces the use of explosives for blasting. At this stage, the most important geotechnical aspect is assuring the stability of rock slopes.

Figure 1.2 Rock Slope for Bauxite Mining (http://www.greatmining.com)

✓ Screening and Crushing:

After excavation, high-grade ore materials are crushed, washed and prepared for shipment, whereas low-grade ore materials are deposited in waste rock dumps. This structure resembles rockfill dams and typically reaches heights of over 200 m.

Figure 1.3 Waste Rock Dump (http://www.acidmetalliferousdrainage.com/)

✓ Transportation:

Aluminum Ore is then stored in heaps inside vessels (bulk cargoes). Typical heap dimensions are 38m of diameter and 14m height. A vessel can transport up to 9 heaps.

Figure 1.4 Bauxite Bulk Cargo (https://www.alcircle.com)

✓ Refinery:

Finally, Bauxite is subjected to metallurgical process for its conversion into industrial products (automobiles, electronic devices). By-products from this process are called

Tailings which are of toxic nature. Safe storage of tailings is usually performed by constructing tailings dams.

Figure 1.5 Tailings Dam - Ring Type (http://www.wikiwand.com)

1.2 PROBLEM STATEMENT

It is important to ensure the safety and serviceability of the structures mentioned above to avoid economic and human life losses as well as environmental damage. However, there have been many cases of failure of bulk cargoes in the last 2 decades due to dynamic liquefaction (figure 1.6). Munro and Mohajerani (2016) reported at least 24 cases of failure of Bauxite bulk cargoes from 1988 to 2015 with subsequent capsizing of the vessels generating 164 deaths. This led to the creation of the Global Bauxite Working Group (GBGW) aiming to determine possible instability mechanisms controlled by water content concluding that liquefaction and dynamic separation are the main phenomena jeopardizing vessels (GBGW, 2017).

Figure 1.6 Capsizing of bulk cargo containing Bauxite in Hong Kong (http://worldmaritimenews.com)

Hence, it is of paramount importance to study the susceptibility of Bauxite to such mechanisms. This can be done in laboratory through model and element tests. This thesis studies liquefaction in element tests only. To do so, there are two approaches. One based on undrained cyclic testing originated in the pioneering work of Seed and Lee (1966), and Seed and Idriss (1971), and the other based on undrained monotonic behavior at large deformations by using the concepts of Critical Void Ratio and Steady State proposed by Casagrande (1936), Poulos (1971) and Castro (1969). Despite being of static nature, the latter approach has contributed greatly to the improved understanding of dynamically induced liquefaction by identifying the effective stress conditions at which liquefaction phenomena are initiated (Kramer, 1997).

While there are studies on the cyclic behavior of Bauxite (GBGW, 2017; Tan Tian, 2018; Mele et al, 2018), there is a lack of research addressing its monotonic behavior and post-liquefaction shear strength. This thesis conducted undrained monotonic test with pore water pressure measurement on Bauxite under several conditions of density and effective confining stress to fill that gap. Furthermore, an estimation of the residual shear strength for post-seismic stability analysis was carried out. It is worth mentioning that Bauxite have different mineralogy and particle shape than most "academic" soils normally used in research (e.g. Toyoura, Ottawa and Silica Sands among others) and therefore it is necessary to study its behavior directly.

1.3 THESIS OBJECTIVES

1.3.1 Main Objective

The main objective of this thesis is:

- ✓ To study the undrained monotonic behavior at large deformations of Bauxite under several conditions of density and effective confining stress

1.3.2 Specific Objectives

The specific objectives are:

- ✓ To verify the applicability of the Steady State theory to this type of soil
- ✓ To estimate undrained residual shear strength for the post-seismic stability analysis of bauxite heaps

- ✓ To compare the behavior of Bauxite with a mix of Silica Sands of similar particle size distribution

1.4 OVERVIEW OF THE THESIS

This thesis project is divided in 6 chapters:

Chapter 1 describes the background, the problem statement and the objectives of this thesis

Chapter 2 summarizes the literature review conducted on the undrained monotonic behavior of granular soils and the factors affecting it.

Chapter 3 shows the geological and geotechnical characterization of Bauxite; laboratory testing standards of the Japanese Geotechnical Society were used. In addition, the main features of the triaxial apparatus are described and a brief operation manual for future applications is provided.

In chapter 4, test results of consolidation and monotonic loading are presented and analyzed. These were divided according to the type of response of the soil (dilative or contractive) showing the stress paths, pore water pressure increments and mobilized friction angles. Then, all results are integrated to obtain the steady state line. Finally, the shear strength mobilized at the quasi steady state is estimated for applications in post-seismic stability analysis.

Chapter 5 presents a structure similar to chapter 4 with the difference that the soil test is a mixture of Silica Sands of different gradation whose particle size distribution resembles Bauxite's. This was done for comparison purposes to determine effects of fines content and mineralogy.

Finally, chapter 6 lists the conclusions in relation with the specific objectives and provides recommendations for further research.

2. LITERATURE REVIEW

2.1 LIQUEFACTION

2.1.1 Liquefaction Phenomena

Liquefaction occurs in loose sandy ground that is saturated with water. When pore water rises due to an external shear load, the effective stress decreases until zero in extreme cases which leads to a loss in interparticle contact between soils grains transforming the soil into a liquid state from where the name "liquefaction" was given. After a complete loss of effective stress, the sand has very small shear modulus and shear strength and consequently undergoes large deformations (Towhata, 2008). Liquefaction phenomena can be divided into two different groups: Flow Liquefaction and Cyclic Mobility.

2.1.2 Flow Liquefaction

Also known as True Liquefaction, it occurs when the static shear stress required for static equilibrium of a soil mass is greater than the shear strength of the liquefied soil mass making the soil flow like a liquid until the shear stresses are low enough (Kramer, 1996).

$$\tau_{static} > S_u \rightarrow Flow\ Failure$$

$$S_u: Liquefied\ Shear\ Strength$$

This type of liquefaction is responsible for the most dramatic failure of ground structures (Flow Failures or Flow Slides) given its sudden nature and the large distances the soil moves. Flow slides were seen in the failure of many water and tailings dams, some well-known cases are Fort Peck Dam in Montana (1938) studied by the U.S. Army Corp of Engineers (1939), the Lower San Fernando Dam in California (1971) analyzed by Castro et al (1992) and Mochikoshi Gold Tailings Dam in Japan (1978) evaluated by Ishihara (1984).

Since static shear stresses are involved, flow failure is most likely to be triggered in sloping ground especially if the slope is greater than 6° (Youd, 1973) as in embankments, dams and ore heaps.

2.1.3 Cyclic Mobility

Cyclic Motility occurs in the opposite case of Flow Liquefaction, when the static shear stresses required for equilibrium are less than the residual shear strength (Kramer, 1997). However, cyclic mobility can also occur in dense soils that show dilative behavior manifesting itself as a progressive softening due to initial pore water pressure rise when cyclic loading is applied leading to large deformations (Castro and Poulos, 1976). If sloping ground undergoes liquefaction, but flow failure does not occur, the accumulation of deformations due to cyclic mobility phenomena can be seen externally as the so called "Lateral Spreading" which is often reported in damage reports after earthquakes.

2.2 UNDRAINED MONOTONIC BEHAVIOR OF COHESIONLESS SOILS

2.2.1 General Behavior under Undrained Conditions

When saturated granular soils are subjected to monotonic loading, three types of response can be obtained (Ishihara, 1996):

- ✓ Non-Flow Type (Dilative): In this type of soils the shear stress always goes up with the strain (Strain Hardening behavior). These soils, when subjected to shearing in drained conditions will present volume increments (positive dilatancy).
- ✓ Flow Type (Contractive): These soils show a peak deviator stress followed by softening until a constant residual value. This type of response is commonly seen in loose sands that will present volume reduction upon shearing in drained conditions (negative dilatancy)
- ✓ Flow Type with Limited Deformation: These soils show -at the beginning- similar behavior to contractive soils reaching a peak and then softening; but, after a minimum deviator stress, the behavior changes to hardening.

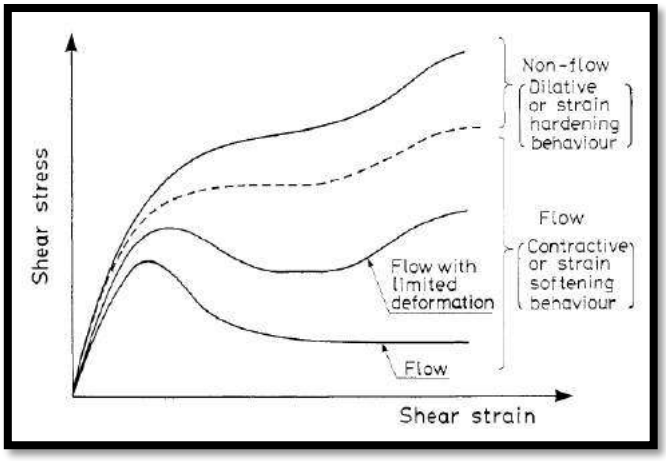

Figure 2.1 Classification of Sandy Soil based on Shearing Behavior (Ishihara, 1996)

Yoshimine and Ishihara (1997) proposed a scheme of these 3 types of behavior depending on the state of the soil (i.e. void ratio and effective confining stress conditions).

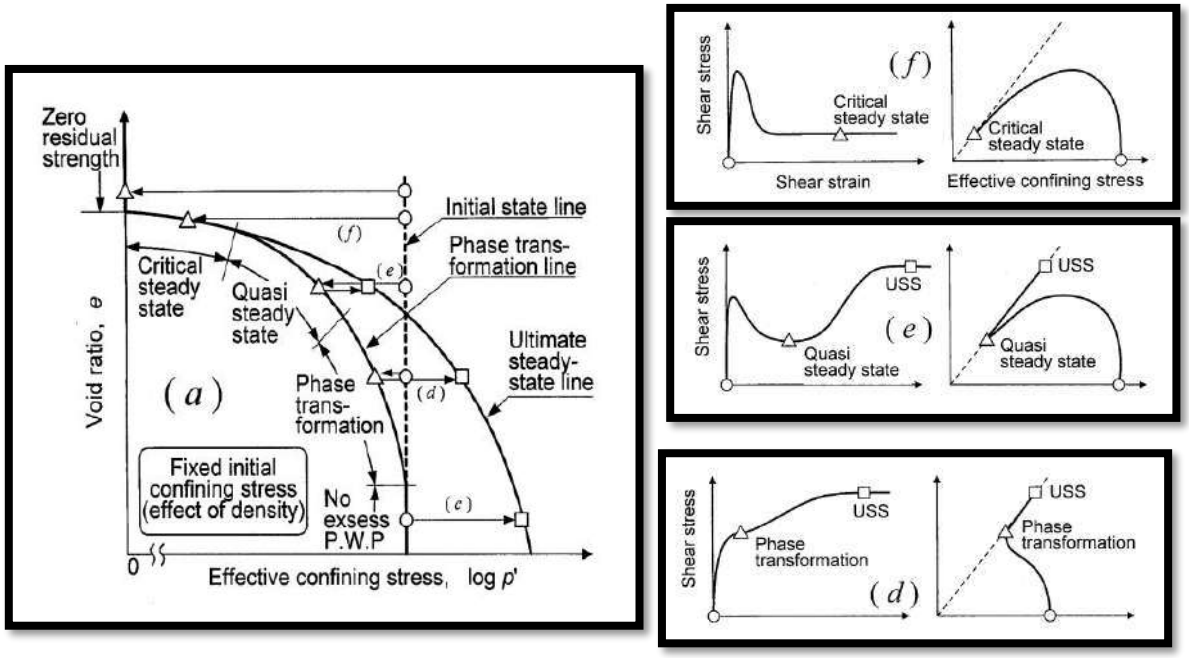

Figure 2.2 General Undrained Shear Behavior of Sand under Large Deformation (Yoshimine and Ishihara, 1998)

2.2.2 Steady State of Deformation

Castro (1969) performed undrained triaxial tests in clean sands noting that, for the same density, the three types of behaviors converge on the same pressure of effective confining stress and constant shear strength. This singular state was called "Steady State" and was subsequently defined by Poulos (1981) as "the state in which the soil flowed

continuously under constant shear stress and constant effective confining stress at constant volume and constant velocity". When joining all the points corresponding to the steady state in the e-p' plane, the steady state line can be drawn. This line is similar to the Critical State Line proposed by Casagrande (1936) and divides the state of soils into flow type and non-flow type which is helpful to assess the susceptibly to flow failure. Dilatant soils are located below the Steady State Line and are not susceptible to flow failure because resistance is increased during loading; however, soils above the Steady State Line show minimum resistance in which static stresses can induce flow failure.

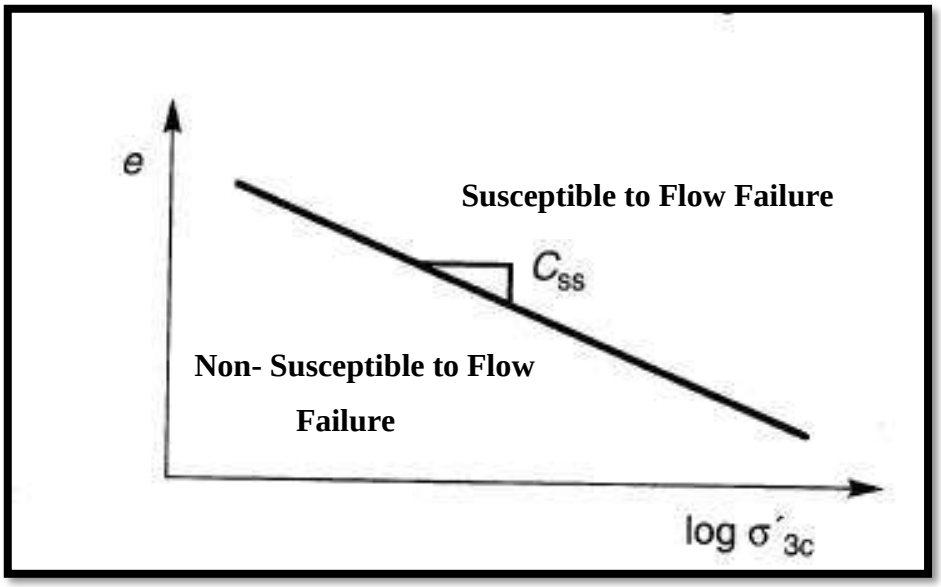

Figure 2.3 Susceptibility to Flow Failure based on the Steady State Line (Kramer, 1996)

2.2.3 Quasi Steady State Response

In effective stress path diagrams of materials presenting "Flow with Limited Deformation", a turning point where contractive behavior changes to dilative can be seen. This point was defined as the Point of Phase Transformation by Ishihara et al (1975) and is the result of a transition from increase to reduction in pore water pressure. Alarcon-Guzman et al (1988) named this state as "Quasi Steady State" which, unlike the actual Steady State, appears at medium levels of strain (typically around 5%-10%).

Verdugo (1992) carried out a comprehensive set of tests on Toyoura sand finding that Quasi Steady State response is predominant even at the loosest possible condition achieved by Japanese Standards for Testing. Hence, this behavior has important engineering applications because soils reaching such state can undergo intolerable

amounts of lateral displacements causing serious damage to embankments or structures lying on such deposits (Ishihara, 1996).

2.2.4 Factors affecting the Undrained Monotonic Behavior of Sands

Understanding factors that affect the behavior of clean sands can provide insight for an appropriate experimental setup of Bauxite.

2.2.4.1 Fines content

Many researchers have studied the influence of fines (silt and clay) on the undrained behavior of sand. From the cyclic viewpoint, Ishihara and Koseki (1989) found that the cyclic strength of soils with low plasticity (IP<10) does not change much but increases thereafter with increasing plasticity index. Alberto Hernandez (2014) compared the behavior of clean sand and sand with non-plastic fines in torsional shear tests and concluded that the cyclic resistance of clean sand is always greater than a mix of sand with non-plastic fines.

From the monotonic viewpoint, Yamamuro and Lade (1998), Yamamuro and Covert (2001), Yang et al (2006), Murthy et al (2007), Phan et al (2016) among others studied the response of sands systematically increasing non-plastic silts, noting that the SSL of sand with fines tend o move downward which can be interpreted as an increased susceptibility to flow failure, but this occurs only until a transitional point after which the response stabilizes. Nevertheless, Kwa and Airey (2017) obtained opposite results showing a movement of the SSL upwards when increasing the content of non-plastic fines, although in cyclic tests they found that soils with the highest content of fines had the lowest resistance to liquefaction.

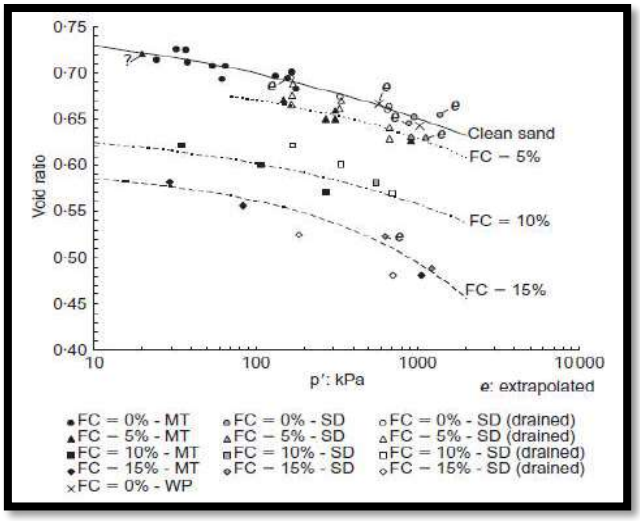

Figure 2.4 Critical state locus in e–p' space for Ottawa sand with 0%, 5%, 10% and 15% non-plastic silt (Murthy et al, 2007)

2.2.4.2 Sample Preparation Method (Soil Fabric)

Each sample preparation method induces a different type of fabric, which affects the stress strain behavior of the soil. Ishihara (1993) showed that the Quasi Steady State Line (QSSL) of soils prepared by Water Sedimentation differs from the QSSL of soils prepared by Dry Deposition. This happens because the QSS occurs in small-to-medium levels of strain where the effects of fabric have not been completely eradicated yet. However, after large deformations, the soils undergo particle re-arrangement and therefore the mobilized friction angle and the critical-state strength will be independent of the sample preparation method.

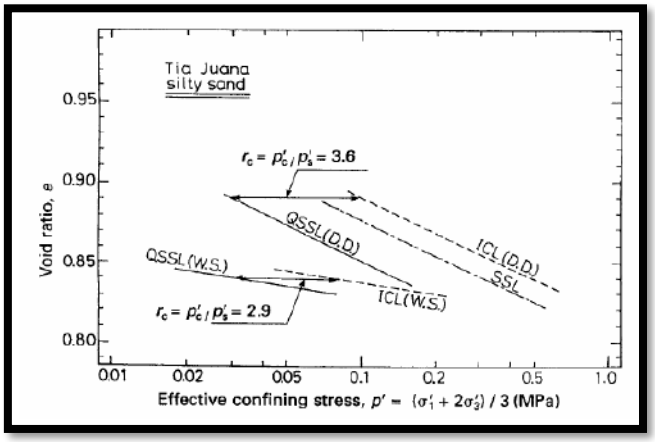

Figure 2.5 QSS and ICL lines from different sample preparation methods (DD-dry deposition and WS-water sedimentation) (Ishihara 1993).

2.2.4.3 Stress-Controlled vs Strain-Controlled tests

Stress-controlled are characterized by increments or decrements on the specimen while recording deformations. Strain-controlled tests, on the other hand, impose deformations at a constant rate and measure the changes in stress. Terzaghi et al (1996) argued that stress-controlled tests are more realistic, but strain-controlled are more convenient. Casagrande (1975) stated that for the undrained condition stress-controlled tests resemble better the flow-structure of soils at the steady state.

However, this supposition has not been borne out by subsequent studies in which it has been shown that strain-controlled tests result in the same steady state condition. Strain-controlled testing is preferable as it provides more detailed data on the post-peak behavior (Jefferies and Been, 2006). Further, according to Zhang and Garga (1997), Stress-controlled tests present issues in recording test data during rapid collapse -as commonly found during softening- which can affect measurements in pore pressure.

2.2.4.4 Particle Characteristics

Particle characteristics are defined as the type of shape of soil's particles and its minerals hardness. Sadrekarimi and Olson (2012) compared soils with similar fabric, but different particle characteristics and density concluding that soils of lower relative density and compressibility (rounded particles and hard minerals) have greater shear strength than soils of higher density and higher compressibility (angular particles and softer minerals).

2.2.4.5 Strain Rate

To examine the effects of the strain rate, Yamamuro and Lade (1998) conducted a series of undrained tests on Nevada Sand with 20% of fines at a relative density of 35% with different levels of strain rate. Their results show that increasing the strain rate produces a significant effect in steepening the effective stress path. For silty sands, an increase in the strain rate reduces contractiveness and therefore the soil is stronger at higher strain rates.

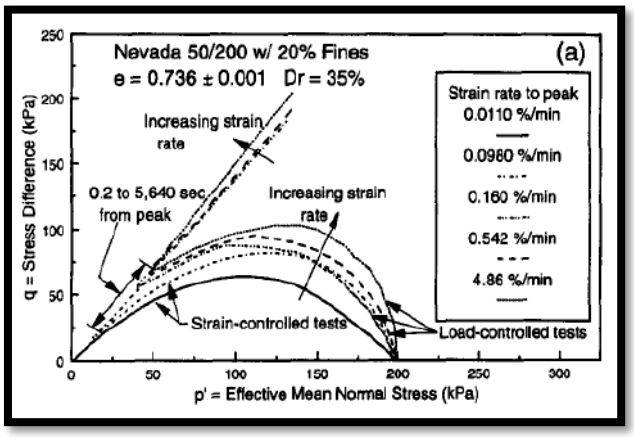

Figure 2.6 Varying strain rates on undrained tests on Nevada sand with 20% of fines (Yamamuro and Lade, 1998)

2.2.4.6 Particle Crushing

According to Vesic and Clough (1968), the critical state line[1] of soils has 3 different zones depending upon the level of stress at which the soil is subjected: First, a zone of low stress in which dilatancy is predominant. Then, after a threshold higher, stresses induce particle crushing suppressing dilatancy. Finally, a zone of very high stresses where the effects of initial density vanish, and the soil behaves like an elastic material. This is shown in figure 2.7 where it can be noticed that after 1000 kPa, the slope of the Critical State Line rotates clockwise.

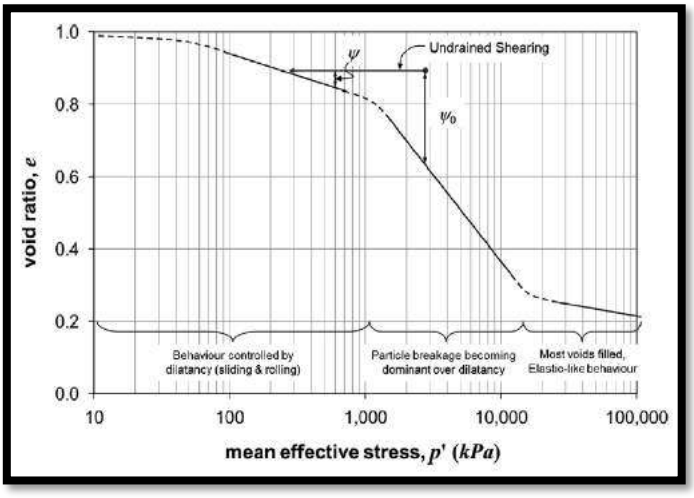

Figure 2.7 Full stress range CSL in e–log p' space and a schematic undrained triaxial test (Ghafghazi et al, 2014)

[1] Both terms Critical State Line (CSL) and Steady State Line (SSL) are interchangeable in this study

Ghafghazi et al (2014) studied Fraser River sand and fixed the threshold to consider the effects of particle crushing at 1000 kPa. Nevertheless, this is not the case for other soils. For instance, Yu (2017) set the threshold at 700 kPa for Silica Sand N°5.

2.2.4.7 Other Factors

Other factors such as stress path, initial static stress and the intermediate principal stress have an important influence on the undrained monotonic behavior, but they are not included in this literature review because the experimental program focused only on compression triaxial tests after isotropic consolidation condition.

2.3 POST-LIQUEFACTION STABILITY ANALYSIS

Ishihara (1993) suggested a flowchart for the analysis of problems in soils undergoing liquefaction. For sloping ground such as embankments or dams, it is necessary to perform a post-seismic stability analysis to estimate the likelihood of flow failure.

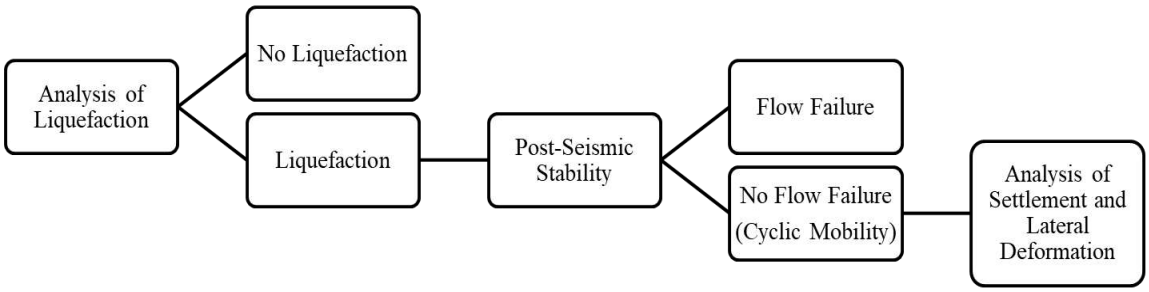

Figure 2.8 Flow chart of the problems associated with liquefaction for sloping ground (Ishihara, 1993)

2.3.1 Engineering Analysis

Finn (1998) proposed the following steps for evaluating the seismic response of embankments containing potentially liquefiable soils:

- ✓ Determine in which soils liquefaction will be triggered during the design earthquake
- ✓ Determine the residual or steady state strengths of the liquefied soils

- ✓ Conduct a stability analysis incorporating residual strengths to determine the factor of safety of the soil structure in its original configuration
- ✓ Depending on the factor of safety, decide whether to conduct a deformation analysis
- ✓ If deformations are unacceptable, plan remedial measures

The key aspect of this procedure is the appropriate estimation of the shear strength of the liquefied soil or post-liquefaction shear strength.

2.3.2 Post-liquefaction shear strength of soils

Current state-of-practice in the estimation of post-liquefaction shear strength includes two main approaches: one based on laboratory element tests and other based on data from real flow failures. Since the post-liquefaction shear strength is strongly dependent on the effective confining stress, both approaches can provide results normalized to the effective confining stress ($\frac{S_{us}}{\sigma_o'}$) which is advantageous in design. Although, this is sometimes difficult because not all soils have a unique relationship, especially sands because they have non-unique isotropic consolidation lines (Kramer, 1996). Furthermore, Olson and Stark (2003) established that this ratio should be used only until 1MPa of effective confining stress as it is not clear whether relations based on state parameter hold after the onset of grain crushing.

2.3.3 Estimation based on laboratory tests

Post-liquefaction shear strengths can be obtained in the laboratory by using the Shear Vane, Shear Ring and Triaxial tests (Reid and Fourie, 2014). In the case of triaxial testing, there are two important strengths: the steady strength mobilized at large deformations, and the strength mobilized at the quasi steady state.

Many researchers have proposed $\frac{S_{us}}{\sigma_o'}$ ratios for the steady strength condition. For example, Pillai and Salgado (1994) carried out undrained monotonic tests in frozen samples of sands from Duncan Dam in Canada obtaining a constant value of 0.21. Baziar and Dobry (1995) obtained a ratio of 0.12 (in Kc=1.0 condition) for Sand Fernando silty sand (figure 2.9). However, Vaid and Sivathalayan, (1996) obtained ratios varying from 0.25 to 0.1 depending on the void ratio (figure 2.10) for Fraser River Sand.

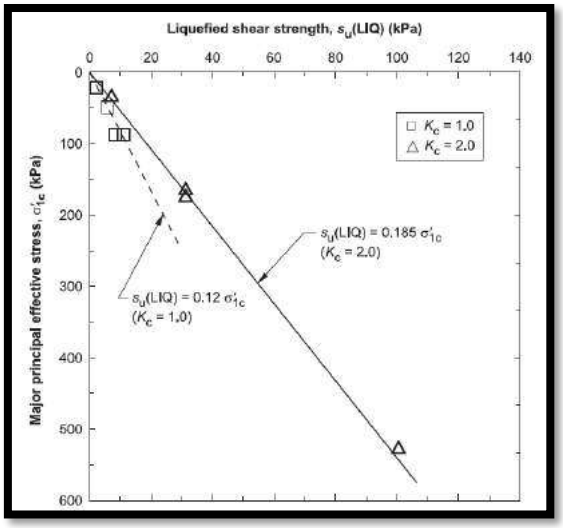

Figure 2.9 Relationship between liquefied shear strength and initial major principal effective stress for remolded layered specimens of silty sand, batch 7, Lower San Fernando Dam (Baziar and Dobry 1995).

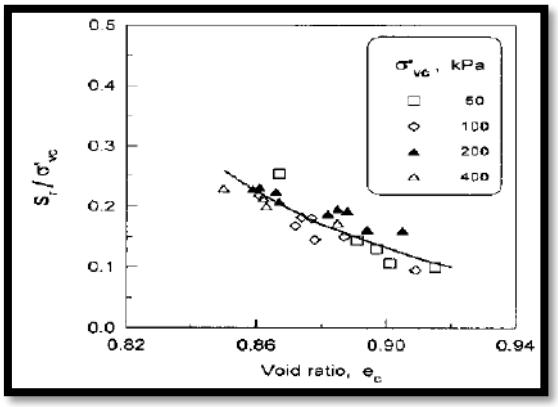

Figure 2.10 Variation of normalized residual strength with void ratio (Vaid and Sivathalayan, 1996)

The aforementioned results were obtained at the steady state; nevertheless, as mentioned in 2.2.3, the quasi-steady-state shear strength plays an important role in the safe design of structures as well. For its calculation, Ishihara (1996) recommended the following expression:

$$\frac{S_{us}}{\sigma'_o} = \frac{q_s}{2} * \frac{\cos \emptyset_s}{\sigma'_o}$$

where $\emptyset_s$ and q_s are the mobilized friction angle and the deviator stress at the quasi steady state respectively. By using this expression, Verdugo (1992) obtained unique $\frac{S_{us}}{\sigma'_o}$ ratios although they depend on the sample preparation method. Figure 2.11 shows the ratios for

Lagunillas sandy silt and Tía Juana silty sand, there is a unique relationship, but values obtained using dry deposition are lower (0.086 and 0.146) than those for water sedimentation (0.134 and 0.181).

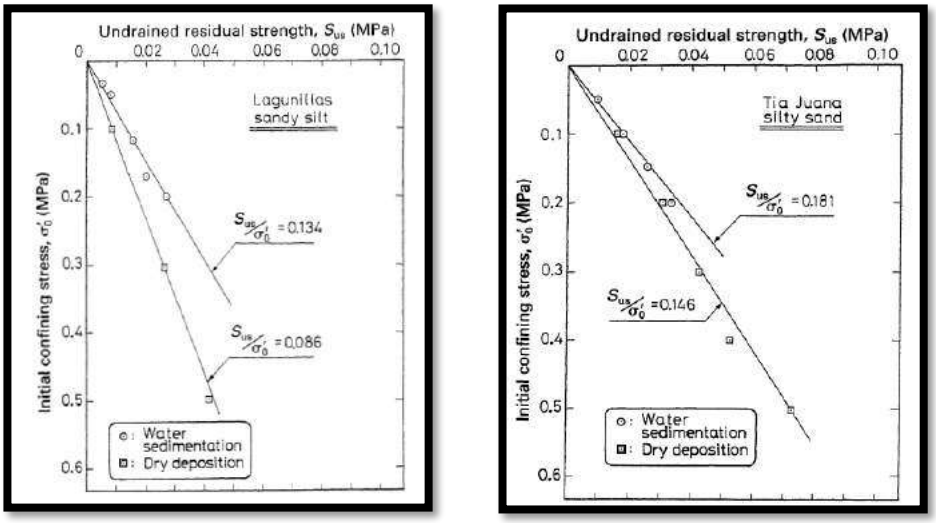

Figure 2.11 Residual strength plotted against initial confining stress for Lagunillas sandy silt and Tía Juana silty sand (Verdugo, 1992)

2.3.3.1 Limitations of the laboratory-based approach

Despite its strong theoretical foundations (Steady State Theory), the use of laboratory tests for evaluating post-liquefaction shear strength has many limitations. First, in granular soils is extremely difficult to obtain undisturbed samples that allow accurate estimations of in-situ void ratio, this aspect is critical in soils whose ratio $\frac{S_{us}}{\sigma_o'}$ is not constant because a small variation in void ratio can have significant effects on the residual strength. Moreover, several studies have noticed that liquefaction in real field conditions has features such as void ratio redistribution, partial drainage and more complex stress paths (Stark and Mesri, 1992) that are not reproduced in laboratory tests. Castro et al (1992) studied silty sands from the failed Lower San Fernando dam by means of triaxial testing and stated that conservative to very conservative interpretation of the laboratory test data was necessary to provide a reasonable level of agreement with the field strength estimated from the observations. Therefore, it is necessary to be very conservative when using ratios from laboratory tests.

2.3.4 Estimation based on field tests and case studies

A less expensive way to estimate the post-liquefaction shear strength is by back analysis of real flow failures. Seed and Harder (1990), Stark and Mesri (1992), Olson (2001), Idriss and Boulanger (2008) among others propose empirical expressions for determining the $\frac{S_{us}}{\sigma'_o}$ in function of field tests (number of blows from SPT test). Olson and Stark (2003) conducted a comparative analysis between ratios obtained for sands in laboratory tests and ratios obtained by Olson (2001) from historic cases. According to this study, laboratory-based $\frac{S_{us}}{\sigma'_o}$ ratios ranges from 0.02 to 0.22 over a wide range of effective stresses, while back-calculated liquefied ratios vary from 0.05 to 0.10 being close to the lower bound of laboratory results (figure 2.12).

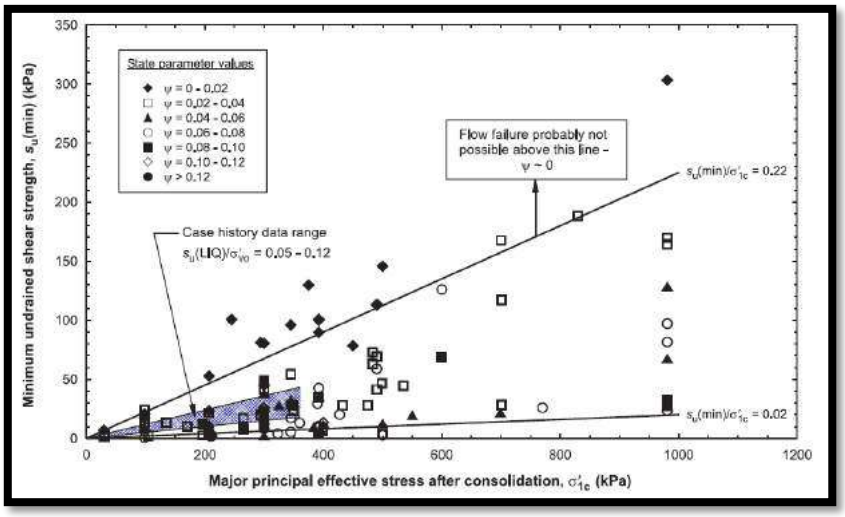

Figure 2.12 Relationships between relative density and liquefied strength ratio for clean sands in laboratory database and case studies (Olson and Stark, 2003)

3. MATERIALS AND EXPERIMENTAL METHODS

3.1 GEOLOGICAL AND GEOTECHNICAL CHARACTERIZATION OF ALUMINUM ORE (BAUXITE)

3.1.1 Geology

Bauxite is a sedimentary rock formed from the weathering of Silicate rocks (Granite, Basalt) or Carbonate rocks (Limestone, Dolomite). Bauxite is commonly found in tropical areas (30° north and 30° south of Equator) near the surface. Tropical weathering conditions remove most soluble minerals leaving insoluble Iron and Aluminum which gives the rock its red color.

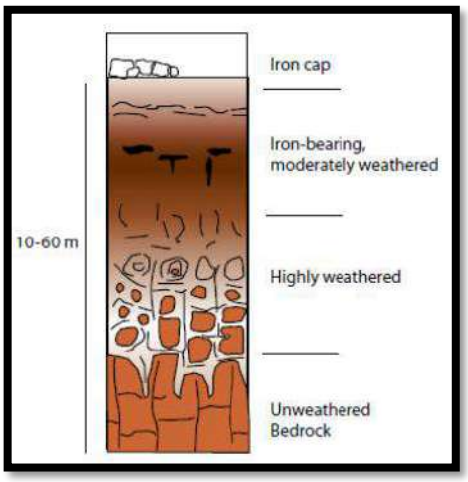

Figure 3.1 Lateritic deposit of Bauxite (https://www.britannica.com/science/laterite)

Figure 3.2 Bauxite rock (http://www.sandatlas.org/bauxite/)

3.1.2 Mineralogy

Mineralogy studies were not conducted in this research, so results from literature review on similar Bauxites will be shown. Gu et al (2013) carried out petrographic analysis on 8 different types of Bauxite from lateritic deposits in China (table 3.1). It is observed that Aluminum hydroxides (Diaspore and Bohemite) are predominant. Diaspore has a hardness on the scale of Mohs similar (6.5 - 7.0) to the hardness of quartz (7.0) and feldspar (6.0 - 6.5) which are the primordial minerals of most sands, while the Bohemite has a hardness of 3.5 approximately.

Table 3.1 Bauxite Mineralogy (Gu et al, 2013)

Mineral	**Hardness in Mohs Scale**	**W-1**	**W-2**	**W-3**	**S-3**	**S-4**	**X-1**	**X-5**	**X-8**
Diaspore	6.5 - 7	**68.6**	**87.6**	**45.49**	1.57	2.4	**91.21**	16.18	**56.87**
Boehmite	3.5	0.15	Y	Y	**94.5**	**88.96**	-	**67.69**	3
Kaolinite	2 - 2.5	21.65	4.71	3.61	0.46	3.88	0.24	5.25	-
Illite	1-2	0.17	1.42	22.43	1.82	0.43	-	0.22	23.15
Iron Minerals	4.5	2.4	0.72	2.62	Y	Y	6.1	0.46	0.47
Smectite	1-2	3.2	1.15	5.76	-	1	-	3.66	1.28
Quartz	7	0.3	0.88	7.18	1.65	2.11	-	-	5.42
Anatase	5.5–6	Y	Y	4.16	Y	Y	2.45	-	Y
Chlorite	2–2.5	-	-	-	-	-	-	2.62	6.45
Feldspar	6.0–6.5	3.47	-	2.77	-	-	-	-	3.36
Calcite	3	-	-	4.06	-	1.22	-	-	-
Gibbsite	2.5 - 3	-	-	-	-	-	-	3.92	-

3.1.3 Particle Size Distribution

Global Bauxite including gravels and pebbles is shown in figure 3.3. Its gradation along with the gradations of Toyoura sand in Japan and San Agustino sand in Italy for comparison is shown in figure 3.4. For particles with a diameter smaller than 0.075mm, Hydrometer tests were conducted. The material presents good gradation (Cu = 42.9) with 25.7% fines content.

Figure 3.3 Global Bauxite including gravels and pebbles

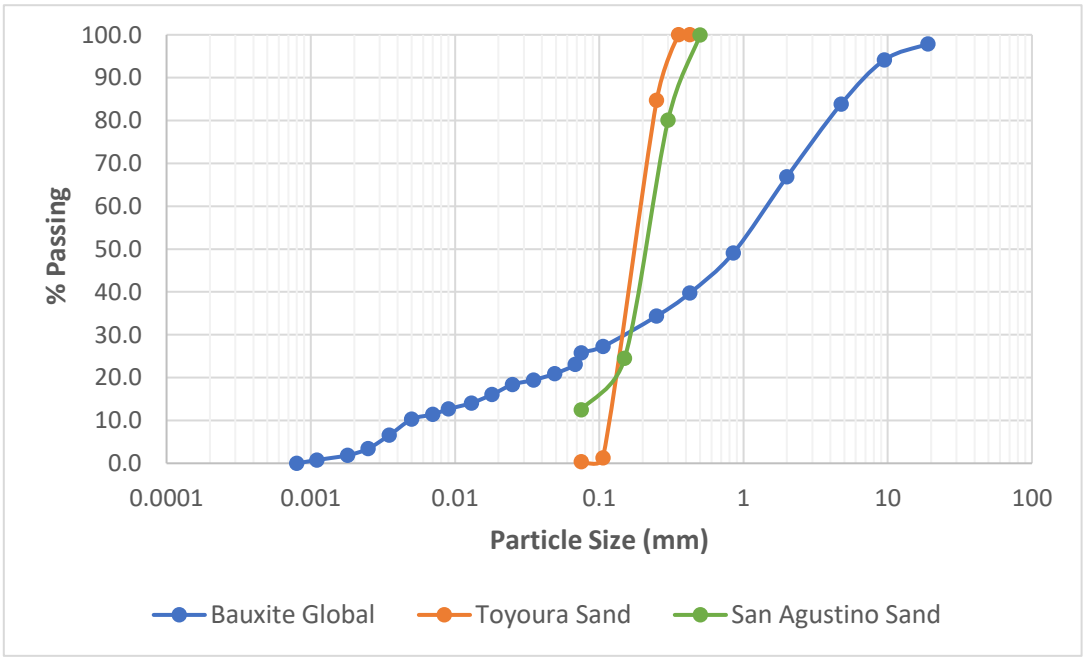

Figure 3.4 Particle Size Distribution of Bauxite

Table 3.2 Summary of Bauxite Gradation

Gravel (%)	33.2
Sand (%)	41.1
Silt (%)	15.5
Clay (%)	10.2
Fines Content (%)	25.7
D_{60} (mm)	1.5
D_{30} (mm)	0.160
D_{10} (mm)	0.035
Coefficient of Curvature (Cz)	0.49
Coefficient of Uniformity (Cu)	42.9

3.1.4 Particle Size Distribution and Soil Classification of Bauxite for Testing (Adjusted Bauxite)

For triaxial tests it was decided to eliminate the gravel and pebbles (particles with diameter greater than 2mm) because the dimensions of the specimen (75mmx160mm) are not large enough to accurately test coarse-soils. Figure 3.5 shows the Bauxite used for testing without coarse particles.

Figure 3.5 Adjusted Bauxite

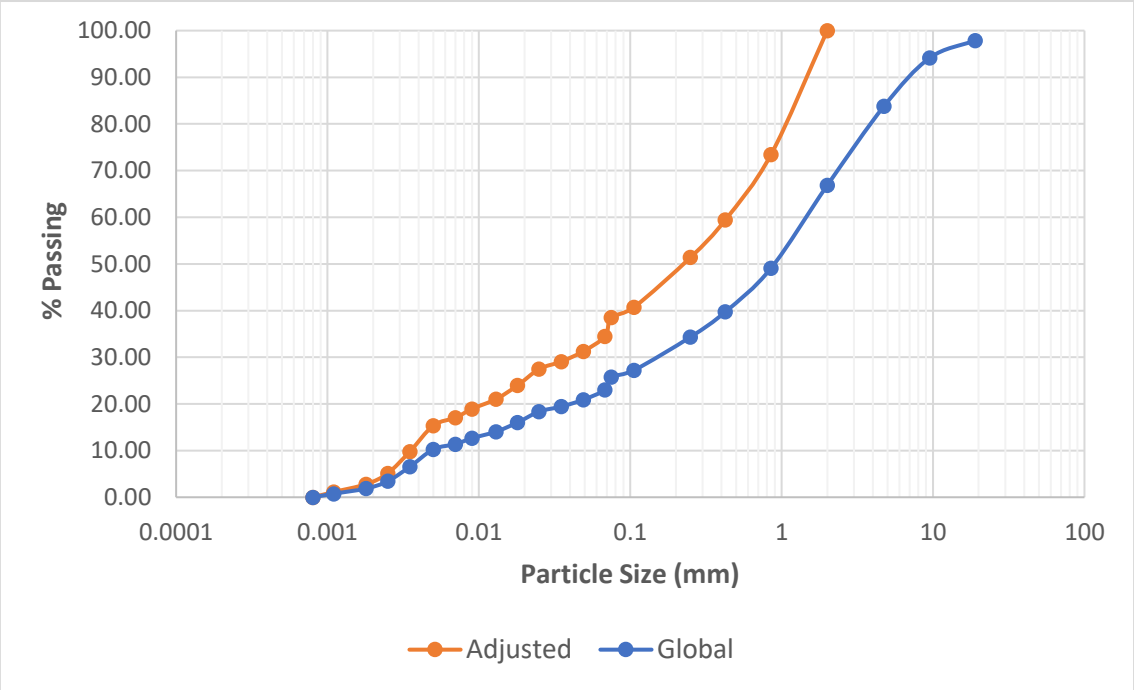

Figure 3.6 Particle Size Distribution of Adjusted Bauxite

Table 3.3 Summary of Adjusted Bauxite Gradation

Gravel (%)	0
Sand (%)	61.4
Silt (%)	23.2
Clay (%)	15.4
Fines Content (%)	38.6
D_{60} (mm)	0.42
D_{30} (mm)	0.04
D_{10} (mm)	0.005
Coefficient of Curvature (Cz)	0.76
Coefficient of Uniformity (Cu)	84.0

3.1.5 Atterberg Limits

- ✓ Plastic Limit (PL): Bauxite showed plasticity when mixed with water. After several trials, the Plastic Limit was established as 25.6%.

✓ Liquid Limit (LL): For adjusted Bauxite, the Liquid Limit was established as 36.5% based on figure 3.7.

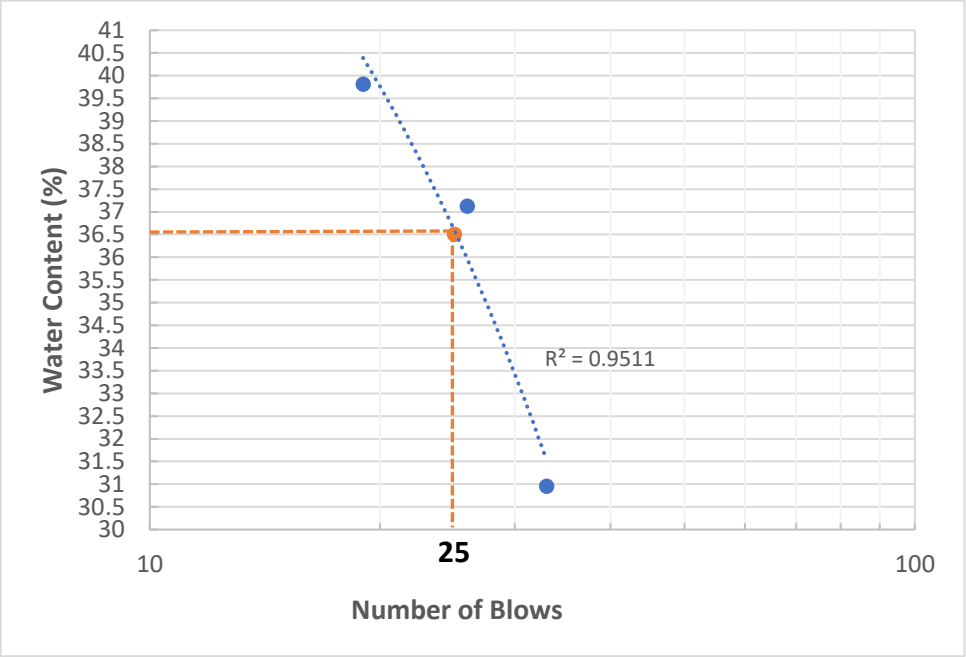

Figure 3.7 Water Content and Number of Blows for Bauxite

✓ Plasticity Index: From the above two test results, the Index of Plasticity can be established as 10.9. Both Plasticity Index and gradation properties are used to classify the soil as SM (silty sand) in the Unified System of Classification of Soils.

Table 3.4 Atterberg Limits of Bauxite

Liquid Limit (LL)	36.5%
Plastic Limit (PL)	25.6%
Index of Plasticity (IP)	**10.9**

3.1.6 Specific Gravity

Six specific gravity tests were performed on the adjusted Bauxite, obtaining an average of 2.642.

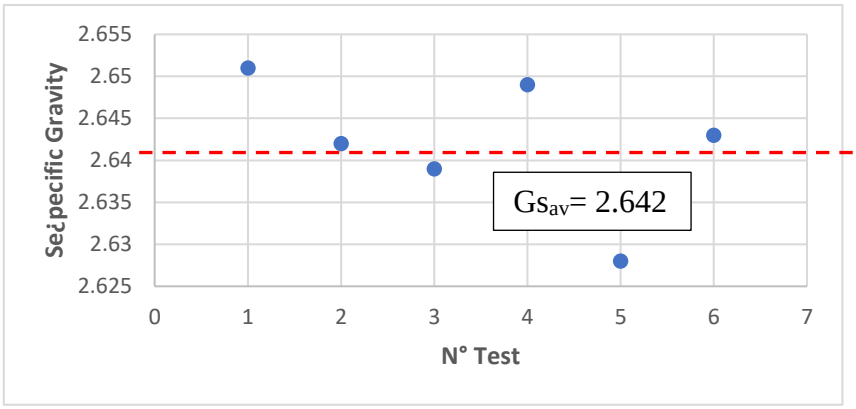

Figure 3.8 Specific Gravity of Adjusted Bauxite

3.1.7 Modified Proctor Test

The maximum dry density was 1.70 gr/cm^3 corresponding to 19.2% moisture content (optimum water content) from the modified Proctor test.

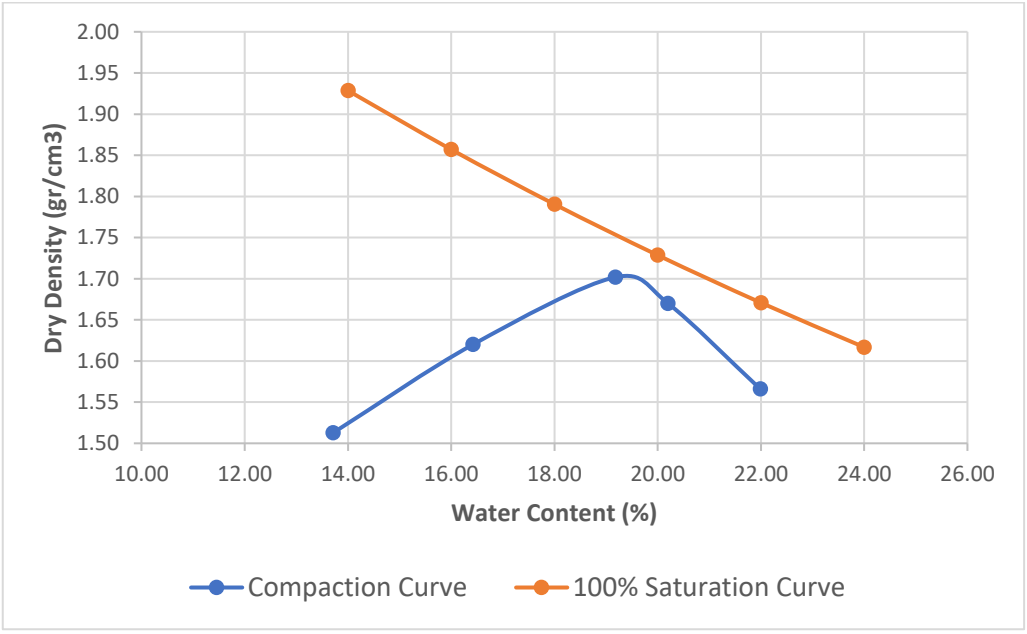

Figure 3.9 Compaction and 100% Saturation Curve for Adjusted Bauxite

3.1.8 Electronic Microscope

Microscopic images of adjusted Bauxite were taken with magnification of 25, 50 and 100 times. The shape of the coarse particles is mainly sub-angular. Furthermore, it can be observed a tendency of fine particles to stick to the surfaces of coarse sand indicating clayey minerals.

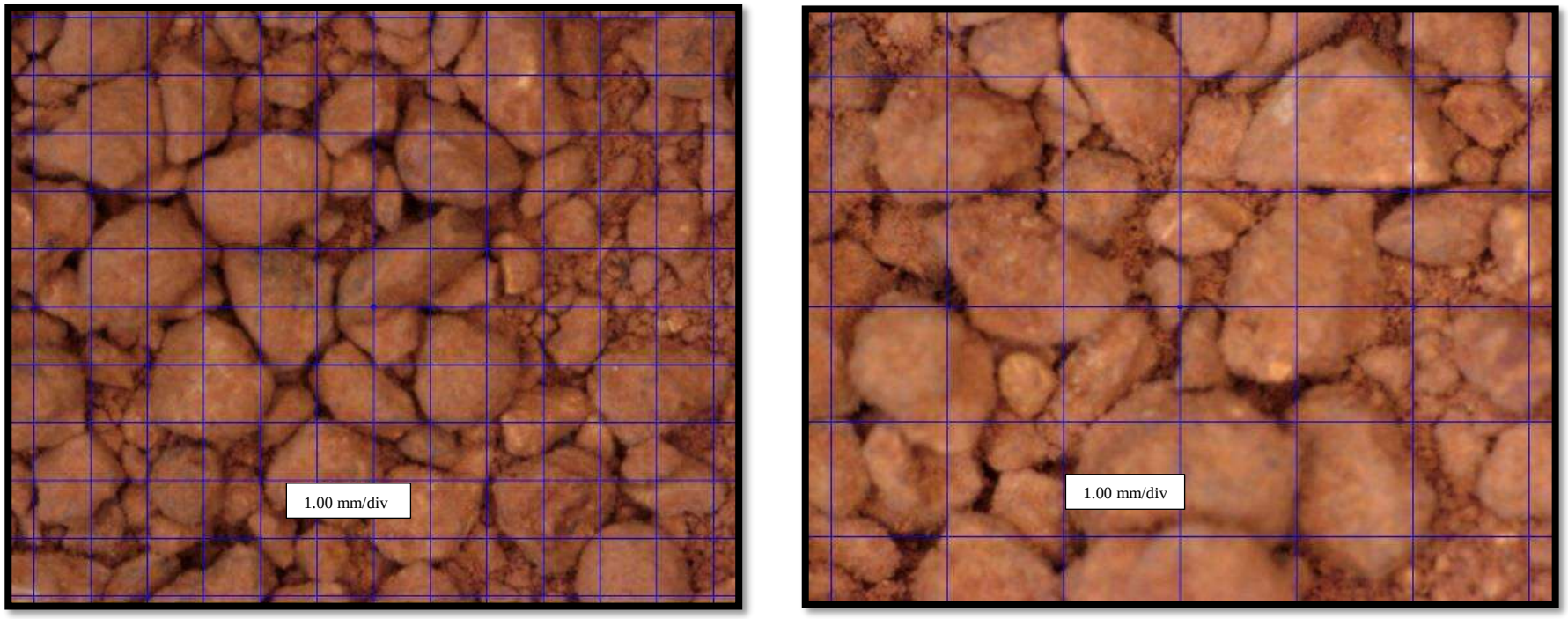

Figure 3.10 and 3.11 Microscopic images of Adjusted Bauxite magnified 25 and 50 times

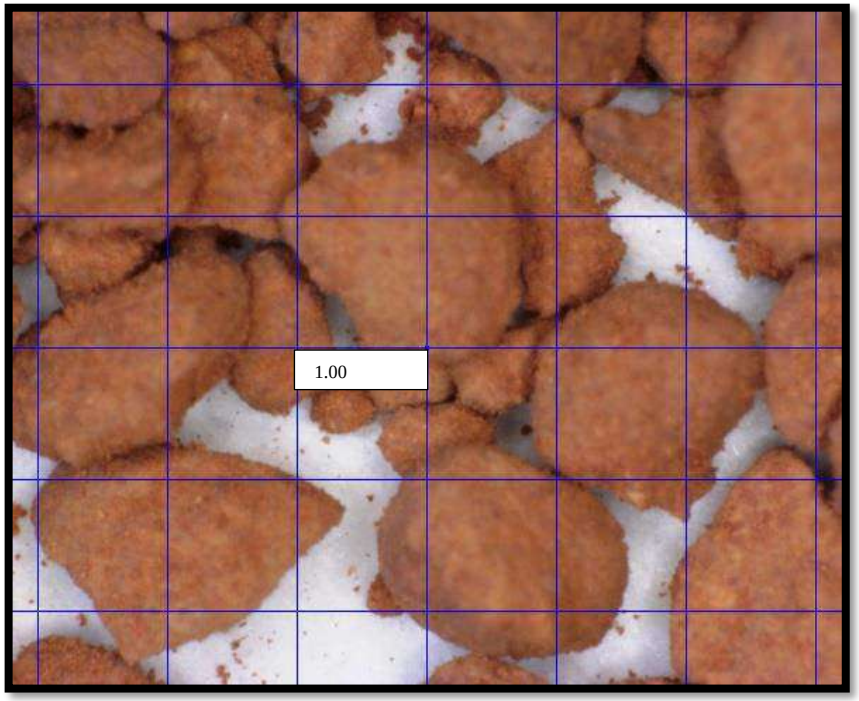

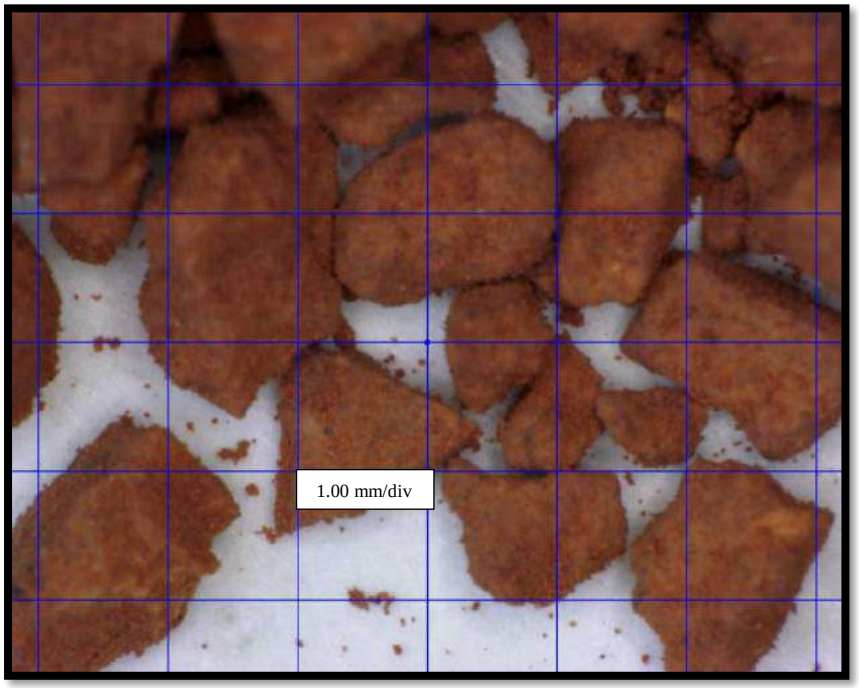

Figure 3.12 and Figure 3.13 Microscopic images of Adjusted Bauxite magnified 100 times

3.1.9 Summary

Adjusted Bauxite is a well-graded silty sand (SM) of low plasticity (IP = 10.9). Its most abundant minerals are of metallic nature (Diaspore, Bohemite) due to its geological formation although some amount of clayey minerals exists which explains its plasticity. The predominant form of its particles is sub-angular. To the touch, its texture feels smooth. Its specific gravity is (2.642), slightly below the typical range for silty sands (2.67-2.70) according to Bowles (2012). From the Modified Proctor's test, the maximum dry density obtained is 1.70 gr/cm^3 with an optimum moisture content of 19.2%.

3.2 GEOLOGICAL AND GEOTECHNICAL CHARACTERIZATION OF SILICA SAND MIXTURE (SIMULATED BAUXITE)

3.2.1 Background

A mixture by weight was designed using several Silica Sands until obtaining a similar gradation to the sandy part of adjusted Bauxite.

- ✓ Silica Sand N° 3 was used for the fraction of Bauxite with diameters larger than 0.85mm, but smaller than 2mm (coarse sands)
- ✓ N° 5 for the ones larger than 0.425mm, but smaller than 0.85mm. N° 7 for the ones larger than 0.25mm, but smaller than 0.425 (medium sands)
- ✓ N° 7 for those larger than 0.106mm, but smaller than 0.25mm. No. 8 for those larger than 0.075mm, but smaller than 0.106mm (fine sands)
- ✓ Finally, Silica Sand N ° 9 passing the sieve #200 was used for the fine particles.

A blender was used to prevent segregation in the mix. Table 3.5 shows the distribution of soils used based on the percentage retained and passing through each standard sieve.

Table 3.5 Types of Silica Sands used

Sieve	Diameter (mm)	% Retained	% Passing	Type of Silica Sand Used
3	2	-	100.0	-
4	0.85	26.6	73.4	**N° 3**
5	0.425	14.0	59.5	**N° 5**
6	0.25	8.1	51.4	**N° 7**
7	0.106	10.7	40.7	**N° 7**
8	0.075	2.2	38.5	**N° 8**
Fines		38.5	-	**N° 9**

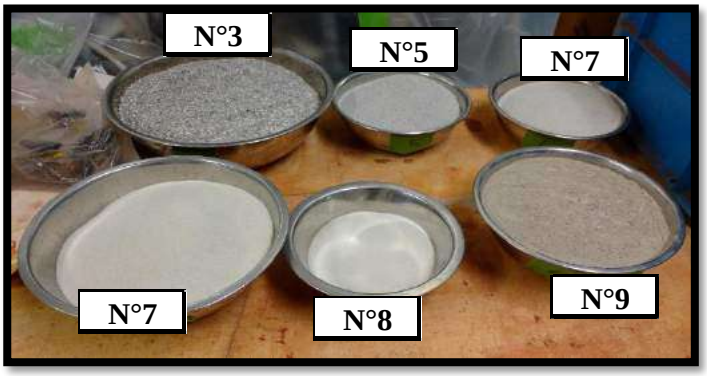

Figure 3.14 Types of Silica Sand Used

Figure 3.15 Mixture of Silica Sands resembling adjusted Bauxite gradation

3.2.2 Geology and Mineralogy

Silica sand is a quartz sand that can be obtained naturally from beach deposits or artificially by grinding and sieving quartzite ore (generally from Sandstone and Schist). It is often used in construction (aggregate of concrete and pavements) and for steel making. The Silica Sand used in this thesis is Mikawa quartz sand made from high-quality

quartz schist rocks spreading around the eastern part of Okazaki city in Aichi prefecture. It is an artificial silica sand which was pulverized and sieved.

The material is of very high purity presenting 98% Quartz (SiO2) with a hardness of 7 on the Mohs scale.

3.2.3 Particle Size Distribution and Soil Classification

The sandy fraction of the mixture has the same gradation as the Adjusted Bauxite, but the fine fraction is different being poorly graded.

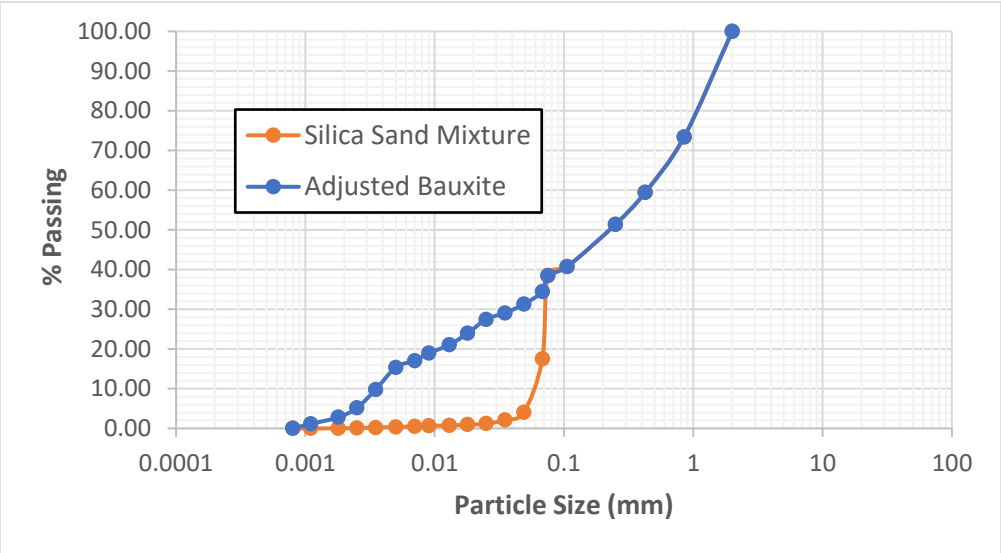

Figure 3.16 Particle Size Distribution of Silica Sand Mixture

Particle size distribution test was done in the mixture (Simulated Bauxite) to study its actual gradation since unexpected fines may change it. As seen in figure 3.17 and table 3.6, there is a small increment in the retained percentage of medium sands (0.5% on average) and 3.1% in fines sands which accounts for the reduction of fines. These is due to some fines loss during the procedure and because some fines are retained together with medium and fine sands.

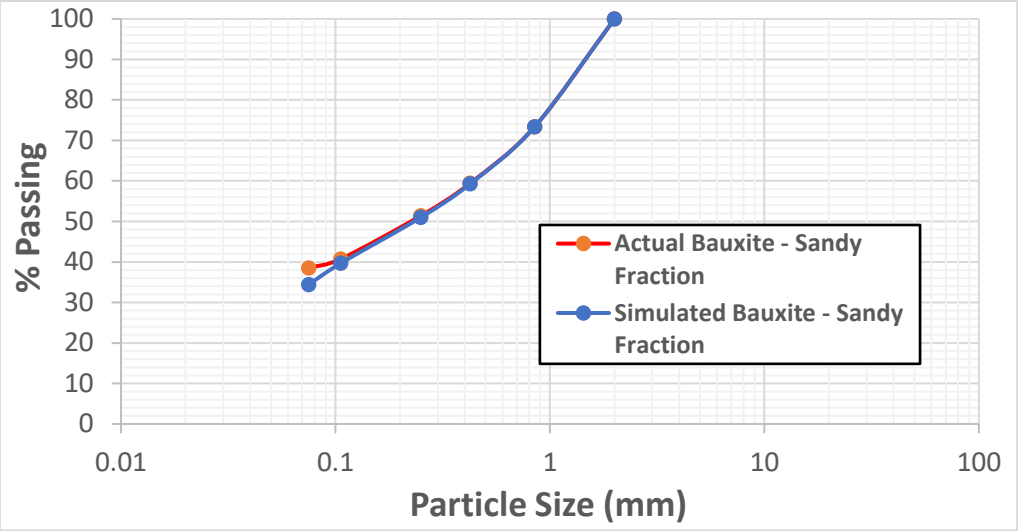

Figure 3.17 Particle Size Distribution of the sandy fraction of Simulated Bauxite and actual Bauxite

Table 3.6 Gradation of the sandy fraction of Simulated Bauxite and actual Bauxite

Sieve	Diameter (mm)	Actual BX (% Retained)	Actual BX (% Passing)	Simulated BX (% Retained)	Simulated BX (% Passing)
3	2	-	100	-	100
4	0.85	26.6	73.4	26.6	73.4
5	0.425	14.0	59.5	14.1	59.3
6	0.25	8.1	51.4	8.3	51
7	0.106	10.7	40.7	11	39.7
8	0.075	2.2	38.5	5.3	34.4
Fines	< 0.075	38.5	-	34.7	-

Table 3.7 Summary of Simulated Bauxite Gradation

Gravel (%)	0
Sand (%)	61.4
Silt (%)	38.2
Clay (%)	0.35
Fines Content (%)	38.6
D_{60} (mm)	0.42
D_{30} (mm)	0.07
D_{10} (mm)	0.06
Coefficient of Curvature (Cz)	0.19
Coefficient of Uniformity (Cu)	7.0

3.2.4 Atterberg Limits

The soil mixture does not present any liquid limit nor plastic limit.

3.2.5 Specific Gravity

Six tests were carried out, establishing the average as the specific gravity of the material (2.613). This value is lower than the specific gravity of Bauxite (2.642) which means that the Silica Sand mixture is lighter than Bauxite, probably because of the heavier metallic minerals of the latter.

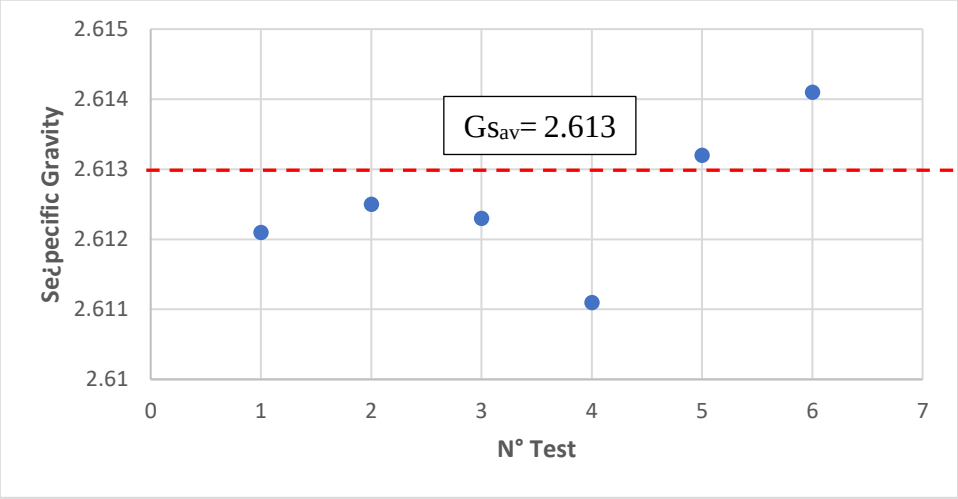

Figure 3.18 Specific Gravity of Silica Sand Mixture

3.2.6 Modified Proctor Test

Simulated Bauxite has a maximum dry density of 1.95 gr/cm^3 and an optimum water content of 9.6%. Bauxite has a lower dry density value (1.70gr /cm^3) but requires a higher moisture content to achieve it (19%). This shows that Bauxite has a higher water absorption capacity.

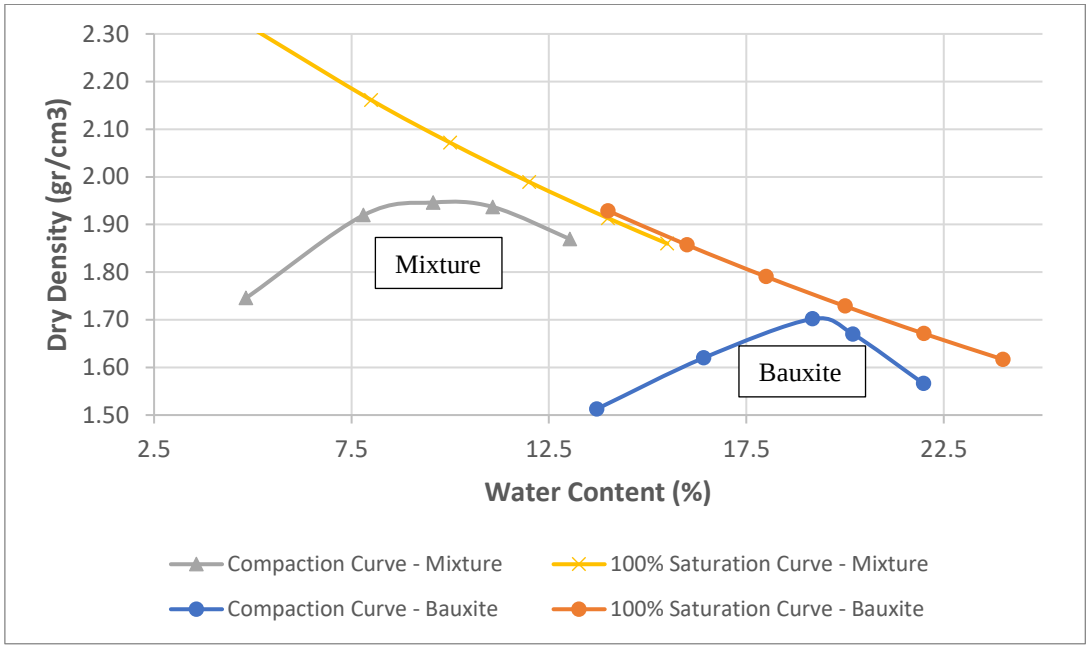

Figure 3.19 Compaction Curves of Silica Sand Mixture and Bauxite

3.2.7 Electronic Microscope

Microscopic images of the mixture were taken at magnification of 25, 50 and 100 times. The shape of the coarse sand's particles was found to be mainly angular. The maximum capacity of the microscope used is 100 times of magnification which does not allow an in-depth study of the Surface texture, but almost all the quartz grains have undergone edge and surface abrasion (Shrivastava et al, 2012). These angularities may explain the roughness of the material to the touch.

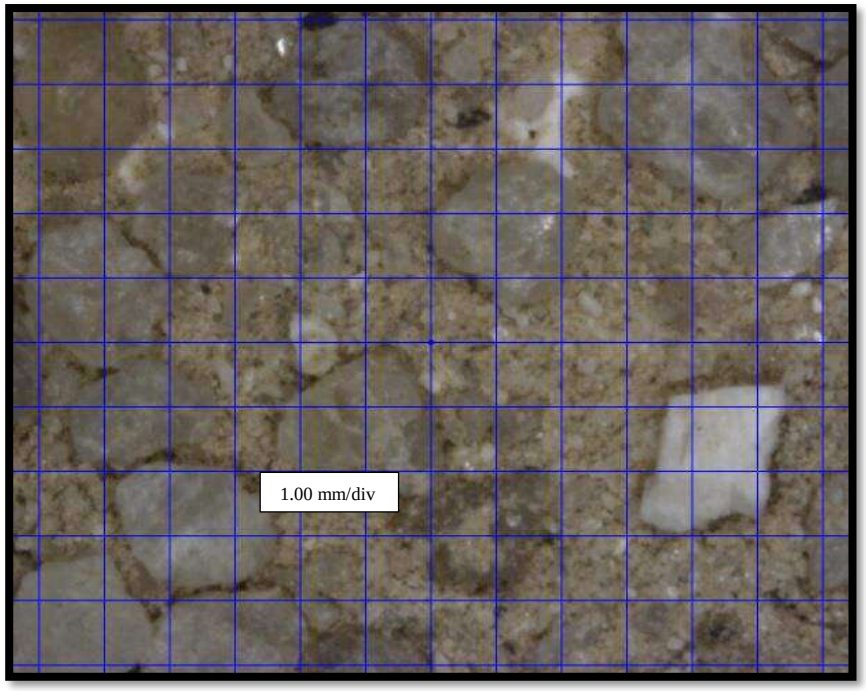

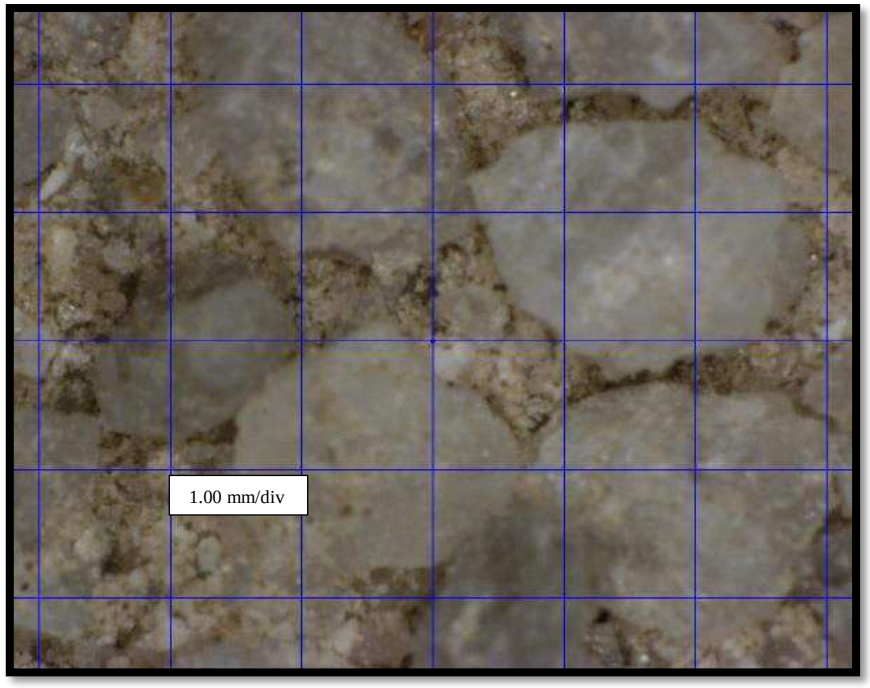

Figure 3.20 and Figure 3.21 Microscopic images of Simulated Bauxite magnified 25 and 50 times

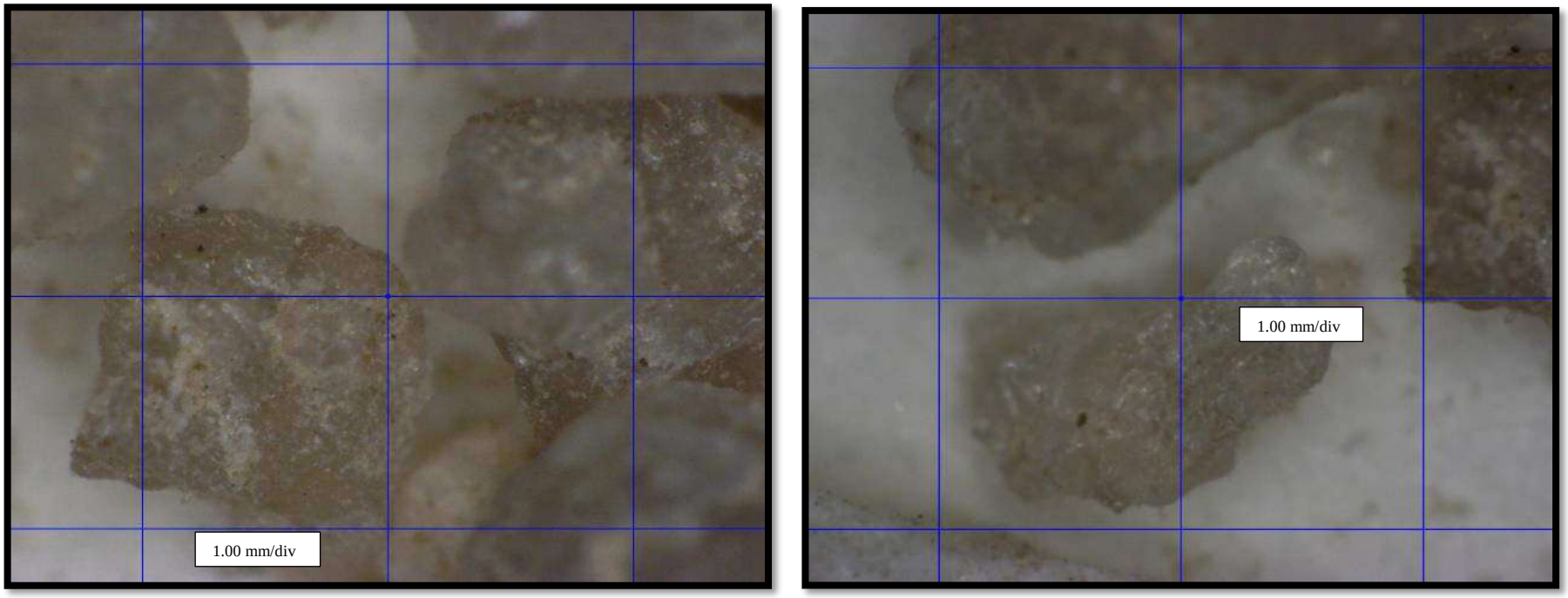

Figure 3.22 and Figure 3.23 Microscopic images of Simulated Bauxite magnified 100 times

3.2.8 Summary

Simulated bauxite is a silty sand (SM) with discontinuous granulometry. The sandy fraction is well graded, but the fine fraction is poorly graded with almost no content of clay particles. It does not show any plasticity. It is almost completely composed of Quartz minerals which is observed in the crystalline structure of the sandy particles. The particles are predominantly angular and feel rough due to the surface texture including Edge abrasions and the high hardness on the Mohs scale (7) of Quartz. Its specific gravity is 2.613, lower than Silica Sand No. 5 (2.761) and No. 6 (2.640) probably due to the inclusion of finer fractions. Its maximum dry density obtained in the Modified Proctor test is 1.95 gr/cm^3 for an optimum moisture content of 9.6%.

3.2.9 Comparison with Bauxite

Figure 3.24 shows Simulated Bauxite and the adjusted Bauxite. The mixture was intended to be as similar as possible, but there are some key differences that cannot be controlled.

Figure 3.24 Silica Sand Mixture and Adjusted Bauxite

- ✓ Fines gradation: The fines content is the same, but the fines of the Bauxite have better gradation and higher clay content (15.4% against 0.35%).
- ✓ Plasticity: Bauxite has a certain level of plasticity (IP = 10.9), but the mixture does not present any plasticity at all

- ✓ Mineralogy: Mineralogy studies were not conducted, but from the literature review it is observed that all the Bauxites have predominantly metallic minerals and in smaller proportion clayey minerals (Montmorillonite). The hardness of these minerals in the Mohs scale is generally less than the hardness of Quartz (7) which is the main component of the simulated Bauxite.
- ✓ Particle shape: Coarse sands included in the simulated Bauxite possess predominantly angular particles, while Bauxite's particles are mainly sub-angular
- ✓ Surface Textures: The mixture of Silica Sands feels rougher to the touch.

3.3 TRIAXIAL TESTING PHASE

3.3.1 Principles of Triaxial Testing

3.3.1.1 Simulation of Field Conditions

The triaxial equipment applies vertical (deviator stress) and horizontal (confining stress) stresses on a soil specimen. These is similar to the principal stresses existing on soil elements of an embankment, dam or ore heaps as shown in the following scheme:

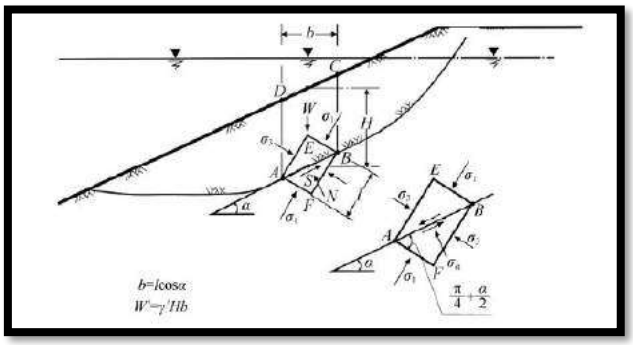

Figure 3.25 Simulation of Field Stresses in Triaxial (Ishihara, 2008)

From the aforementioned analogy, Ishihara (2008) conceptually simulated the Flow Failure of sloping ground in static conditions (static liquefaction). Figure 3.26 shows the Flow Failure sequence of a dredged submarine slope. The initial state shows a slope with inclination angle "α" and the principal stresses of an inclined soil mass of it that resembles the state of an element of soil in triaxial testing after isotropic consolidation. Then, an external load "$\Delta\sigma$" is applied in undrained condition (deviator stress in triaxial tests). This triggers a slip in the slope. After the slip had been triggered, the soil undergoes softening until reaching the steady state where a new deviator stress (0.26 σ_1' for this case) and a

reduced effective confining stress is applied. If the shear strength mobilized at this state is lower than the static shear stress, flow failure will occur.

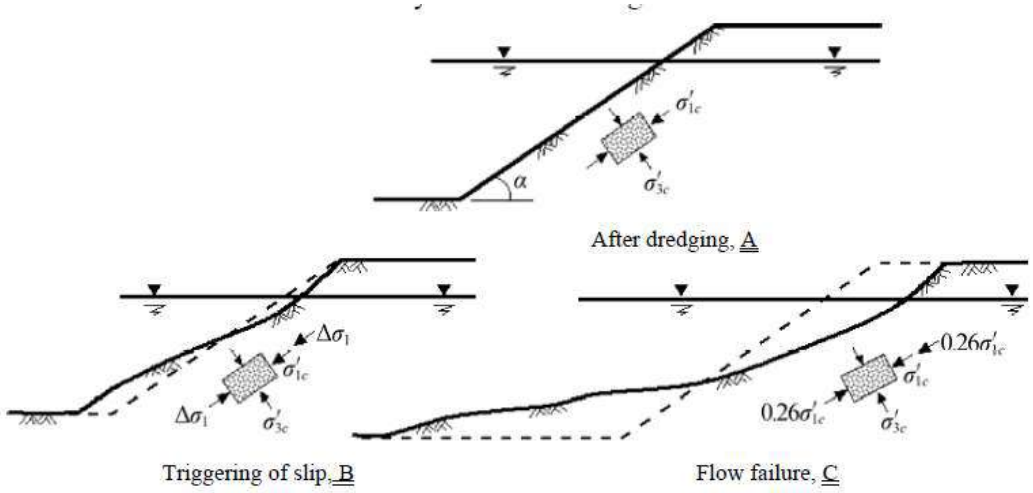

Figure 3.26 Sequence of Events Leading to Flow Failure (Ishihara, 2008)

3.3.1.2 Derivation of Stress and Strain

The Triaxial test is commonly performed in cylindrical specimens. First, a confining stress "σ_3" is applied in axisymmetric condition to the specimen and therefore the intermediate horizontal stress is the same (σ_2=σ_3). At this point, the vertical principal stress "σ_1" is also equal to the confining stress in isotropic consolidation. Then an additional stress named deviator stress "q" is applied in axial direction.

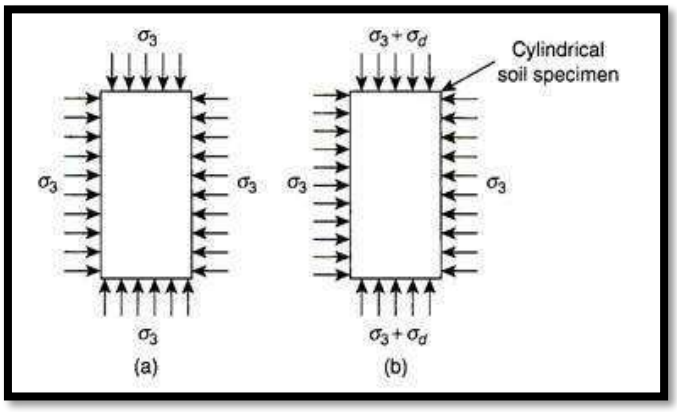

Figure 3.27 Consolidation and shear stage of triaxial compression test (http://www.soilmanagementindia.com)

Since the specimen is cylindrical, the principal stresses are vertical and radial:

$$\sigma_{Vertical} = \sigma_1$$

$$\sigma_{Radial} = \sigma_3$$

And the deviator stress can be computed as:

$$q = \sigma_1 - \sigma_3 = \sigma_{Vertical} - \sigma_{Radial}$$

These equations are valid in effective stresses:

$$\sigma'_{Vertical} = \sigma'_1 = \sigma_1 - u$$

$$\sigma'_{Radial} = \sigma'_3 = \sigma_3 - u$$

$$q' = \sigma'_1 - \sigma'_3 = \sigma'_{Vertical} - \sigma'_{Radial}$$

The mean effective stress can be calculated in Cambridge type by:

$$p' = \frac{\sigma'_{Vertical} + 2\sigma'_{Radial}}{3}$$

The axial strain and volumetric strain can be derived from the initial values of height (H0) and volume (V0).

$$\varepsilon_v = -\frac{\Delta H}{H0}$$

$$\varepsilon_{vol} = -\frac{\Delta V}{V0}$$

3.3.2 Triaxial Equipment

3.3.2.1 Triaxial Setup

Figure 3.28 shows a picture of the triaxial equipment used in this test and figure 3.29 a drawing scheme. This apparatus consists basically of the following parts:

- ✓ Specimen of soil of 75mm of diameter and 160mm height
- ✓ Metallic cell filled with water
- ✓ Pressure supply (EPT) up to 1.0 MPa
- ✓ Vertical loading equipment
- ✓ Instrumentation system for measurement and control

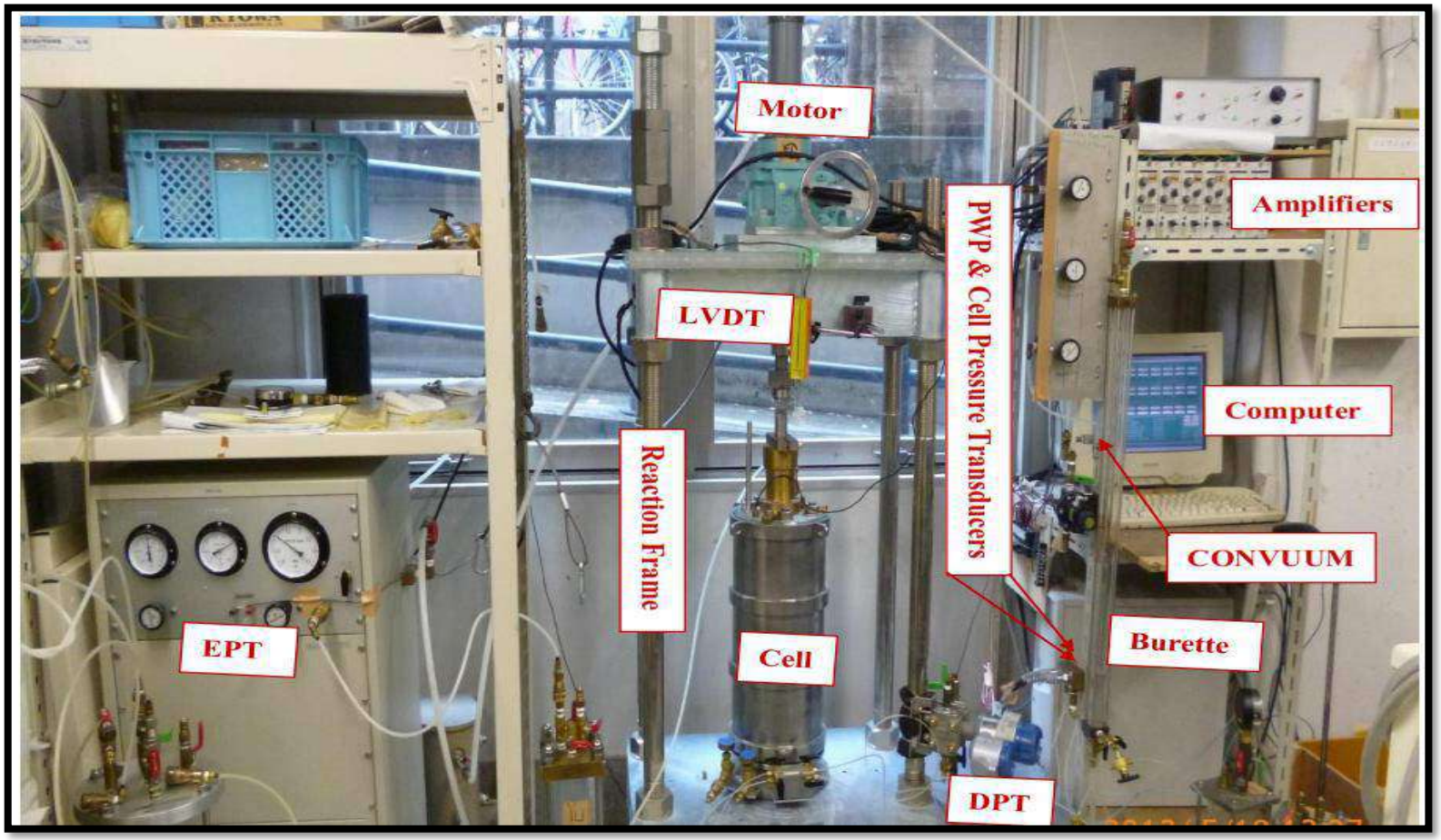

Figure 3.28 Picture of high-pressure Triaxial Test (Ahmed, 2016)

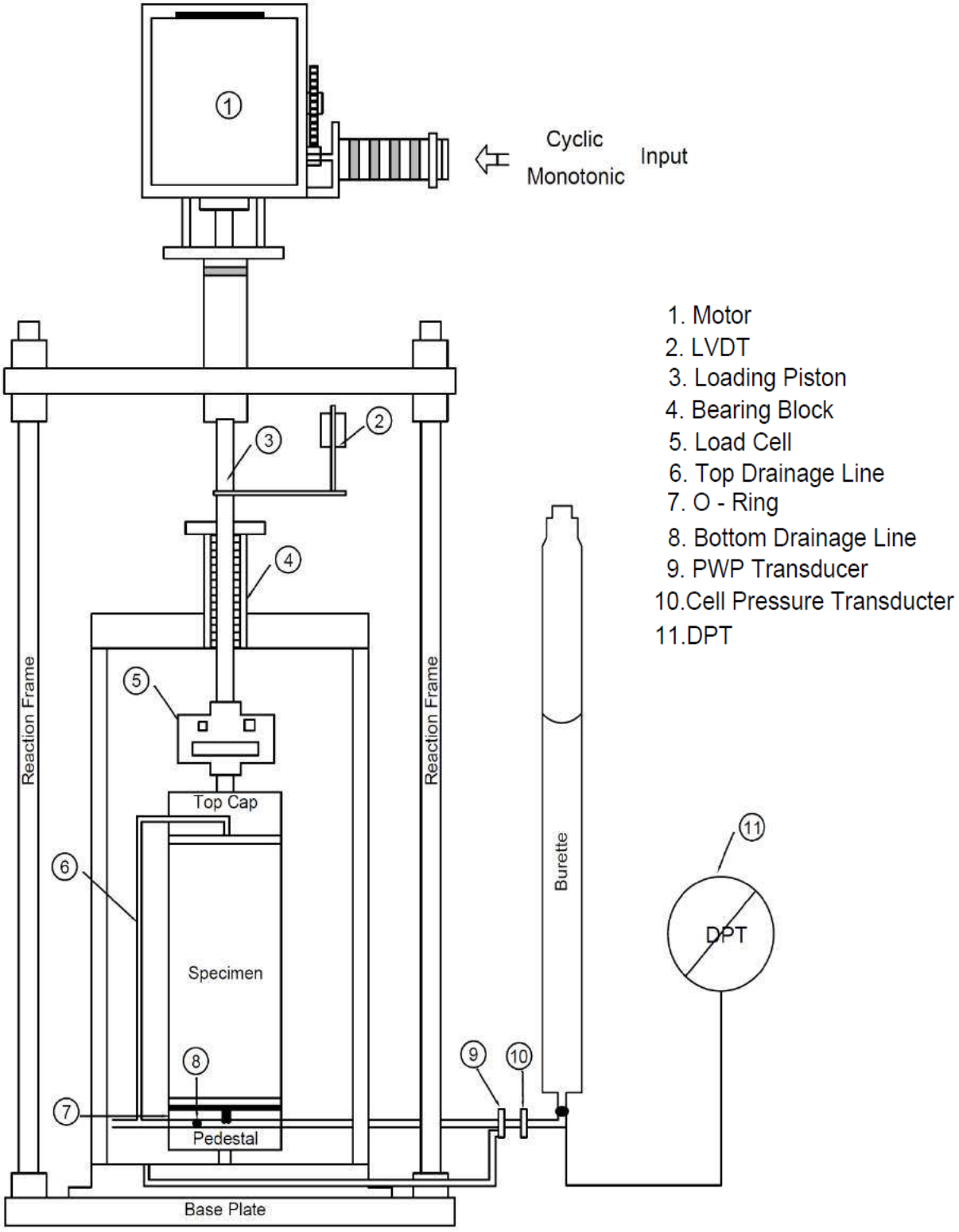

Figure 3.29 Scheme of High-pressure triaxial test

3.3.3 Instrumentation, Measurements and Control

3.3.3.1 Purpose of Instrumentation

The purpose of instrumentation is to measure the physical processes that occur in a test to be able to describe it. The physical quantities of interest (e.g. stresses, strains) require transformation into more usable and more easily measured quantities. Thus, the purpose of instrumentation is to transform one physical quantity into another physical quantity that can be measured. This process is called "Transduction" (Lade, 2016).

The triaxial apparatus used in this thesis has 5 different transducers to measure linear deformations, volume changes, axial loads and pressures (cell and pore water).

3.3.3.2 Measurement of Linear Deformations

A Linear Variable Differential Transformer (LVDT) or External Deformation Transducer (EDT) is used to measure displacements. Its working range is linear, and its maximum capacity is 100mm. The calibration curve of LVDT was obtained by using standard block gauges. Figure 3.30 show the calibration curve of the LVDT.

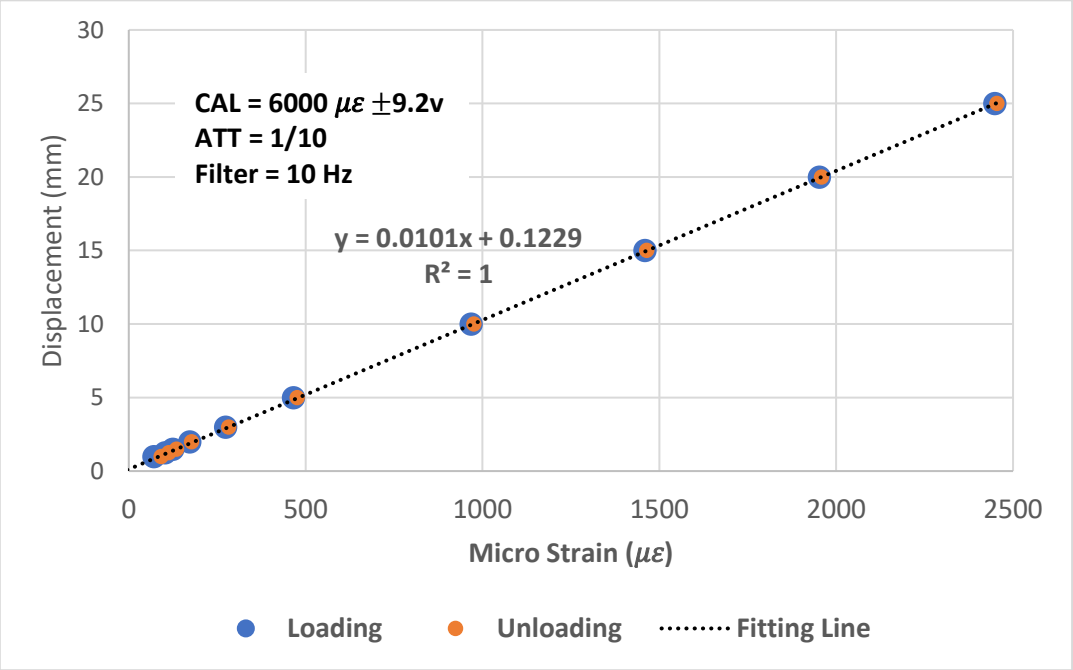

Figure 3.30 Calibration of LVDT

3.3.3.3 Measurement of Volume Changes

Volume changes are measured by a Burette with a Differential Pressure Transducer (DPT) connected to it. This device measures the volume of water expelled from saturated specimens (the water is deemed incompressible). The calibration curve is shown in figure 3.31.

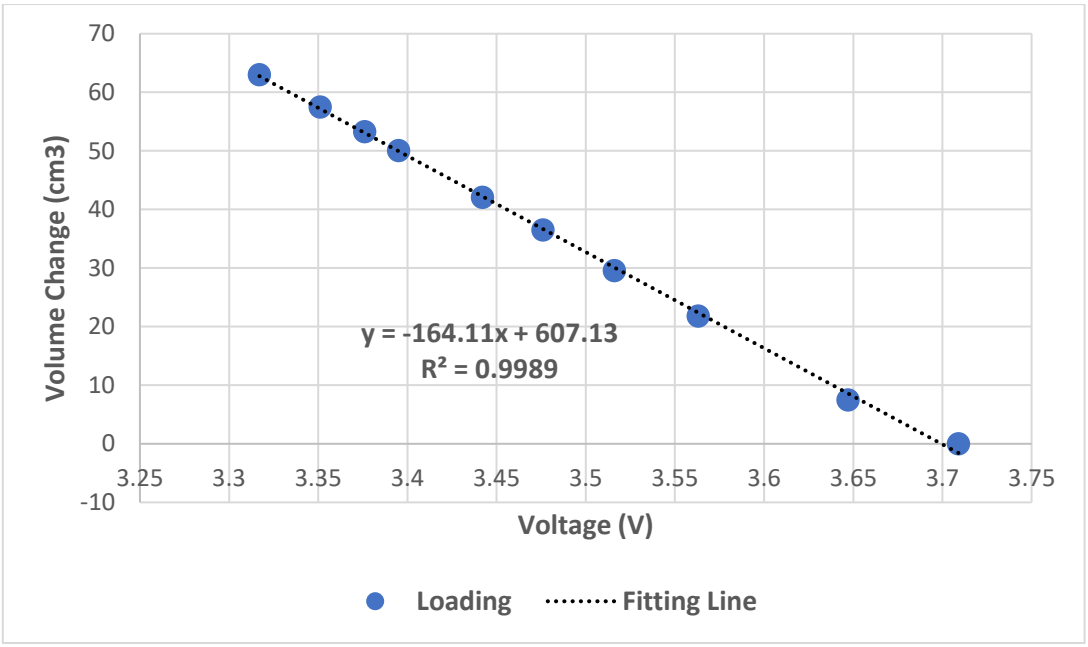

Figure 3.31 Calibration of DPT

3.3.3.4 Measurement of Axial Load

The axial force is measured by a Load Cell composed of an electrical resistance strain gauge type which is fixed on the loading piston. Calibration of the load cell was done by progressively increasing weights of 11.7 kg approximately to the piston while using a dummy specimen. The resulting curve is shown in figure 3.32.

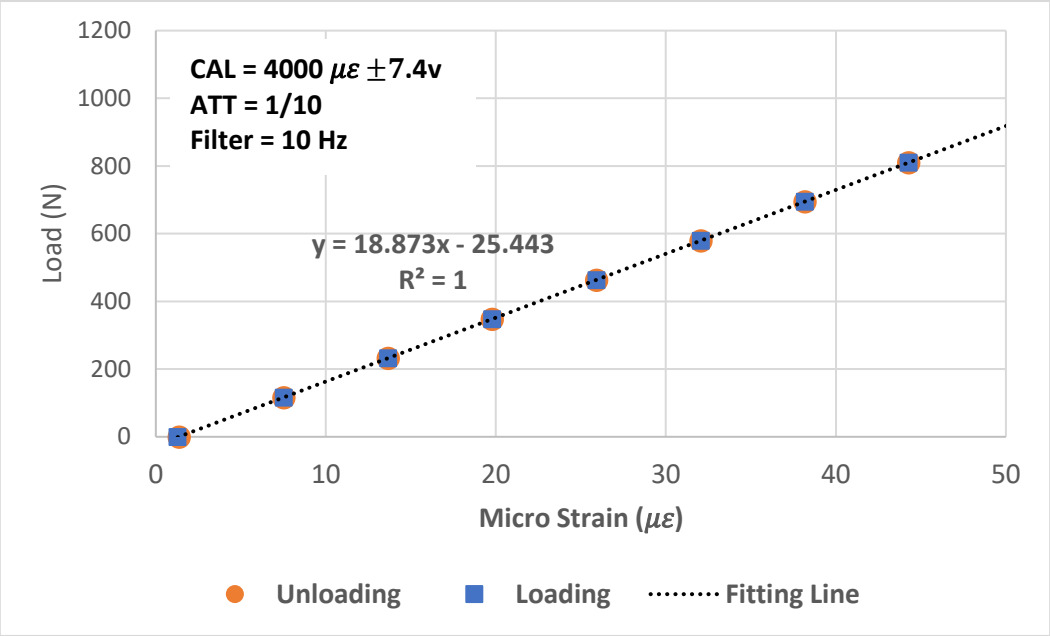

Figure 3.32 Calibration of Load Cell

3.3.3.5 Measurement of Pressure

Cell pressure and pore water pressure are measured by pressure transducers located together outside of the triaxial cell. The calibration characteristics of these transducers are shown in figures 3.33 and 3.34.

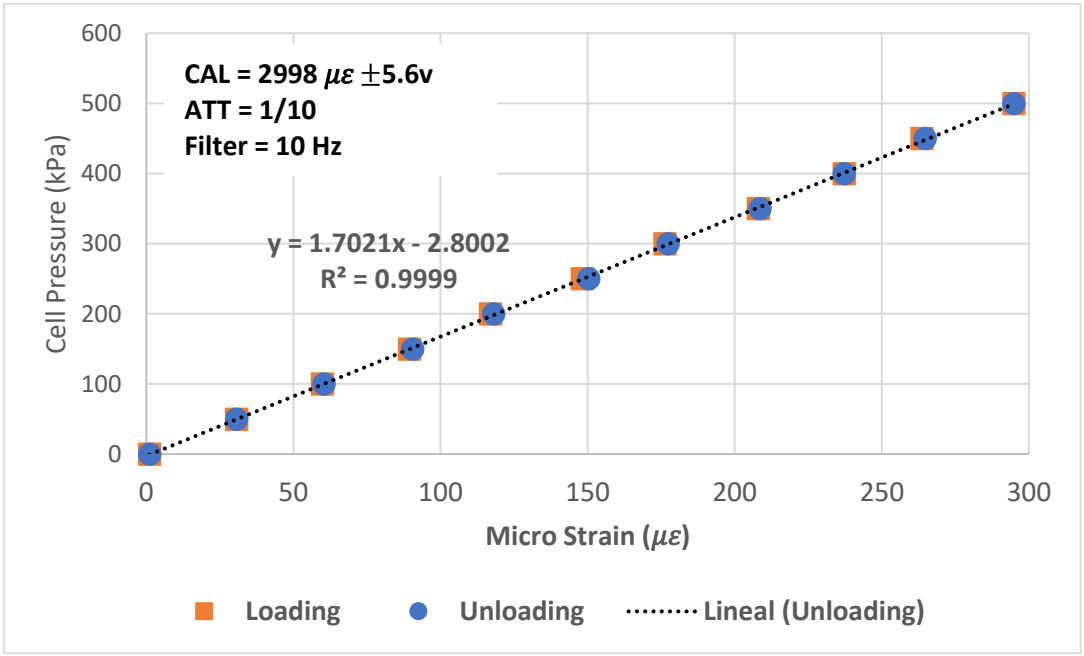

Figure 3.33 Calibration of Cell Pressure Transducer

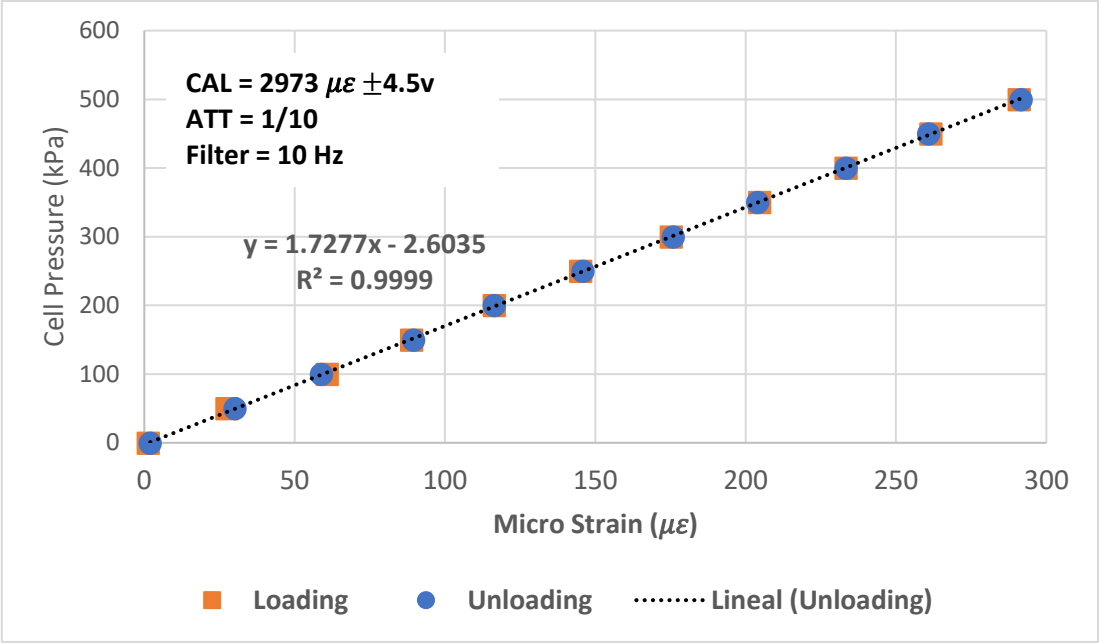

Figure 3.34 Calibration of Pore Water Pressure Transducer

3.3.3.6 Summary of transducers

Table 3.8 shows the maximum capacity and calibration factors of each of the transducers:

Table 3.8 Summary of Transducers

Transducer	Serial N°	Maximum Capacity	Calibration Factor
LVDT	SD-1000R N° 031811	100 mm	0.0101 mm/με
DPT	A1B3273T	10 kPa	-
Load Cell	-	100 kN	18.873 N/με
CP	FD2950015	5 MPa	1.702 kPa/με
PWP	FD2950014	5 MPa	1.728 kPa/με
E/P	-	1.0 MPa	-

3.3.3.7 Data Acquisition

Datalogging is made automatically by using a computer. The instrumentation system provides electrical signals of analog type from transducers of volume changes, axial loads, linear deformations and pressures that are converted into digital signals from an A/D converter board. The digital signals are then recorded with a data acquisition software

(Digit Show Basic) and finally converted into physical values by using calibration factors. The channel arrangement is as follows:

- ✓ CH1: Load Cell
- ✓ CH2: Displacement (LVDT)
- ✓ CH3: Pore Water Pressure (Pressure Transducer)
- ✓ CH4: Cell Pressure (Pressure Transducer)
- ✓ CH5: Volume Change

3.3.3.8 Test Control and Feedback

The software Digit Show Basic allows both datalogging and test control. Main features of the test such as the strain rate in strain-controlled tests or keeping a fixing a minimum deviator stress during consolidation can be set from the computer by assigning a motor speed. Further, it is possible to establish a certain value of confining stress to the E/P transducer. The procedure to control the test follows the process of data acquisition, but inversely. The assigned values of motor speed or confining stress are of digital type which are converted to analog by a D/A converter board. The scheme 3.35 displays the procedure of data acquisition and control.

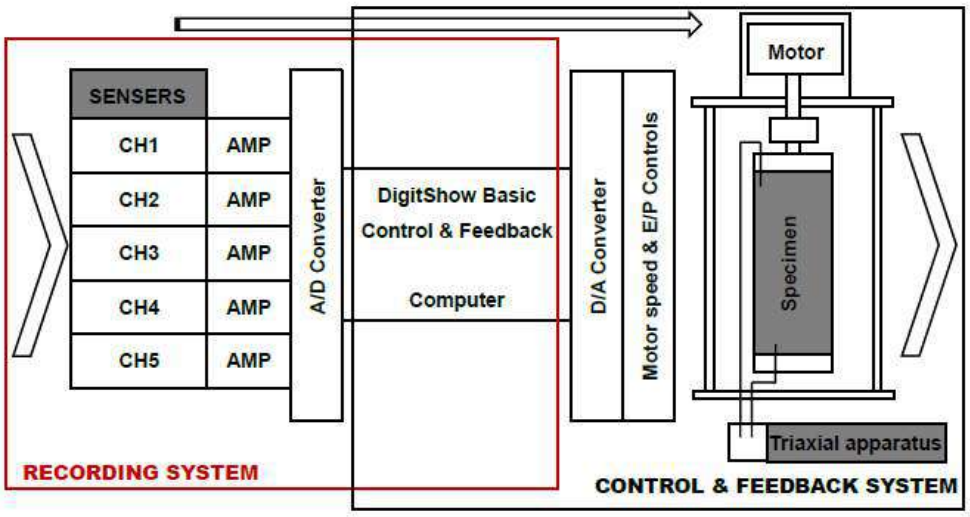

Figure 3.35 Schematic Diagram of recording and control and feedback system (Yu, 2014)

Calibration procedures were done for the motor speed in terms of number of revolutions per minute against displacements to determine appropriate values of Strain Rate for monotonic loading stage (figure 3.36). However, the calibration of the E/P transducer was not conducted because the transducer was not functioning at the time of this research.

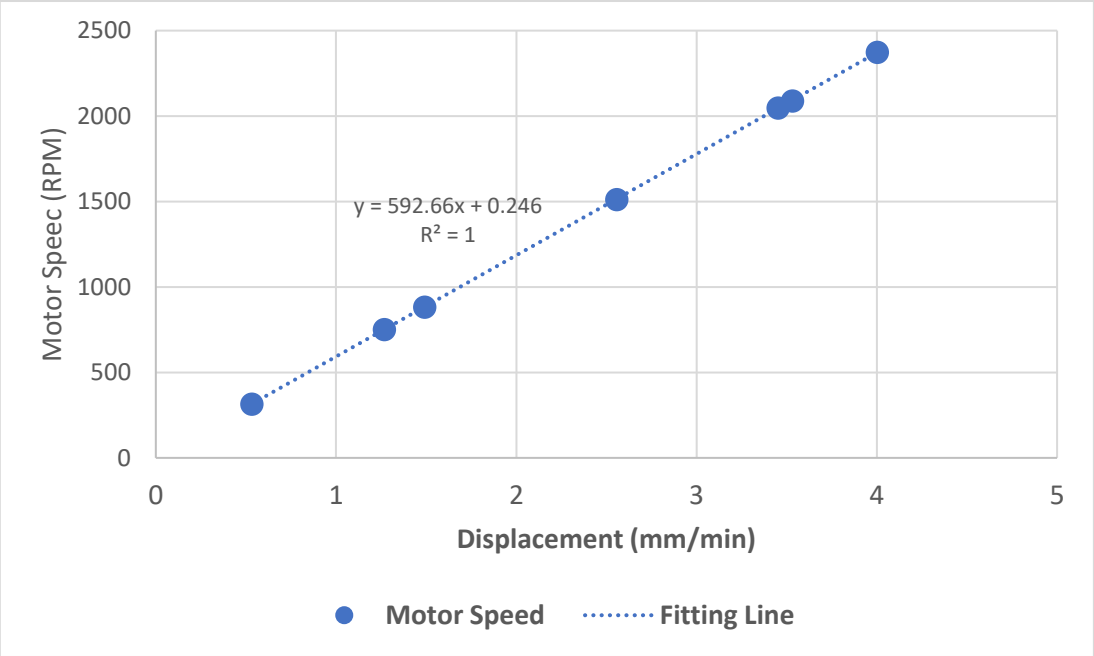

Figure 3.36 Calibration of Motor Speed

3.3.4 Test Procedure

3.3.4.1 Preparation of Triaxial Specimens

1. Before each test, the adequate supply of 75mm diameter and 1mm thick membranes should be ensured, as well as sufficient de-aired water. In addition, the calibration values of the transducers must be entered to the software Digit Show Basic
2. Both the pedestal and the top cap must be lubricated using silicone grease and a membrane of 0.3mm of thickness. This is of paramount importance because the measured strengths and the non-uniformities of stresses and deformations will depend on the quality of lubrication of platens (Tatsuoka et al, 1984). If the lubrication is of high quality, the specimen will deform as right cylinder during shear with consequent uniform strains and uniformly distributed pore pressures in undrained tests (Lade, 2016).

3. Then, filter paper should be placed on the porous stones of the top cap and the pedestal to avoid fines particles of soil to prevent the flow of water during flushing.
4. Vacuum grease is applied to the sides of the pedestal and top cap to avoid leakages from the cell pressure to the specimen. Then, a membrane of 200mm height and 0.75mm of diameter is placed and fixed with a rubber O-ring.
5. The Split Mold is placed around the membrane and negative pressure of -30kPa is applied to ensure that the specimen remains vertical.
6. In this thesis the Wet Tamping method was used for sample preparation because it allows obtaining larger ranges of density (Verdugo, 1992) and because the resulting soil fabric does not present high level of anisotropy as other methods such as Dry Deposition (Sze and Yang, 2013). In addition, this method of preparation resembles better the actual procedure of construction of embankments, dams and ore heaps.

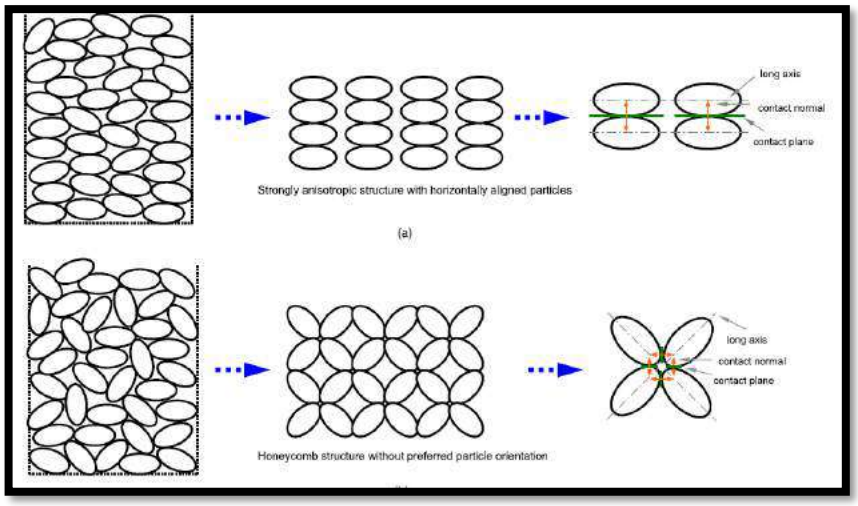

Figure 3.37 Schematic illustration of fabrics of sand specimens prepared by (a) dry deposition; (b) moist tamping (Sze and Yang, 2013)

7. The density level desired for the test will be a percentage of the maximum density obtained in the Modified Proctor test. For adequate compaction and saturation, a proper moisture content must be chosen. It is recommended to use a water content close to the optimum (16% was used for Bauxite and 7.5% for the Silica Sand Mixture).
8. To assure that the compaction energy is transmitted uniformly, it was decided to use 8 layers of 2cm each. According to Sasaki (2017), resistance to

liquefaction in cyclic tests does not vary greatly for samples prepared in 4, 6 and 8 layers if the same moisture content is maintained during the preparation. After finishing the tamping of a layer, the soil surface must be scratched to assure adherence between it and the next layer. This is like grading embankments layers in earthmoving construction.

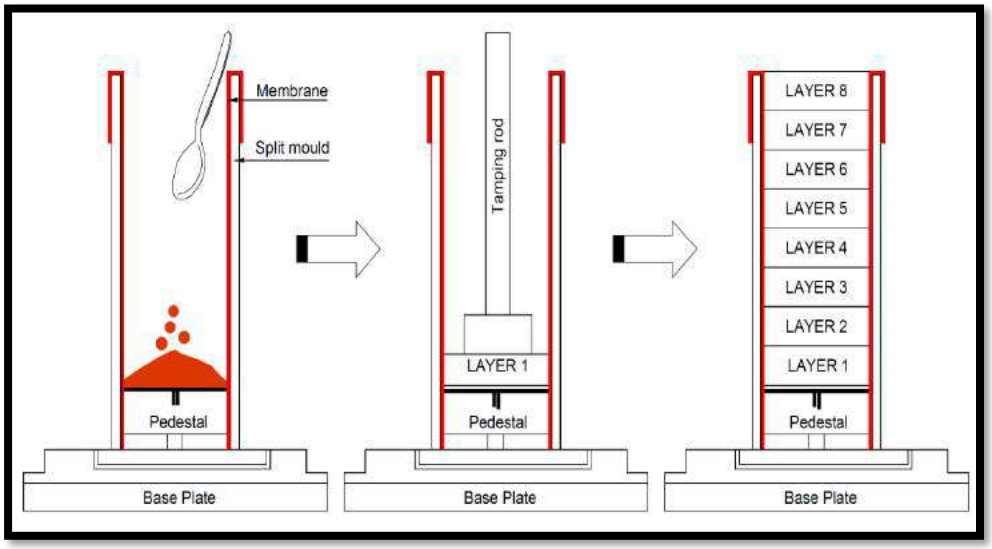

Figure 3.38 Moist Tamping method of sample preparation

Figure 3.39 Finished Sample

9. After the preparation of the sample is finished, the 4 steel pillars are placed, and the top part is mounted.
10. The membrane is fixed to the top cap using a rubber O-ring, it should be noted that the top cap should also be spread with vacuum grease to avoid leakage. The drainage line of the top cap should be connected as well.
11. A negative pressure of -30kPa is applied to the specimen to keep it standing and then the split mold is removed. At this stage, the equipment looks like figure 3.40.

Figure 3.40 Triaxial equipment after fixing the top part

12. The metallic cell must be placed using a crane, then the 4 pillars will be adjusted with 4 screws and the equipment will be moved until its exactly position under the piston.

Figure 3.41 Triaxial with metallic cell

13. Subsequently, the cell is filled with water up to the height of the membrane to assure a better transmission of the confining stress.
14. The residual pressure is removed inside the cell and the pressure measurement sensor is connected adjusting its value to zero.
15. The displacement measurement sensor LVDT is placed, ensuring its horizontal and vertical orientation with the bubble level.

3.3.4.2 Specimen Saturation

16. Prior to the saturation process, it is suggested to use the "Pre-consolidation" option with a speed of 200 RPM to keep the isotropic consolidation condition throughout the saturation process.
17. Saturation will be done using the "Double-vacuuming" method (Ampadu and Tatsuoka, 1993) with an external vacuuming pump. Negative pressure in the specimen will be -100kPa and in the cell -70kPa so that the effective stress in the specimen remains 30kPa. At these high negative pressures, air bubbles will be enlarged and sucked. The vacuuming will be done for 1.5 hours for loose specimens and at least 3 hours for denser specimens (more than 85% of degree

of compaction). The configuration of water tanks and the pump for double-vacuuming is shown in Figure 3.42.

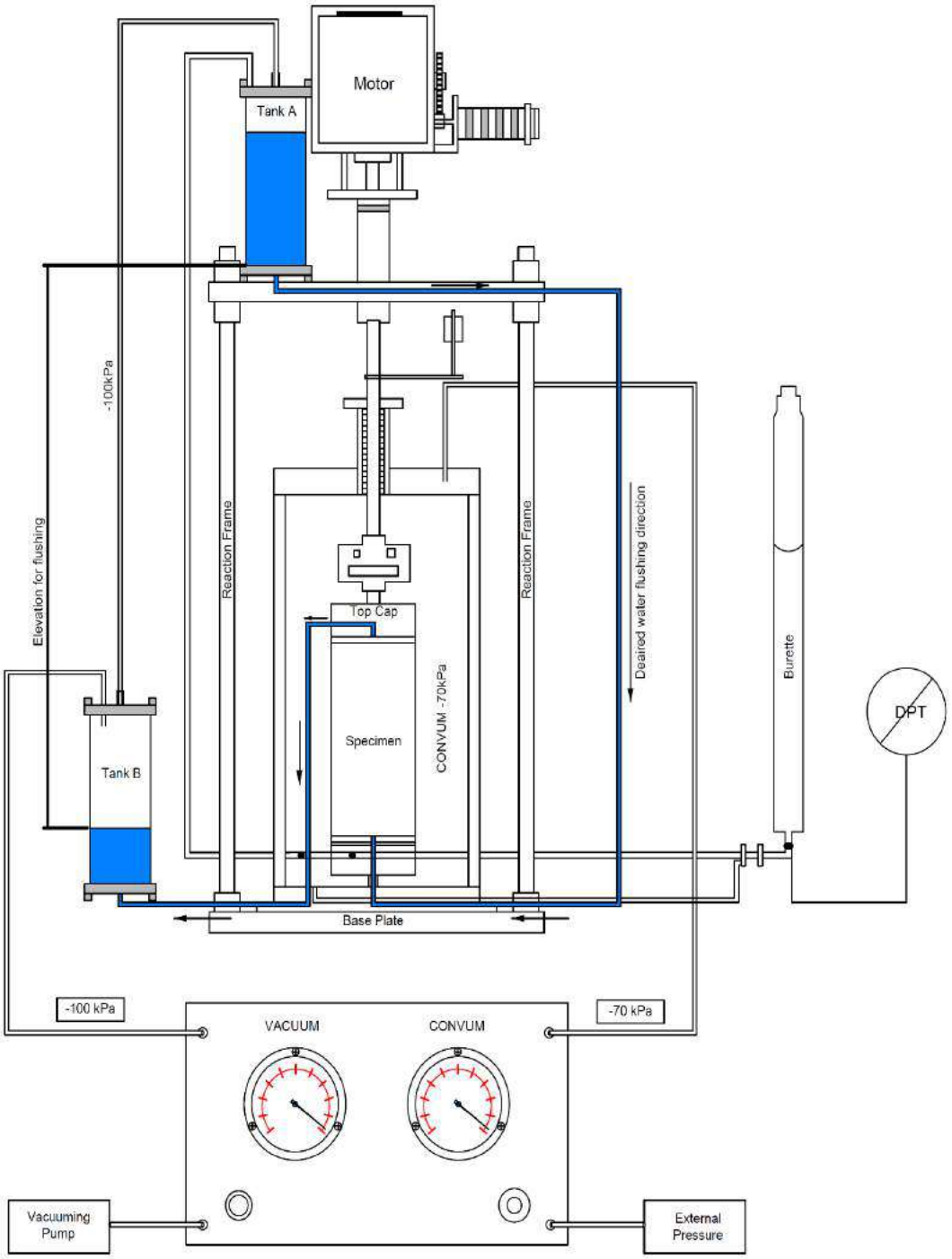

Figure 3.42 Configuration for Double Vacuuming

18. Then, percolation is carried out using de-aired water, since the lower and upper tanks and the specimen are at the same pressure (-100kPa), the water will flow by gravity. The water is introduced through the bottom drainage line and it will

saturate the specimen by flushing the air out though the top drainage line. It is recommended the water level in the upper tank to be reduced at least the same height of the specimen (16cm) and consequently the water level of the bottom tank to rise a similar height to ensure a good level of saturation.

19. At the end of the percolation, the tanks and the vacuum pump must be removed, and the specimen should be connected to the burette and to the pore water pressure sensor
20. Back Pressure will be applied to dissolve the remaining air bubbles. In order to determine the degree of saturation, the "B-value" defined by Skempton (1954) is used.

$$B = \frac{\Delta\mu}{\Delta\sigma_3}$$

Where, $\Delta\mu$ is the change in pore water pressure as a result of an imposed change in isotropic cell pressure $\Delta\sigma_3$. If a specimen is fully saturated, a given increment in isotropic cell pressure will reflect the same increment in pore water pressure giving a B value of 1.0. Nevertheless, this case is impossible as there will always remain some isolated air bubbles. B values greater than 0.97 are acceptable since they represent approximately 99% of degree of saturation for soft, medium and stiff soils (Black and Lee 1973).

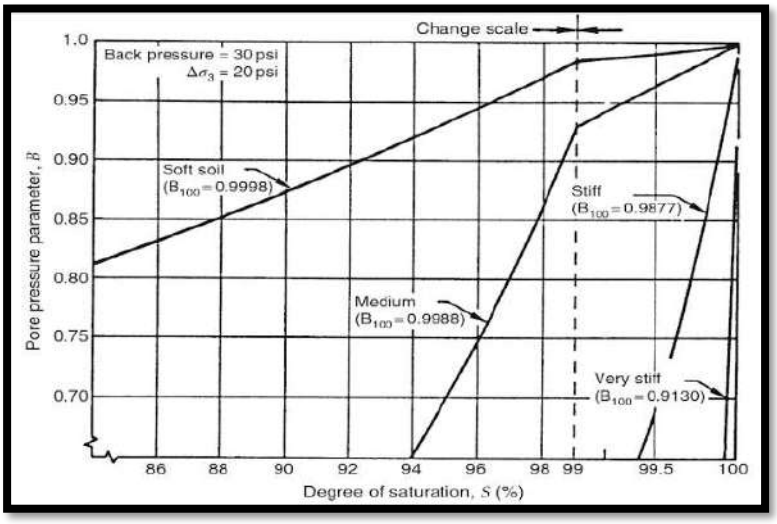

Figure 3.43 Variation of B Values with degree of saturation for four classes of soil (Black and Lee, 1973)

21. Usually 200kPa of Back Pressure is sufficient for Bauxite and the mixture in loose state. For denser samples, until 300kPa might be required. Back pressure must be applied slowly to allow the pore water pressure sensor to read the values accurately.
22. The valve connecting the specimen to the Burette is closed, the current values of cell pressure and pore pressure are recorded (usually 230 kPa and 200 kPa) and 50 kPa of cell pressure is increased. The new value of the pore water pressure is used to estimate the B value. It is advisable to wait at least 2 minutes until the reading of the pore water pressure stabilizes, if the B value is greater than 1.0 it is a signal of leakage from the cell to the membrane since the external air pressure is entering the specimen.

3.3.4.3 Consolidation

23. Once the specimen is saturated, the external source of pressure is replaced by the high-pressure compressor since the former can only reach 600 kPa.
24. The function "Linear Stress Path Loading" is programmed in the software Digit Show Basic setting the target effective confining stress and a suitable motor speed loading that assures isotropic consolidation condition, 220 RPM is highly recommendable in the author's experience for the current motor configuration (3 gears).
25. The DPT is calibrated to zero and the consolidation process is done manually by small increments, 5 kPa every 15 seconds is recommendable.
26. Volumetric and Axial Strains measurements shall be recorded every 1 seg.
27. When the desired level of confinement is reached, consolidation will automatically stop.

3.3.4.4 Shearing

28. Before proceeding with the monotonic loading, it must be assured that the value of the deviator stress is zero and the valve connecting the specimen with the burette must be closed for undrained condition.
29. The "Monotonic Loading" function is used in the software fixing the type of test, the strain rate and the range of strain desired.
30. In this thesis, strain-controlled tests were preferred because they can provide better insight of the undrained post-peak behavior. The Japanese Geotechnical

Society for laboratory shear tests (2015) recommends a strain rate of 0.1%/min for silty samples to ensure uniform distribution of pore water pressure in the specimen; however, the strain rate used was 0.05%/min (50 RPM of motor speed) because -as mentioned in chapter 2.2.4.5- lower strain rates give more conservative results. The target strain level was 30% as it was deemed enough to reach the steady state based on prior studies in similar materials (Santos and Verdugo, 2011; Ahmed, 2016; Kwa and Airey, 2017, Wang et al 2018).

31. Finally, a data collection sample time is set (5 sec for monotonic loading) and the test is started.

3.3.4.5 Leakage

This thesis aims to study the undrained monotonic behavior of soils so a B value of at least 0.95 is mandatory. Even a small amount of air will have a large effect on the pore pressures that develop during an undrained test because the volumetric compressibilities of water and air are vastly different (Lade, 2016). The main source of lack of full saturation in triaxial test is leakage which can take place in several different locations of the apparatus. Leroueil et al (1988) stated that potential sources of leakage are: external fittings, fittings inside the cell and between end plates and the membrane, through the membrane due to osmosis between the pore fluid and the cell fluid and diffusion inside the burette. Figure 3.44 shows a scheme of the sources of leakage.

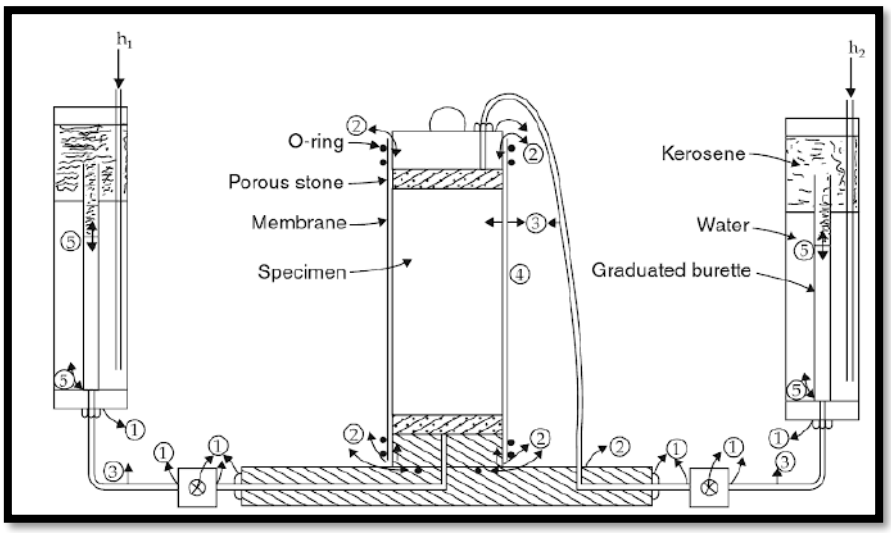

Figure 3.44 Sources of Leakage in Triaxial Tests: (1) Leakage in external fittings; (2) Leakage in fittings inside the cell; (3) osmosis and diffusion through the membrane and lines; (4) saturation of membrane; (5) leakage and diffusion in burette (Leroueil et al, 1988)

To avoid the negative effects of leakage it is suggested the following procedures:

- ✓ Carry out maintenance of fittings replacing old tubes and valves and checking constantly the conditions of upper and bottom tanks and the burette. Teflon tape and Araldite epoxy resin are suggested to seal fittings.
- ✓ Sealing the membrane to pedestal and top cap using vacuum grease. In the authors experience membranes can be used without problems up to 4 times for large deformations tests (30% of strain).
- ✓ For high confining stress (greater than 800 kPa), leakage due to osmosis may take place within the cell. To prevent this, Lade (2016) suggests the use of de-aired water as cell fluid and two membranes instead of one.

4. EXPERIMENTAL RESULTS AND DISCUSSION ON BAUXITE

4.1 GENERAL REMARKS

A set of 16 undrained monotonic tests were conducted on fully saturated Aluminum Ore (Bauxite). Moist-tamping method was used for specimen preparation. The initial void ratio varied from 0.727 to 1.329 corresponding to degrees of compaction of 90.0% and 66.7% of the maximum dry density obtained by the modified Proctor test respectively. The void ratio after consolidation ranged from 0.631(95.3% of DC) to 1.322 (66.9% of DC).

The minimum value of the initial void ratio is the actual minimum obtained for moist-tamping in Bauxite, whereas the maximum initial void ratio was established as the maximum void ratio at which it was practical to obtain fully saturation using the Double-vacuuming method. It was possible to obtain bigger densities using moist-tamping method (more than 90% of DC). However, in those cases, the percolation procedure for saturation required many days to be effective. This excessive time induced long-term leakage in the triaxial system from the interface membrane-pedestal because the water dissolves the high-vacuum grease used to paste the membrane to the pedestal. If water is not used as cell fluid, the cell pressure is not suitably distributed. Therefore, for practical reasons it was decided to conduct tests only until 90.0% of initial Degree of Compaction.

On the other hand, the effective confining stress varied from 25 kPa to 1000 kPa. For the 25kPa case, the external source of pressure was used and the initial confining stress in the specimen was fixed in 12 kPa. For the rest of the tests, the high-pressure compressor was used, initiating consolidation at an effective stress of 30 kPa. Figure 4.1 shows schematically all the tests carried out in the plane e vs p'.

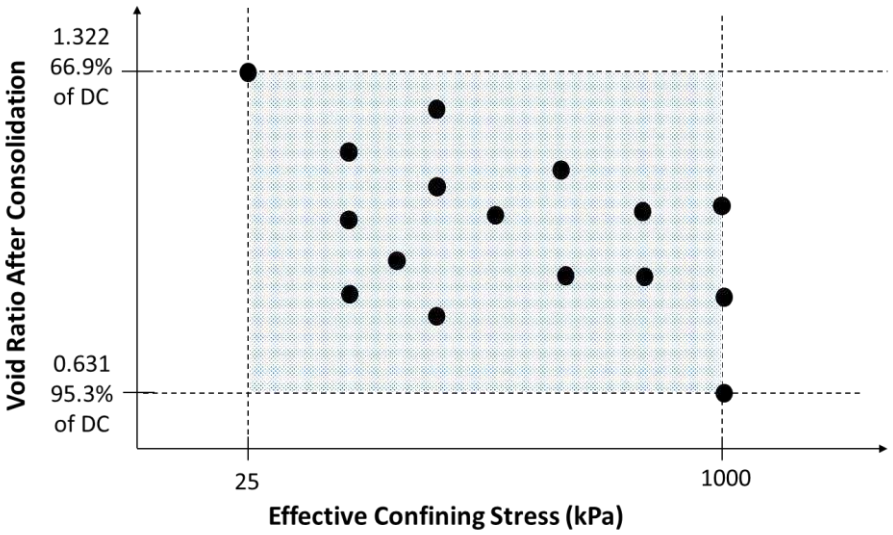

Figure 4.1 Ranges of Void Ratio and Effective Confining Stress of Testing

The summary of all the tests performed considering the effective confining stress and the initial and final density and void ratio is shown in table 4.1.

Table 4.1 Summary of Tests Conducted on Bauxite

Test N°	Initial Degree of Compaction (Dc_i) (%)	Initial Void Ratio (e_i)	Effective Confining Stress (kPa)	Final Degree of Compaction (Dc_f) (%)	Final Void Ratio (e_f)
1	66.7	1.329	25	66.9	1.322
2	90.0	0.727	100	91.2	0.704
3	80.0	0.942	100	80.9	0.920
4	70.0	1.220	100	72.5	1.143
5	80.5	0.931	150	84.7	0.835
6	70.0	1.220	200	77.0	1.019
7	80.0	0.942	200	85.0	0.829
8	83.3	0.865	200	88.0	0.765
9	70.0	1.220	400	79.7	0.950
10	70.0	1.220	600	80.4	0.934
11	80.0	0.942	600	89.8	0.731
12	70.0	1.220	800	82.6	0.882
13	80.0	0.942	800	92.7	0.676
14	73.5	1.115	1000	84.8	0.833
15	83.5	0.861	1000	95.3	0.631
16	78.3	0.985	1000	88.9	0.748

4.2 CONSOLIDATION

Consolidation was done under isotropic conditions. For a more understandable presentation of the test results, it was decided to divide them in 4 groups. The grouping criterion was based on the density level presented by each sample before being consolidated. The summary of each group is shown in table 4.2.

Table 4.2 Groups of tests for presentation of consolidation results

Group	Initial Degree of Compaction (Dc_i) (%)	Initial Void Ratio (e_i)	Effective Confining Stress (kPa)
1	66.7	1.329	25
	70.0	1.220	100
	70.0	1.220	200
	70.0	1.220	400
2	70.0	1.220	600
	70.0	1.220	800
	73.5	1.115	1000
	78.3	0.985	1000
3	80.0	0.942	200
	80.0	0.942	100
	80.0	0.942	600
	80.0	0.942	800
4	80.5	0.931	150
	83.3	0.865	200
	83.5	0.861	1000
	90.0	0.727	100

4.2.1 Effective Confining Stress vs Axial Strain

Figures 4.2-4.5 show the behavior of axial strain with respect to the effective confining stress and figure 4.6 compiles all the results.

Soils with greater density have greater stiffness and therefore the rate of axial and volumetric strain should be smaller in dense soils. This fact is clearly observed in Figure 4.3 (group 2). After 200 kPa, the soil with 78.3% of degree of compaction (DC) undergoes less axial strain than a soil with 73.5% of DC and this one, in turn, undergoes lower axial strain than 2 soils with 70.0% of DC. However, there are some anomalies. For example,

in figure 4.6 a soil with 80% of DC (subjected at 800kPa of confining stress) deforms axially more than a soil with 78.3% of DC (subjected at 1000 kPa of confining stress).

Theoretically, if 2 soils have the same initial density level and are subjected to a consolidation process at the same rate of loading, they should have similar behavior. However, this only occurs in soils with 70% of DC subjected to 800kPa and 600 kPa (figure 4.3). Other specimens at the same density level show different axial strain. These inconsistencies might be explained due to a lack of uniformity in the void ratio of the sample since at the time of tamping the amount of energy applied to each layer is always different. This is supported by Thomson and Wong (2008) who applied X-ray to samples during consolidation and monotonic loading finding that void ratio of each layer of a specimen prepared by moist-tamping varies within 0.65 to 0.75 suggesting increasing the number of layers to improve uniformity.

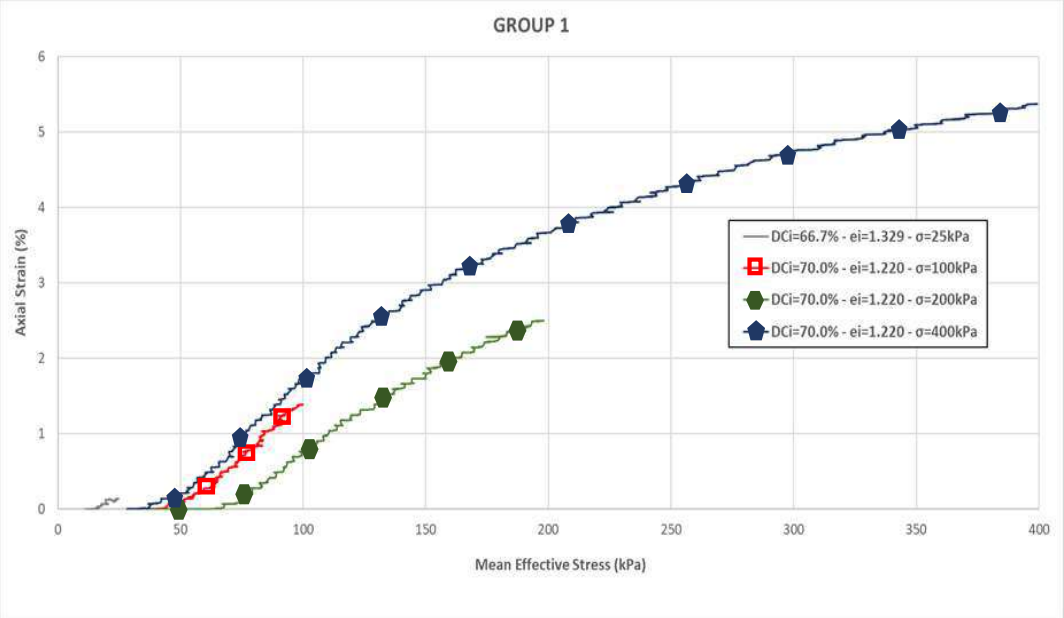

Figure 4.2 Mean Effective Stress (kPa) vs Axial Strain (%) of Group 1

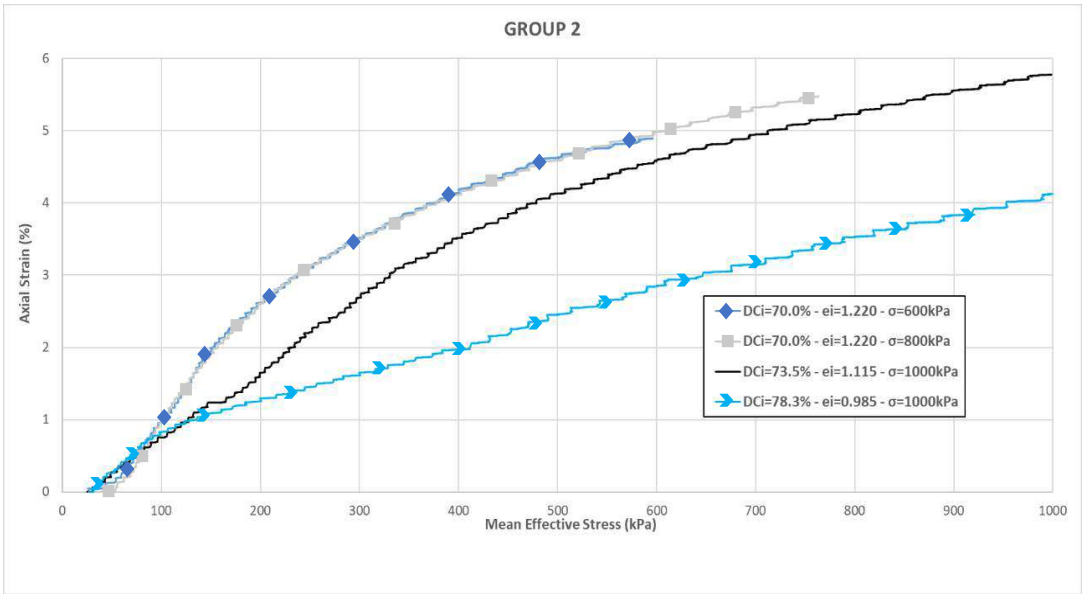

Figure 4.3 Mean Effective Stress (kPa) vs Axial Strain (%) of Group 2

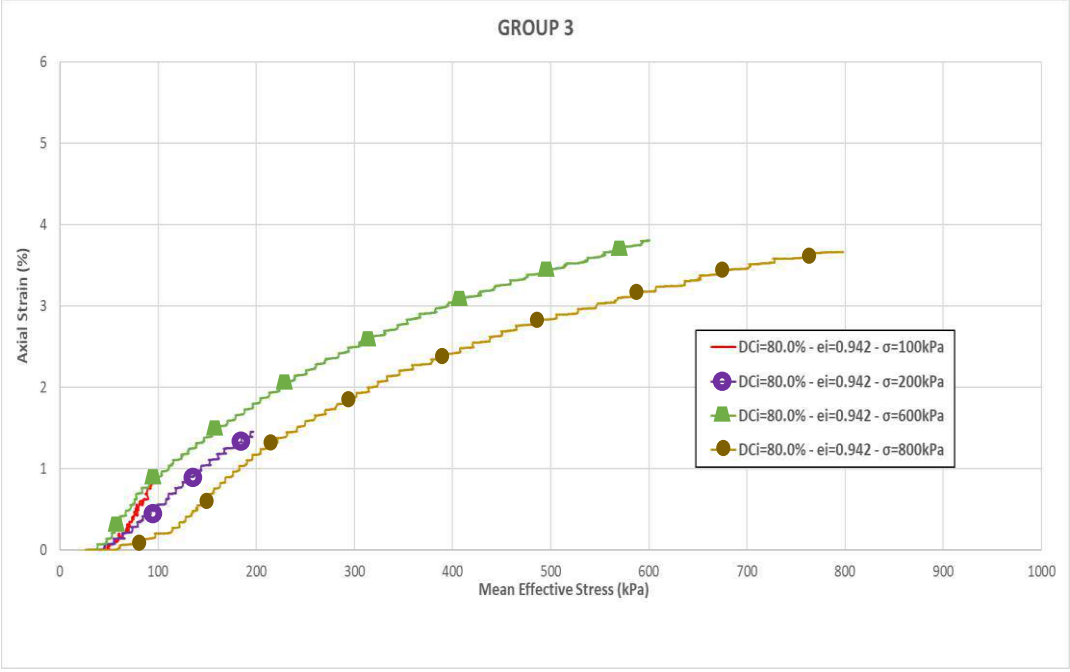

Figure 4.4 Mean Effective Stress (kPa) vs Axial Strain (%) of Group 3

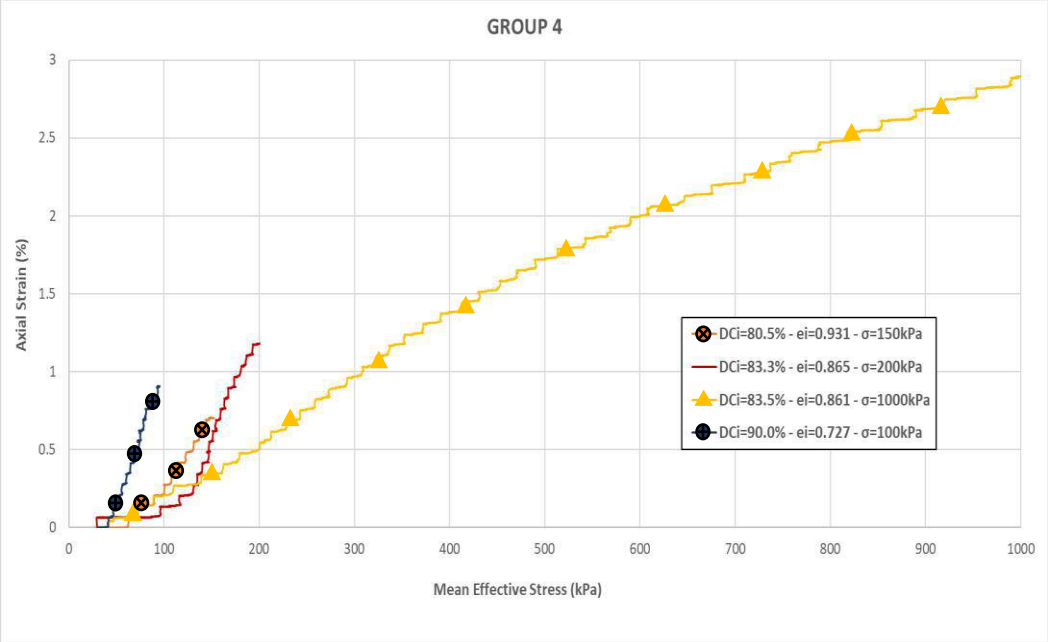

Figure 4.5 Mean Effective Stress (kPa) vs Axial Strain (%) of Group 4

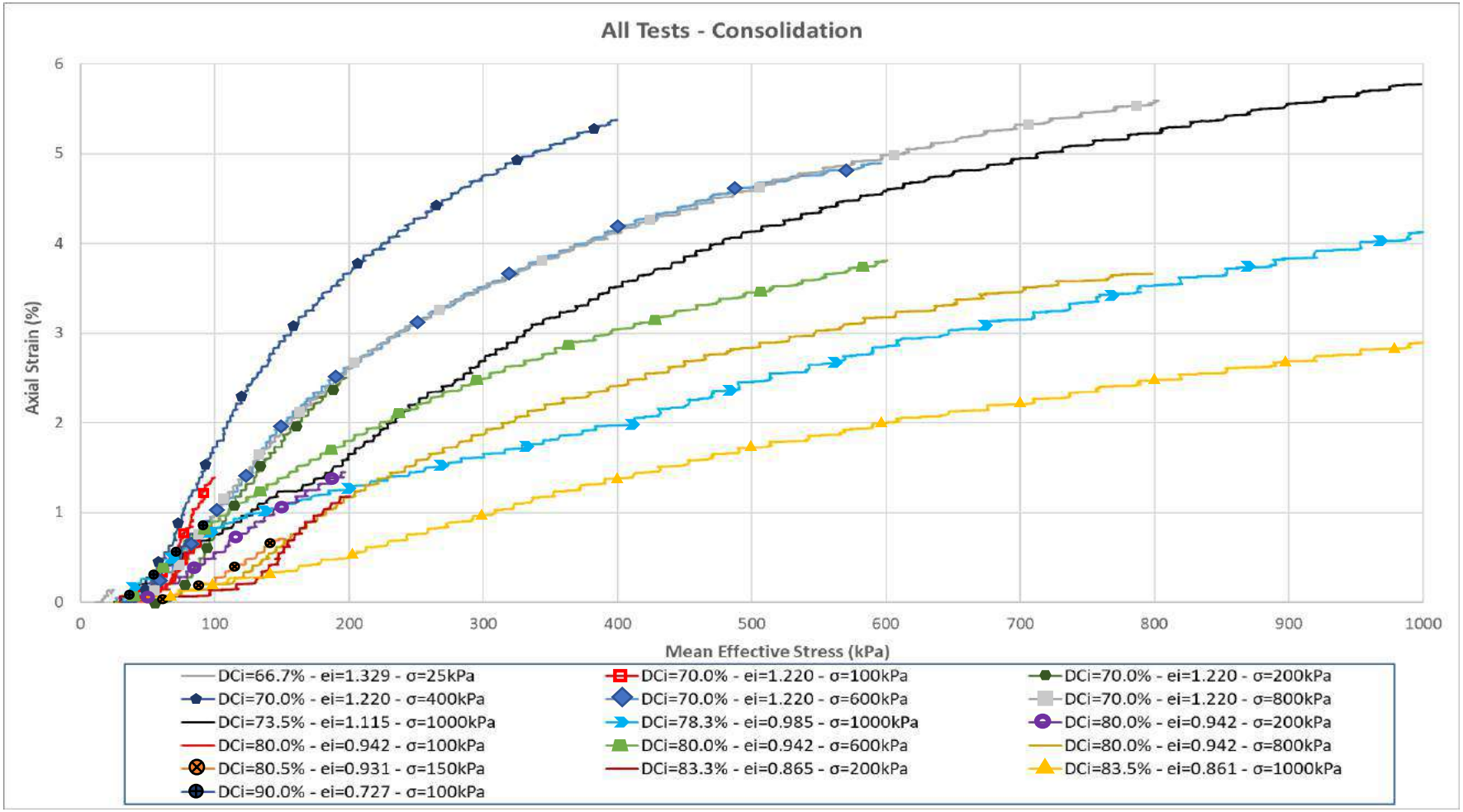

Figure 4.6 Mean Effective Stress (kPa) vs Axial Strain (%) of all tests

4.2.2 Axial Strain vs Volumetric Strain

The data corresponding to the axial and volumetric strain during consolidation are plotted. Figure 4.7 zooms in to observe the behavior of the looser sample. Figure 4.11 shows the results of all the tests performed.

Similarly to the previous topic, some anomalies are observed. For example, in figure 4.8 it is observed that a soil with 78.3% of DC has greater volumetric strain than one with 70.0% of DC.

From all the results, it is possible to conclude that Bauxite is highly compressible since its volumetric strain can vary up to 15% in volume for an effective confining stress of 800 kPa.

In 5 tests, volumetric strain without axial strain can be observed at the beginning, which can be evidence of leakage. Although leakage effects are usually shown in chaotic behavior of volume change.

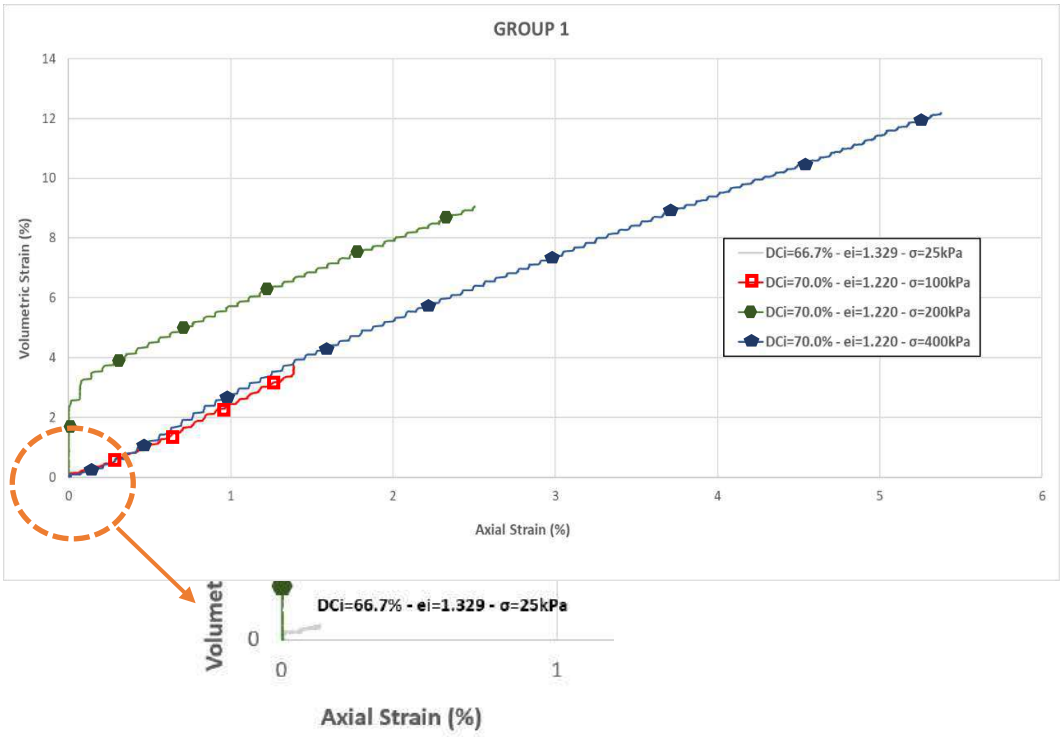

Figure 4.7 Axial Strain (%) vs Volumetric Strain (%) of Group 1

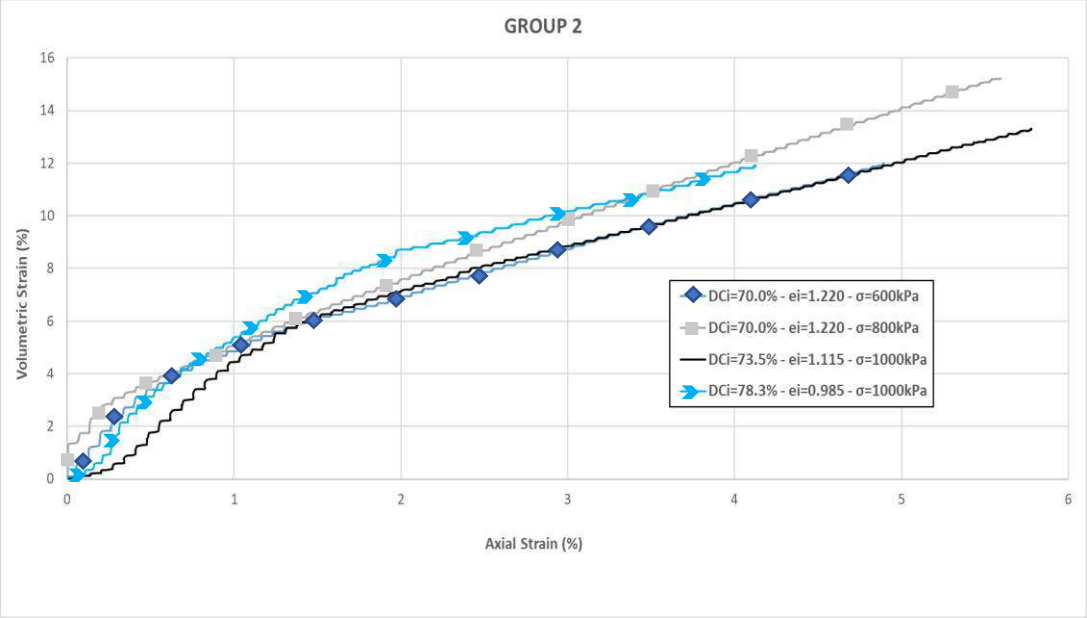

Figure 4.8 Axial Strain (%) vs Volumetric Strain (%) of Group 2

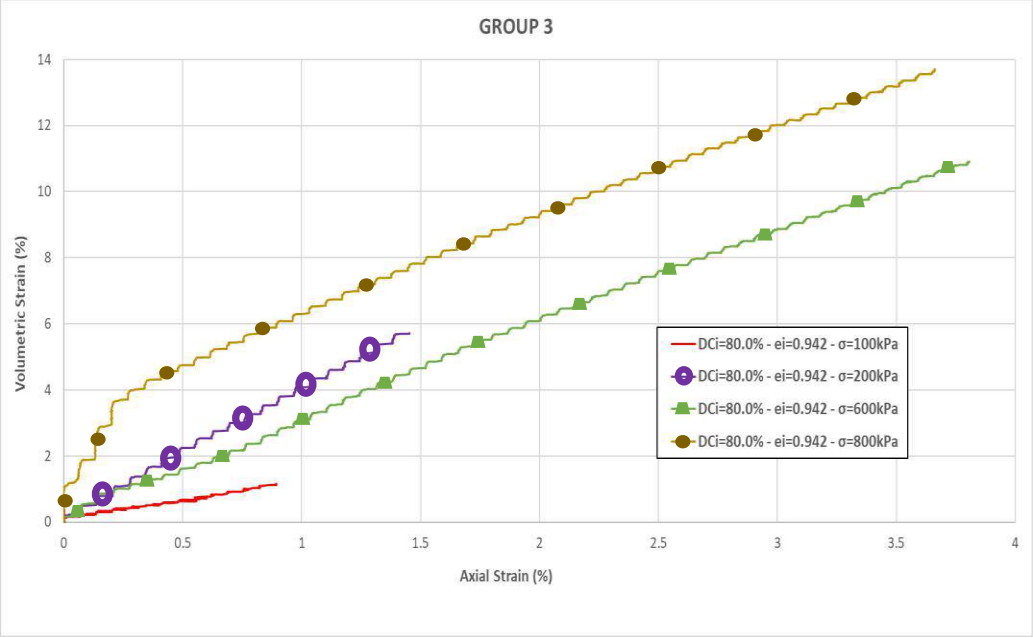

Figure 4.9 Axial Strain (%) vs Volumetric Strain (%) of Group 3

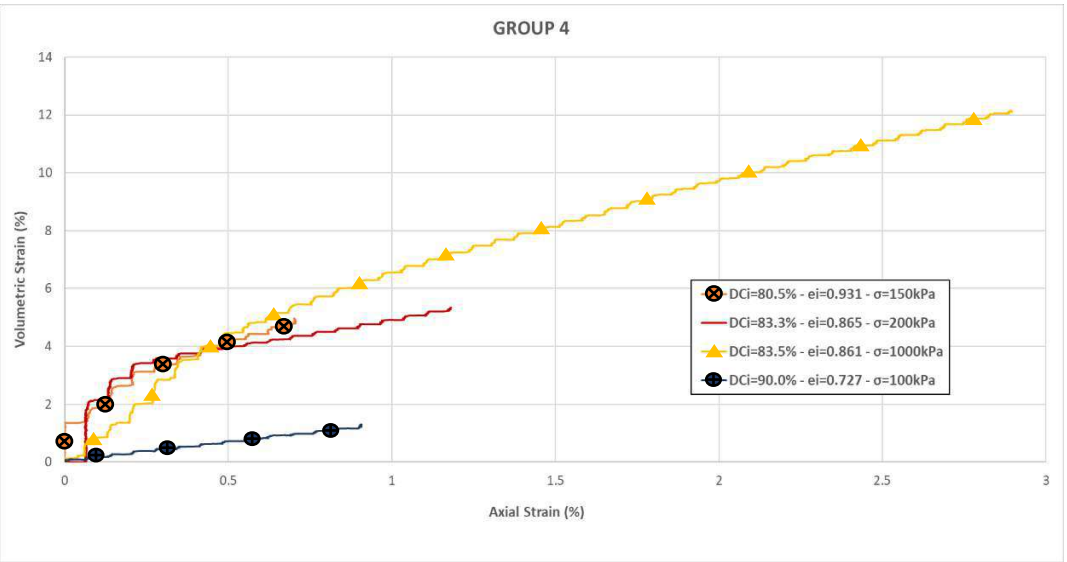

Figure 4.10 Axial Strain (%) vs Volumetric Strain (%) of Group 4

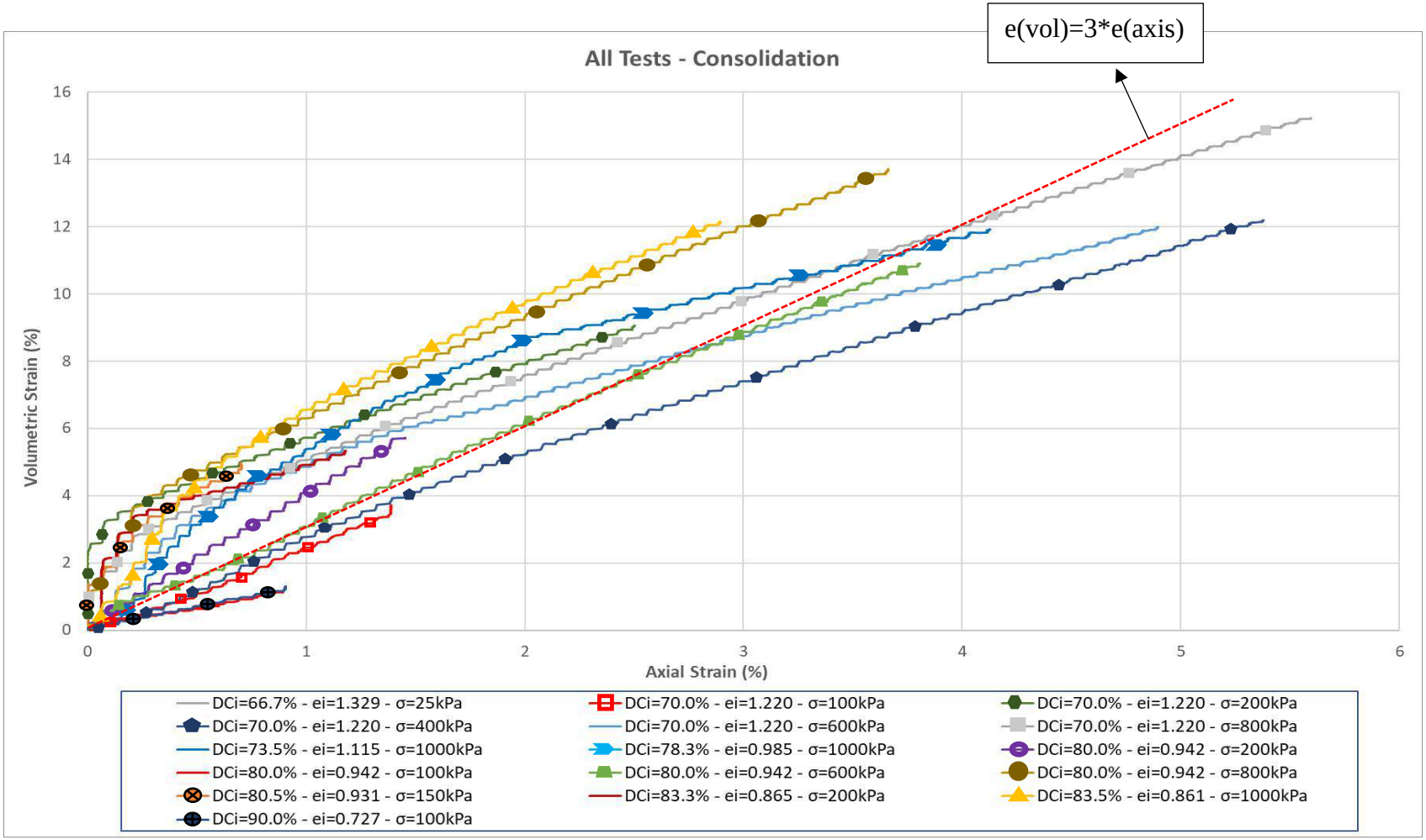

Figure 4.11 Axial Strain (%) vs Volumetric Strain (%) of all tests

4.2.3 Effective Confining Stress vs Volumetric Strain

The relationships between the effective confining stress and the volumetric strain are shown. Figure 4.13 shows the influence of density on the level of volumetric strain. The soil with the highest density (78.3% of DC) undergoes less volumetric strain than soils at 73.5% of DC and 70.0% of DC.

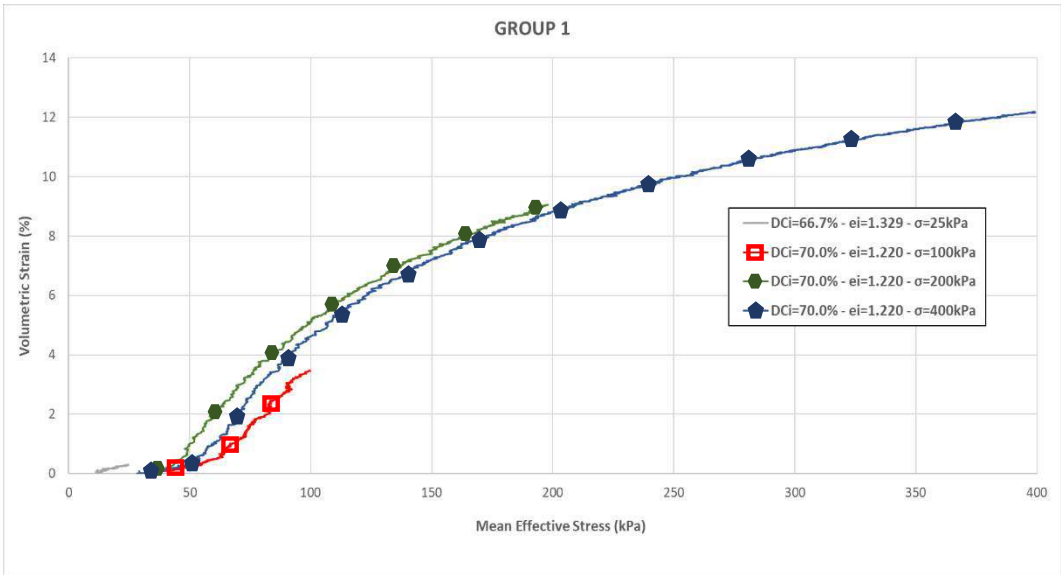

Figure 4.12 Mean Effective Stress (kPa) vs Volumetric Strain (%) of Group 1

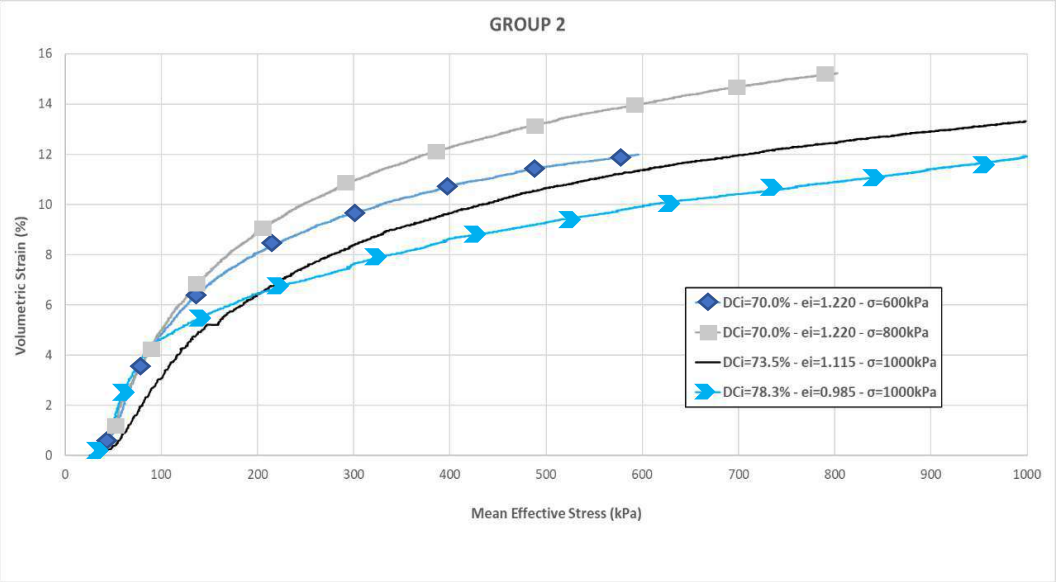

Figure 4.13 Mean Effective Stress (kPa) vs Volumetric Strain (%) of Group 2

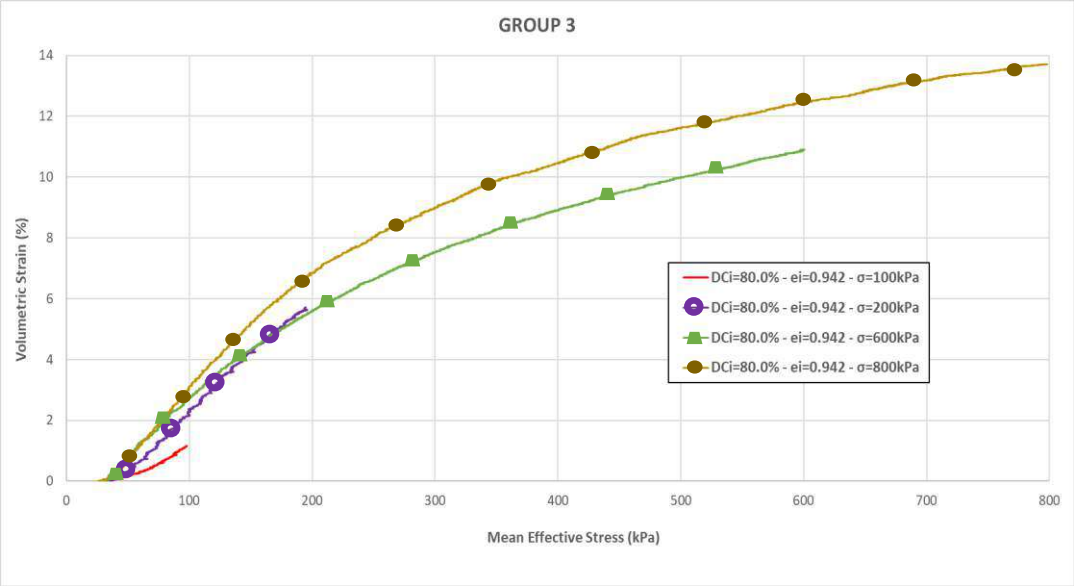

Figure 4.14 Mean Effective Stress (kPa) vs Volumetric Strain (%) of Group 3

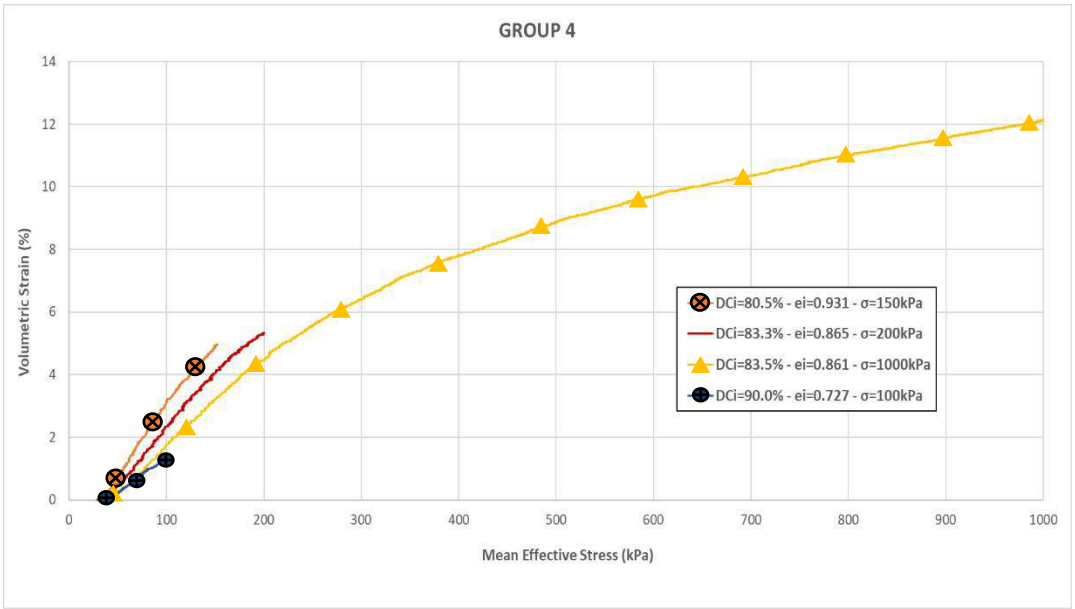

Figure 4.15 Mean Effective Stress (kPa) vs Volumetric Strain (%) of Group 4

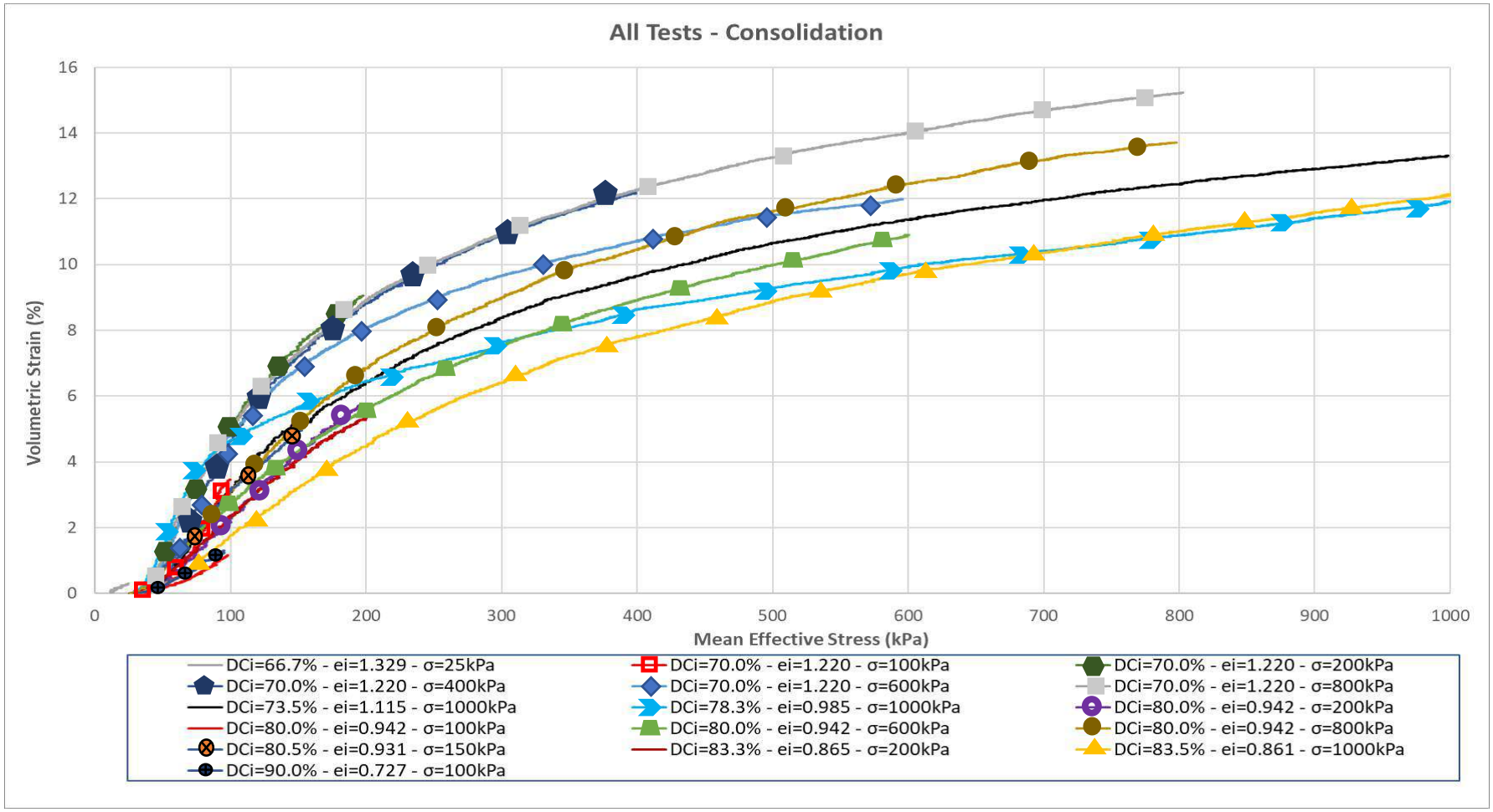

Figure 4.16 Mean Effective Stress (kPa) vs Volumetric Strain (%) of all tests

4.2.4 Isotropic Consolidation Lines

The 16 tests performed were separated in two groups for the presentation of the Isotropic Consolidation Lines (ICL). The first group consists of those tests whose initial density is around 70% of DC, while the second group consists of those with initial density close to 80% of DC. This allows to analyze the uniqueness of the ICL for Bauxite.

Table 4.3 Groups of data for the study of Isotropic Consolidation Lines

Group	Initial Degree of Compaction (Dc_i) (%)	Initial Void Ratio (e_i)	Effective Confining Stress (kPa)
Group A	66.7	1.329	25
	70.0	1.220	100
	70.0	1.220	200
	70.0	1.220	400
	70.0	1.220	600
	70.0	1.220	800
	73.5	1.115	1000
Group B	78.3	0.985	1000
	80.0	0.942	100
	80.0	0.942	200
	80.0	0.942	600
	80.0	0.942	800
	80.5	0.931	150
	83.3	0.865	200
	83.5	0.861	1000
	90.0	0.727	100

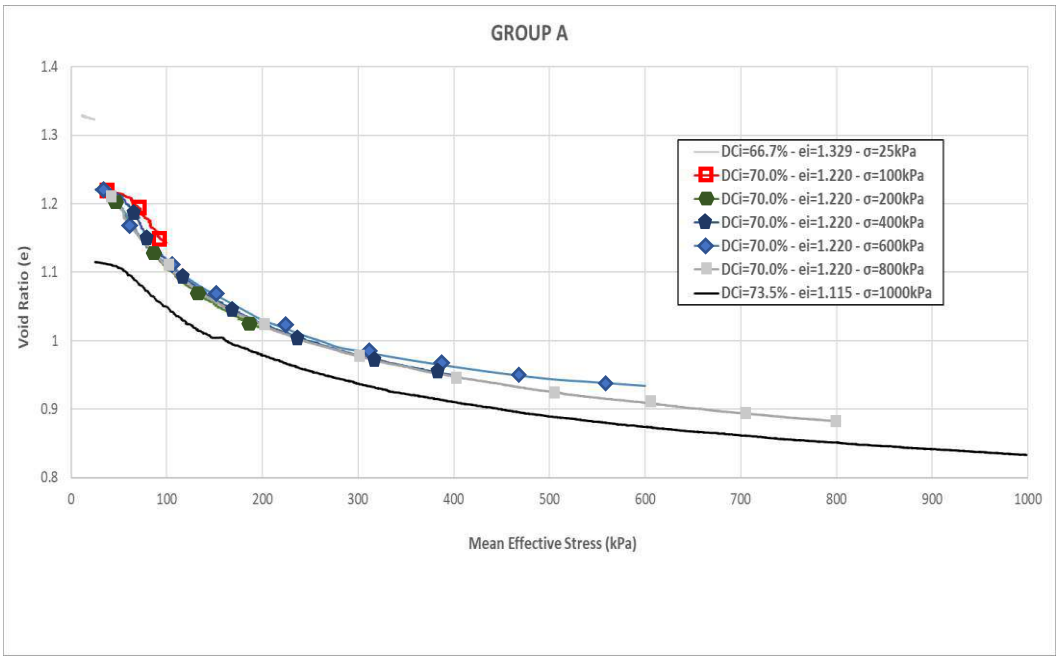

Figure 4.17 Isotropic Consolidation Lines – Group A

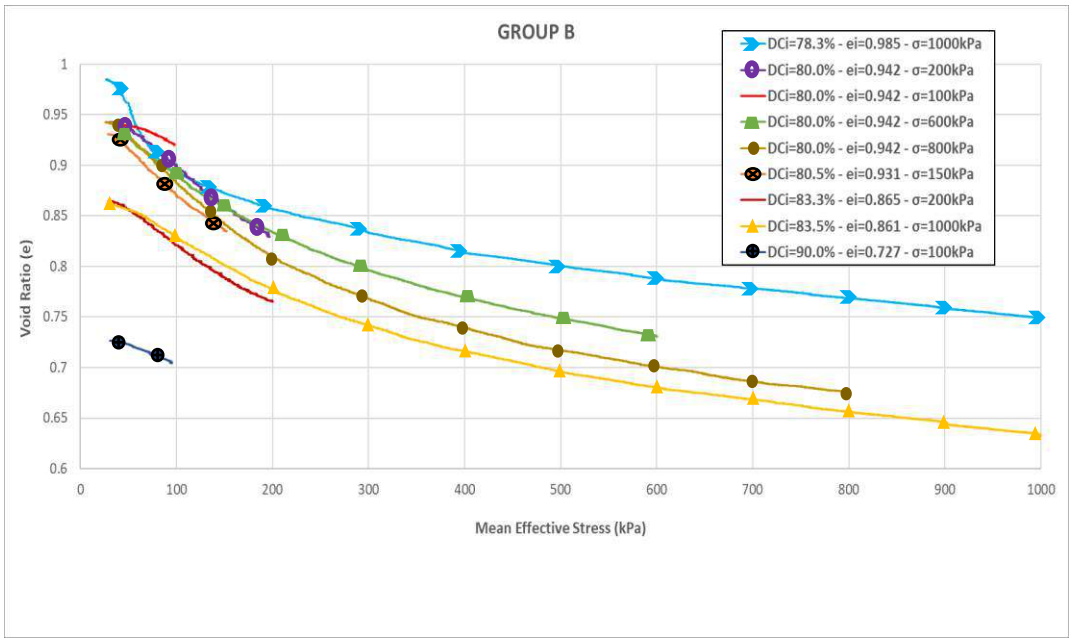

Figure 4.18 Isotropic Consolidation Lines – Group B

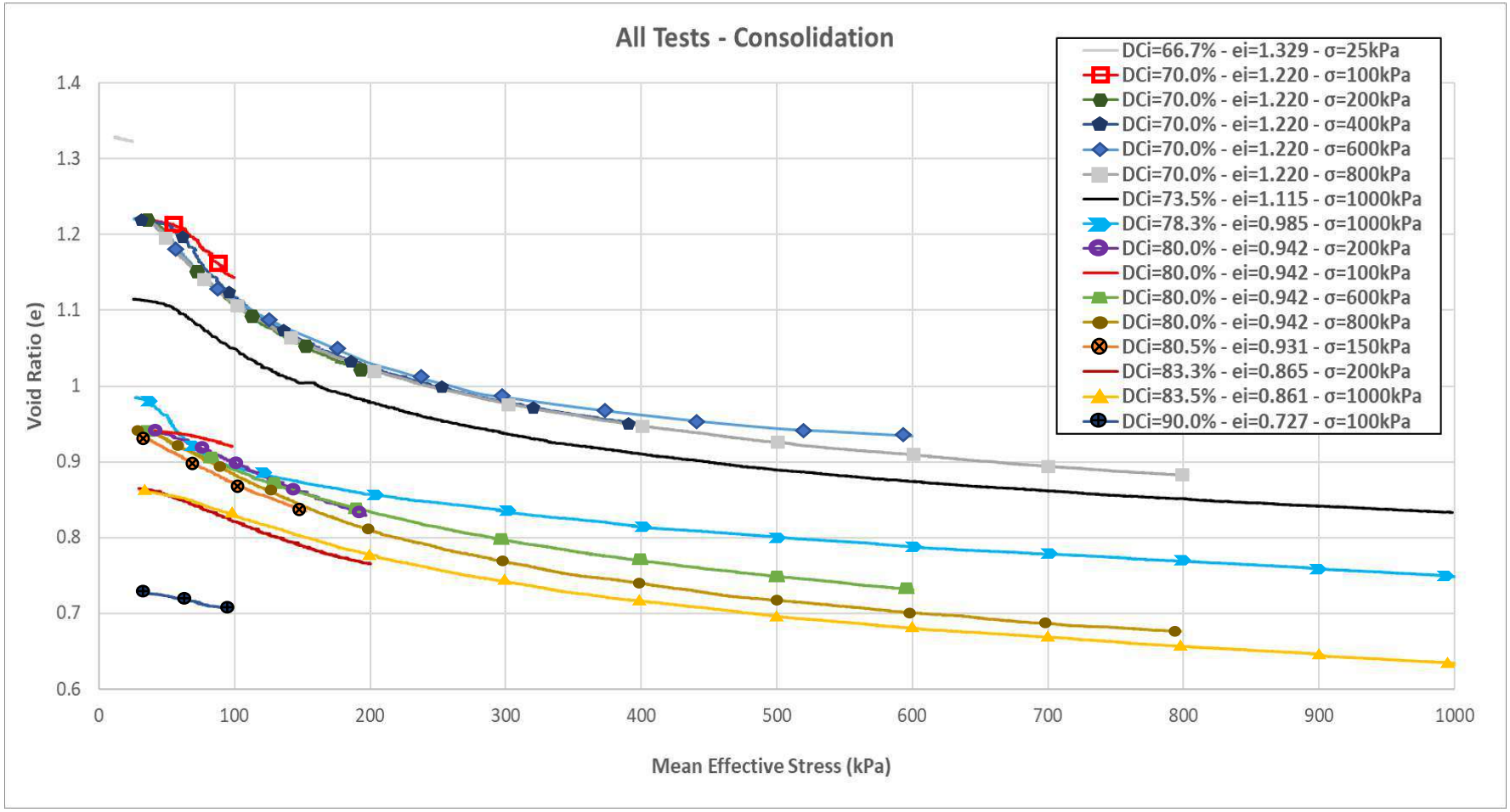

Figure 4.19 Isotropic Consolidation Lines of all tests

As shown in figure 4.17, in loose samples the data obtained fits better in a single ICL being similar for cases with initial density 70% of DC at 200 kPa, 400 kPa and 600 kPa of confining stress. However, as shown in figure 4.18, for denser samples (80% of DC) many different ICL can be seen. Thus, there is not unique ICL for Bauxite. This is supported by Jefferies and Been (2000) who stated that for sandy soils there may be infinite ICL at low confining stresses. Unique ICL may be apparent when stresses are high enough to induce particle crushing (Atkinson and Bransby, 1978).

4.3 UNDRAINED MONOTONIC BEHAVIOR OF BAUXITE

As mentioned in chapter 2.2.1 of literature review, a saturated granular soil shows 3 types of behavior when subjected to monotonic loading under undrained conditions: non-flow type (dilative), flow type (Contractive) or flow with limited deformation (Quasi Steady State). In this thesis, only non-flow type (dilative) and flow with limited deformation (Quasi Steady State) responses were obtained. Even for the loosest possible density state of the moist-tamping preparation method for Bauxite and a very low effective confining stress it was not possible to obtain the flow type behavior. These results are similar to the data provided by Verdugo (1992) in Toyoura sand which does not show flow type response even for the loosest state obtained from moist-tamping method. Therefore, the presentation of test results will be divided between those showing Quasi Steady State (QSS) behavior and those showing dilative behavior.

4.3.1 Flow with limited deformation or Quasi Steady State Behavior

Out of the 16 tests performed in Bauxite, 11 results show Quasi Steady State behavior. For data presentation, 2 groups of 4 test results and one of 3 according to their void ratio after consolidation will be shown as summarized in table 4.4:

Table 4.4 Groups for presentation of results of monotonic loading

Group	Type of Behavior	Initial Degree of Compaction (D_{ci}) (%)	Initial Void Ratio (e_i)	Effective Confining Stress (kPa)	Final Degree of Compaction (D_{cf}) (%)	Final Void Ratio (e_f)
Group X	QSS	66.7	1.329	25	66.9	1.322
	QSS	70.0	1.220	100	72.5	1.143
	QSS	70.0	1.220	200	77.0	1.019
	QSS	70.0	1.220	400	79.7	0.950
Group Y	QSS	70.0	1.220	600	80.4	0.934
	QSS	70.0	1.220	800	82.6	0.882
	QSS	73.5	1.115	1000	84.8	0.833
	QSS	78.3	0.985	1000	88.9	0.748
Group Z	QSS	80.0	0.942	600	89.8	0.731
	QSS	80.0	0.942	800	92.7	0.676
	QSS	83.5	0.861	1000	95.3	0.631

4.3.1.1 Test Results of Group X

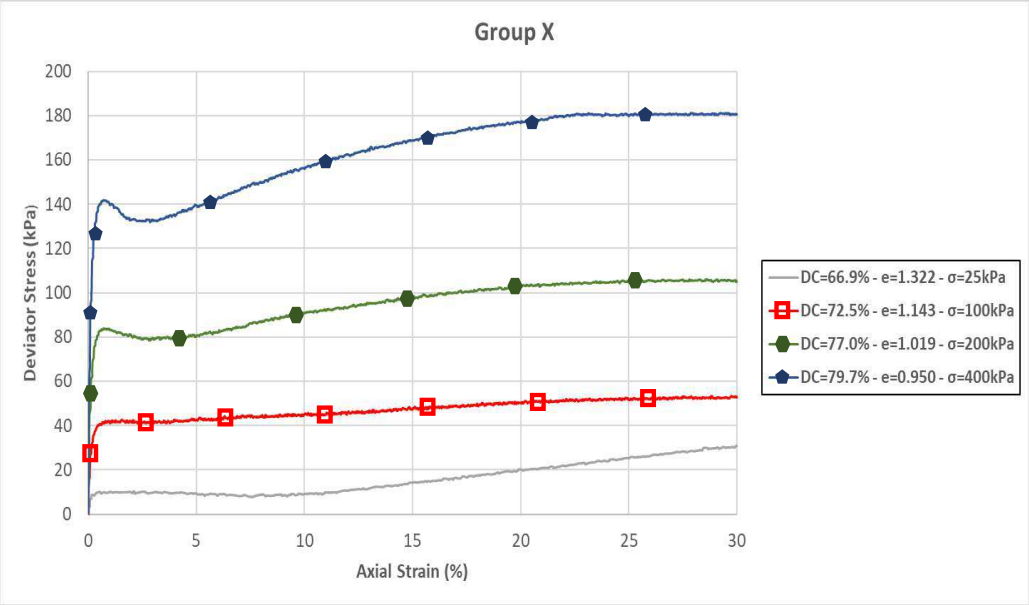

Figure 4.20 Deviator Stress (kPa) vs Axial Strain (%) of Group X

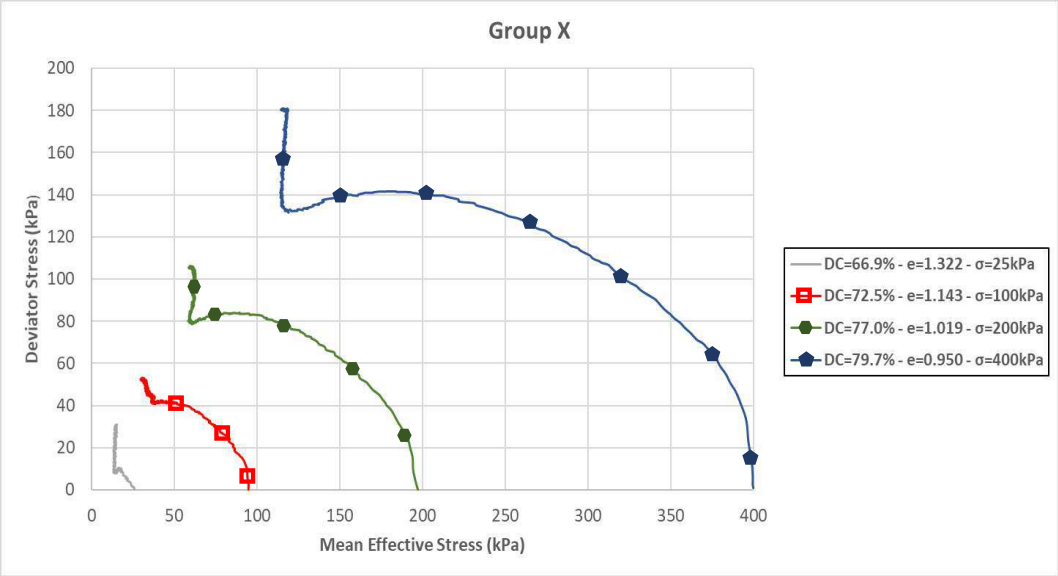

Figure 4.21 Effective Stress Path of Group X

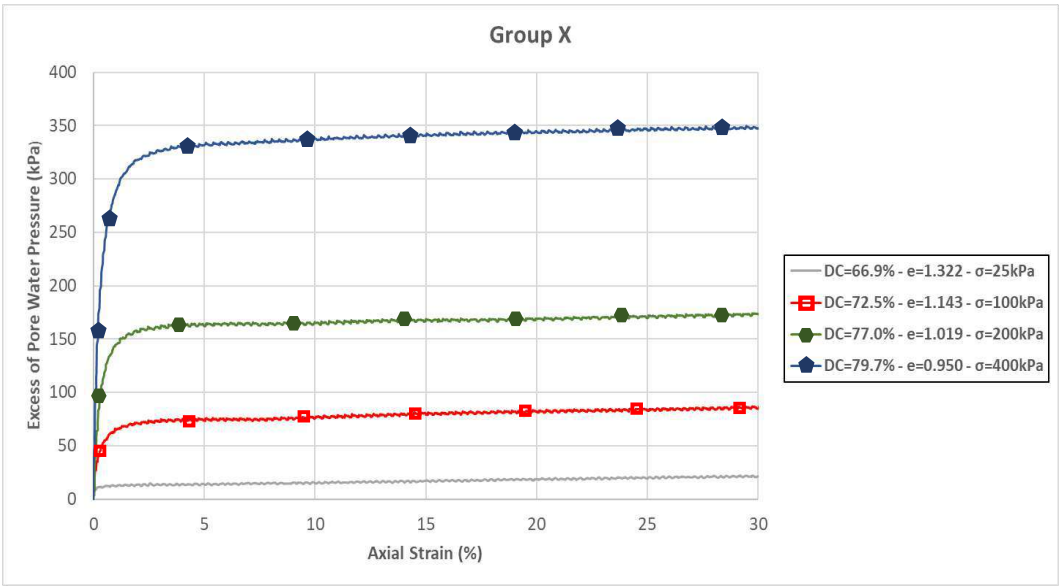

Figure 4.22 Excess Pore Water Pressure of Group X

4.3.1.2 *Test Results of Group Y*

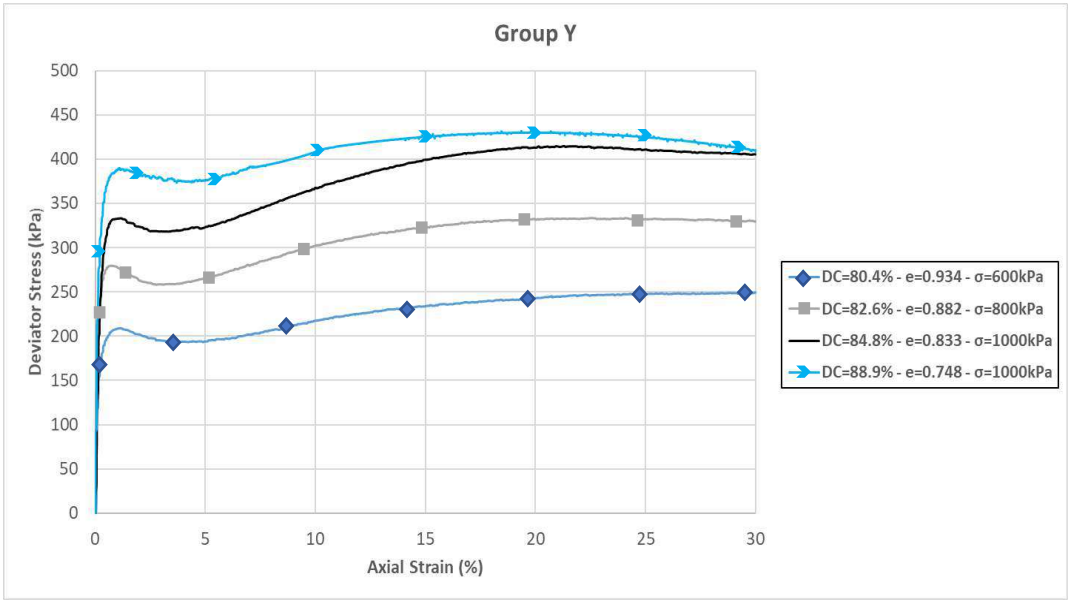

Figure 4.23 Deviator Stress (kPa) vs Axial Strain (%) of Group Y

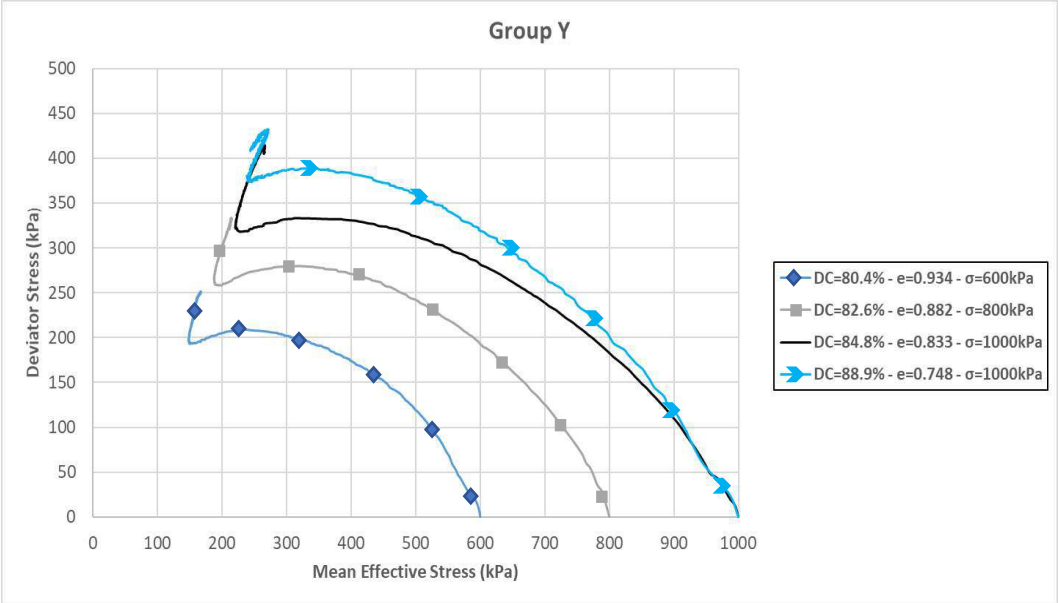

Figure 4.24 Effective Stress Path of Group Y

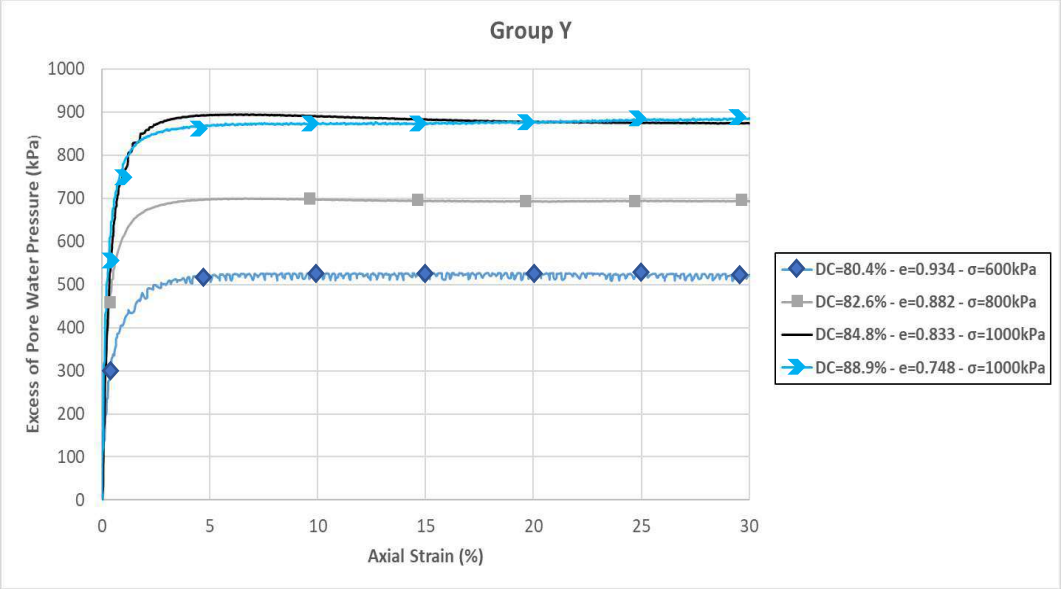

Figure 4.25 Excess Pore Water Pressure of Group Y

4.3.1.3 Test Results of Group Z

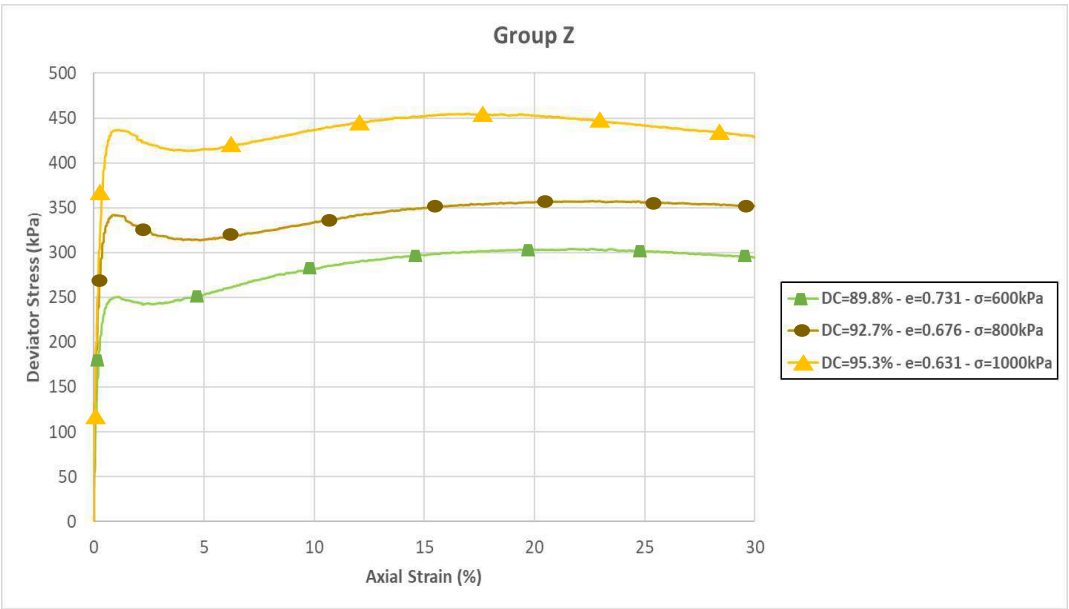

Figure 4.26 Deviator Stress (kPa) vs Axial Strain (%) of Group Z

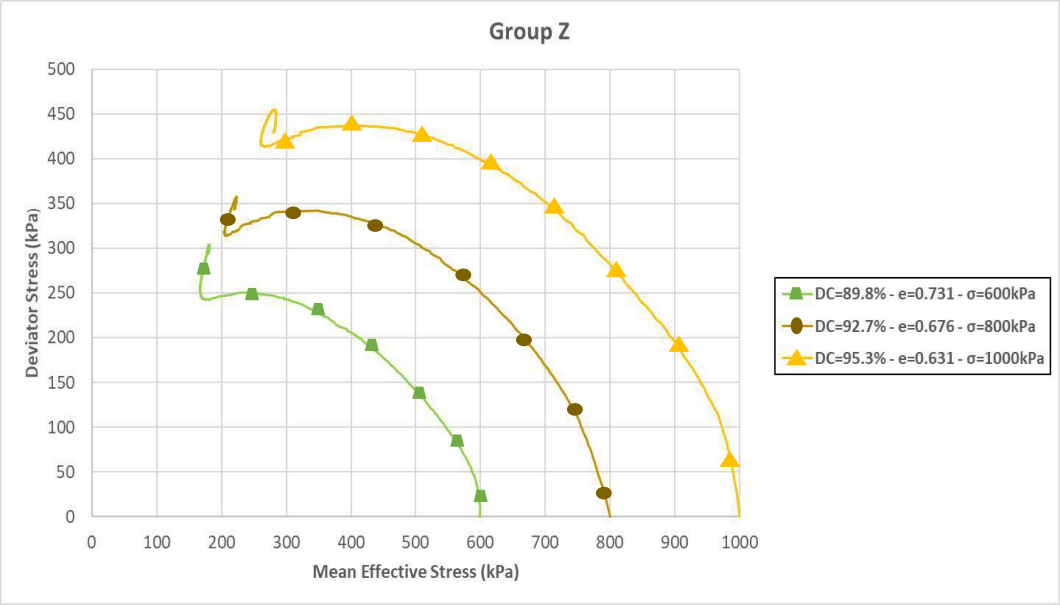

Figure 4.27 Effective Stress Path of Group Z

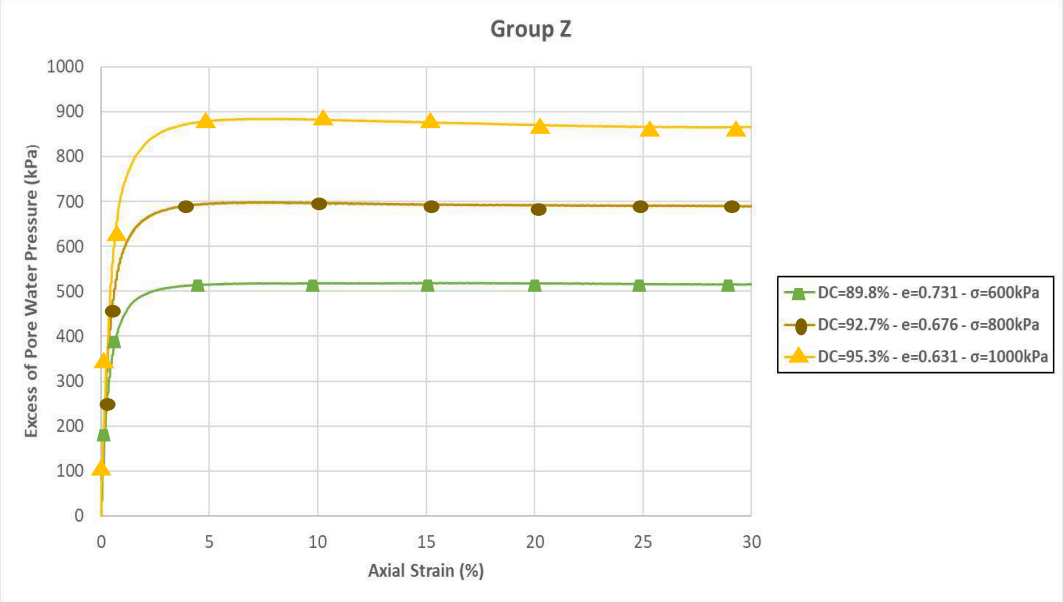

Figure 4.28 Excess Pore Water Pressure of Group Y

4.3.1.4 Results of All tests

Figures 4.29, 4.30 and 4.31 compiles all the tests results. Table 4.5 summarizes the changes in effective confining stress due to the excess pore water pressure at peak and Point of Phase Transformation states.

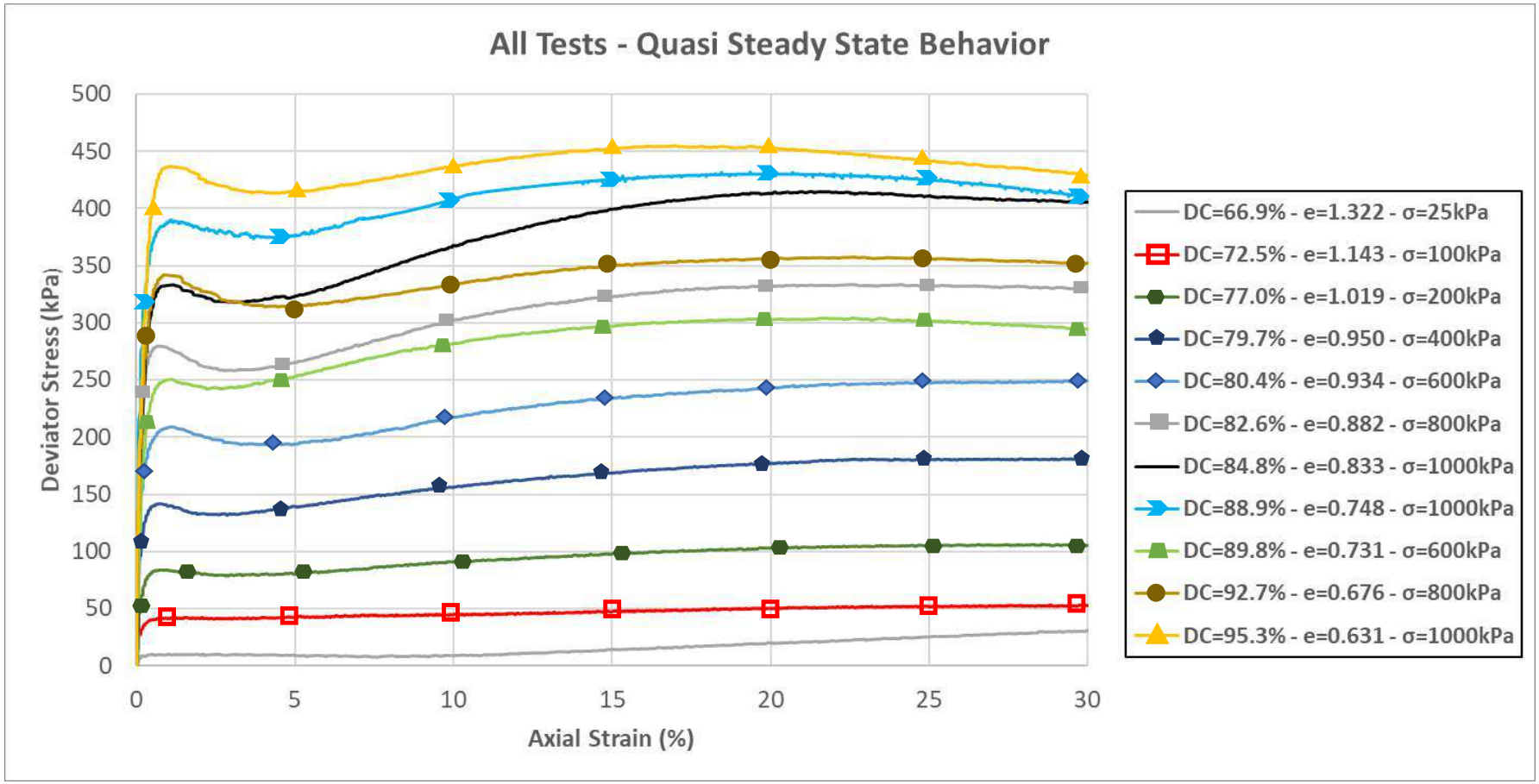

Figure 4.29 Deviator Stress (kPa) vs Axial Strain (%) of all tests showing Quasi Steady State behavior

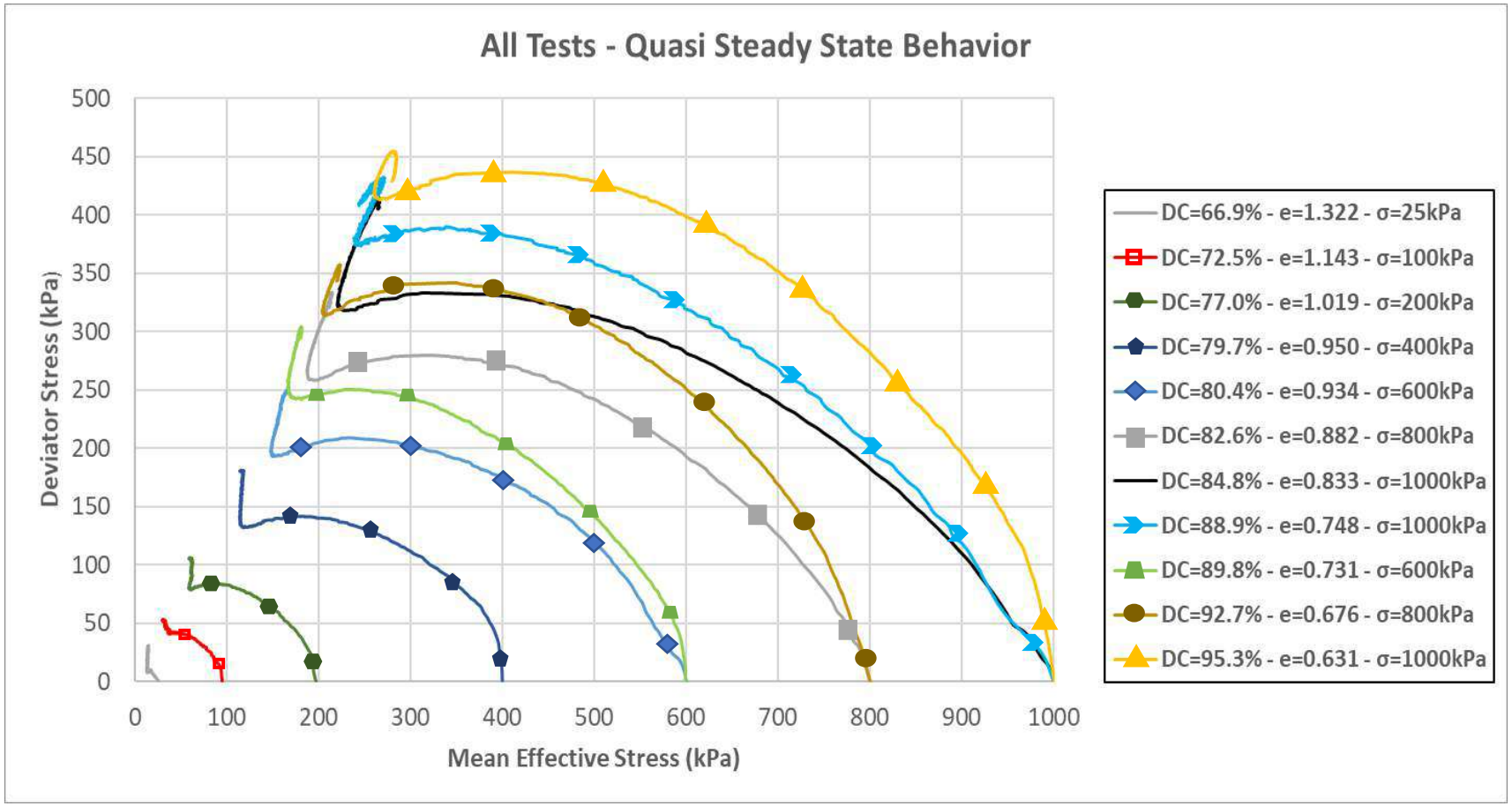

Figure 4.30 Effective Stress Path of all tests showing Quasi Steady State behavior

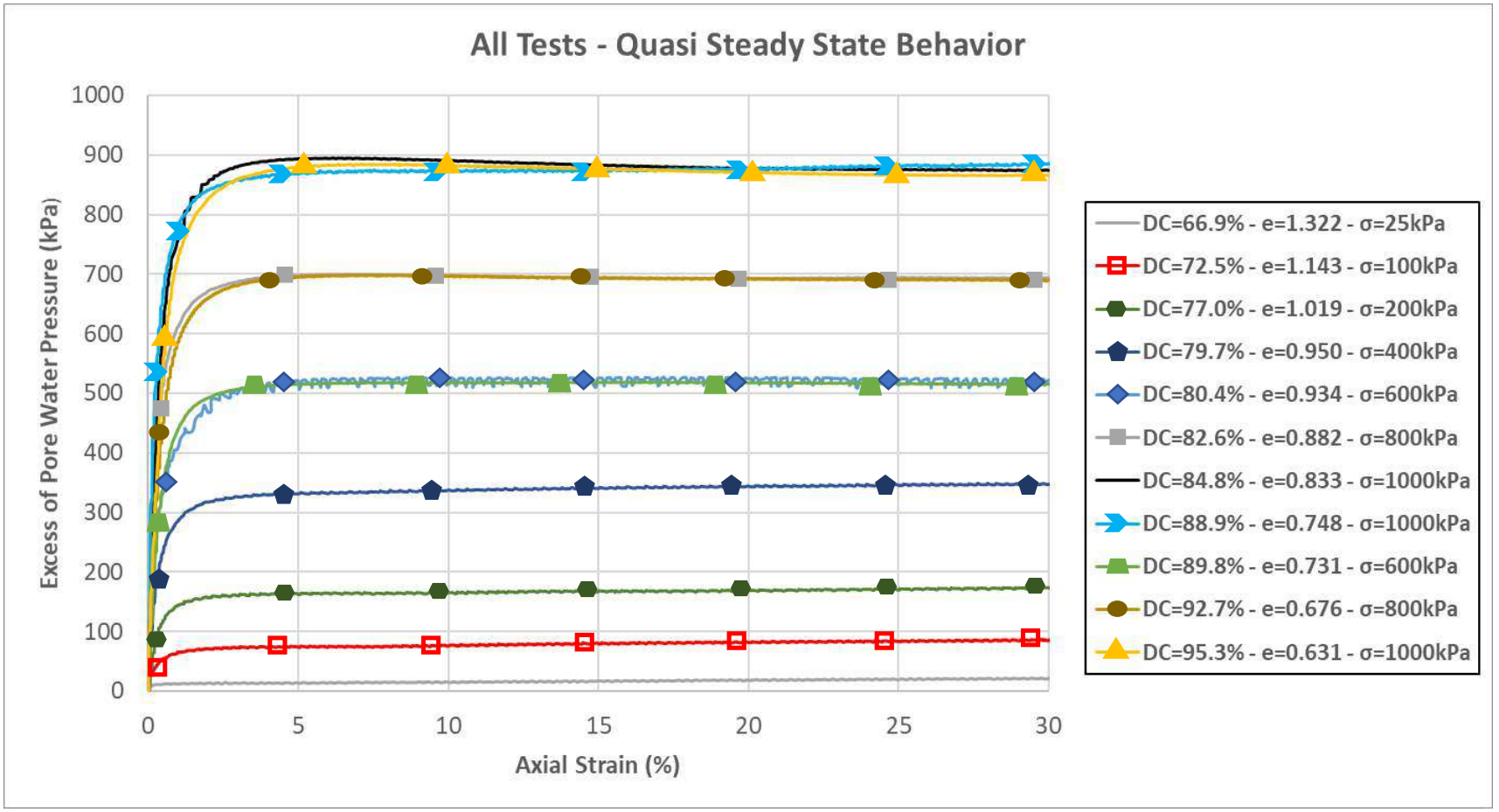

Figure 4.31 Excess Power Water Pressure of all tests showing Quasi Steady State behavior

Table 4.5 Effective confining stress changes due to excess pore water pressure at peak and PPT states

Group	Type of Behavior	Final Degree of Compaction (DC_f) (%)	Final Void Ratio (e_f)	Effective Confining stress (σ'_o) (kPa)	Peak State				Point of Phase Transformation State			
					p'_{peak} (kPa)	p'_{peak}/σ'_o (%)	Excess PWP_{peak}	Excess PWP_{peak}/σ'_o (%)	p'_{ppt} (kPa)	p'_{PPT}/σ'_o (%)	Excess PWP_{PPT}	Excess PWP_{ppt}/σ'_o (%)
1	QSS	66.9	1.322	25	16.3	65.0	11.9	47.6	13.9	55.6	15.4	61.6
	QSS	72.5	1.143	100	42.6	42.6	67.9	67.9	38.6	38.6	71.2	71.2
	QSS	77.0	1.019	200	89.6	44.8	134.1	67.0	60.8	30.4	161.7	80.8
	QSS	79.7	0.950	400	184.2	46.1	262.8	65.7	118.6	29.6	324.8	81.2
2	QSS	80.4	0.934	600	235.9	39.3	440.9	73.5	149.5	24.9	521.3	86.9
	QSS	82.6	0.882	800	316.8	39.6	574.0	71.8	194.3	24.3	688.8	86.1
	QSS	84.8	0.833	1000	311.9	**31.2**	804.7	**80.5**	227.3	22.7	884.8	88.5
	QSS	88.9	0.748	1000	339.0	33.9	792.4	79.2	245.9	24.6	863.0	86.3
3	QSS	89.8	0.731	600	230.0	38.3	452.5	75.4	182.1	30.4	496.9	82.8
	QSS	92.7	0.676	800	349.3	43.7	563.6	70.4	205.9	25.7	694.5	86.8
	QSS	95.3	0.631	1000	412.8	41.3	736.8	73.7	266.9	26.7	875.4	87.5

4.3.1.5 Discussion of Undrained Monotonic Test Results

The above figures show that the deviator stress increases with the confining stress. Post-peak strain-softening is also more pronounced at a higher level of confining stress. The peak deviator stress in soils at the same confining stress increases as a function of density. For example, for 1000 kPa, the soil at 95.3% of DC presents 436.8 kPa, at 88.9% of DC 390.0 kPa and at 84.8% of DC 333.2 kPa.

The confining stress also increases the peak deviator stress in soils with similar density. For the soil with 89.8% of DC at 600 kPa, the peak deviator stress was 250.5 kPa, while for the sample with 88.9% of DC at 1000 kPa, the deviator stress was 390.0 kPa showing an increment of 1.5 times approximately.

The peak deviator stress appears on average at 1.0% of axial strain being up to a maximum of 436.8 kPa for the case of 95.3% of DC at 1000 kPa of confining stress. After the peak state, the soil's shear strength dwindles (visualized in a reduction of the deviator stress) until reaching a temporary minimum or Quasi Steady State in levels of axial strain within 2.2% to 7.6%. The smallest deviator stress corresponds to the loosest state and lowest confining stress (66.9% of DC and 25kPa of effective confining stress) being 7.7kPa.

Subsequently, all the soils undergo strain-hardening surpassing the value of peak deviator stress at approximately 20% of axial strain, after which -in soils subjected to confining stress greater than 600 kPa- a small second strain-softening occurs evidencing the onset of particle crushing

The effective stress path allows to conclude that all soils showing Quasi Steady State behavior are totally contractive, moving since the beginning of shearing to the left unlike similar materials such as Iron Ore Fines (Wang et al, 2018) that even at contractive states tend to move slightly to the right at the beginning, manifesting a small positive dilatancy.

Table 4.5 shows the effects of pore water pressure increments on the effective confining stress at peak and Point of Phase Transformation states. On average, the excess pore water pressure reaches 73% of the initial confining stress with a maximum of 80.5% for the case of 84.8% of DC at 1000 kPa. However, none of these cases fulfills the criteria to define initial liquefaction which requires the water pressure excess to build up to a value of 100% (Seed and Idriss, 1971). Thus, for all these cases the mechanism occurring at the

peak state due to pore water pressure increments can be interpreted as collapse of granular soils (Sladen et al, 1985).

Figure 4.31 shows that the excess pore water pressure has very similar behavior for cases at 600 kPa, 800 kPa and 1000 kPa irrespective of the different density of each sample.

4.3.1.6 Pictures after Shearing

The following 2 figures show the specimens with 77.0% of DC at 200kPa and 84.8% of DC at 1000 kPa after being subjected to monotonic loading until 30% of axial strain.

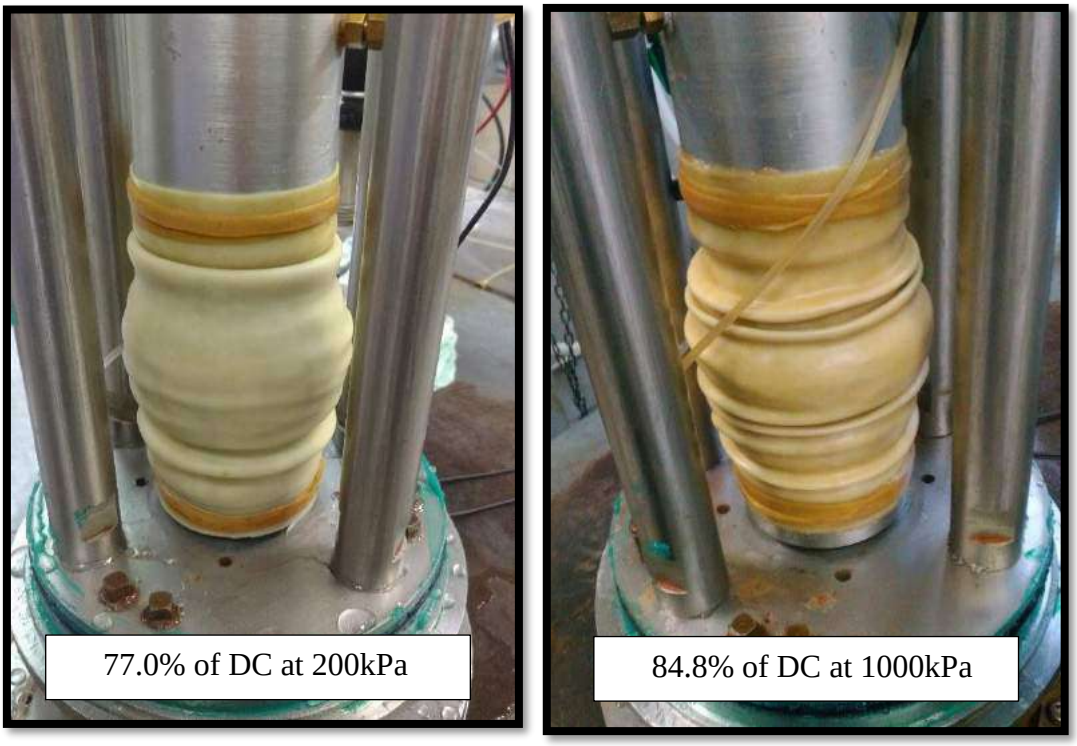

Figure 4.32 and Figure 4.33 Deformation images of specimens after monotonic loading

Figures 4.32 and 4.33 show that deformations, at least globally, were uniform since a good level of axisymmetry is observed in the specimens after shearing. This is probably due to the boundary condition of the pedestal and top cap where lubricated ends were placed.

Lade (2016) stated that in triaxial testing, soils show 3 forms of instability: Smooth Peak Failure, Localization of Plastic Strain (Shear Banding) and Instability inside the collapse surface which lead to liquefaction-type behavior occurring only in undrained condition. The first type of mechanism usually appears in drained tests of dense soils. Shear Bands were not noticed in all the tests conducted in this thesis even for the densest specimens.

Then, it is confirmed that the predominant mechanism occurring is the instability within the collapse surface.

4.3.2 Dilative or Non-flow Behavior

Dilative-type behavior was seen in 5 tests.

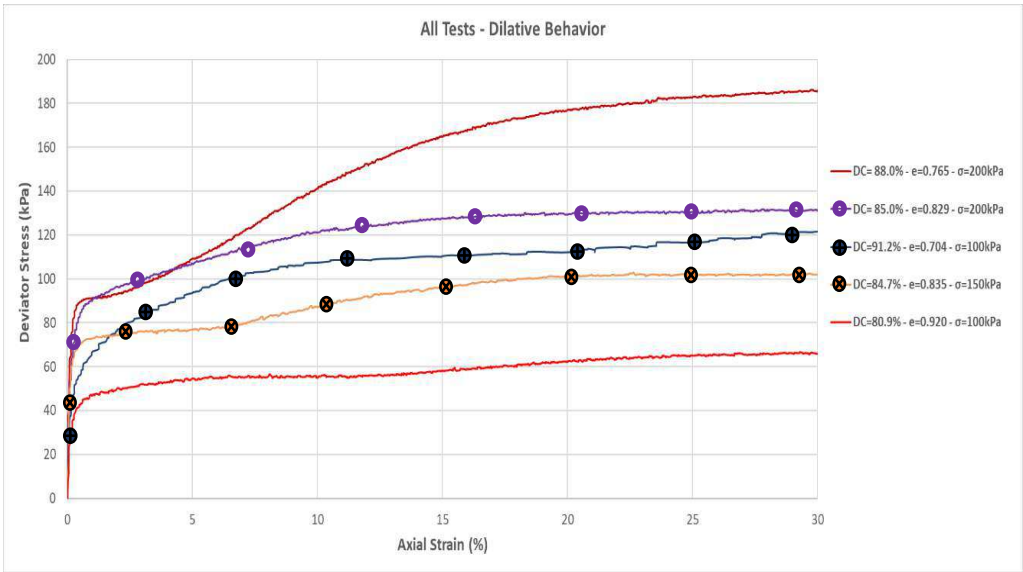

Figure 4.34 Stress (kPa) vs Axial Strain (%) of tests showing dilative behavior

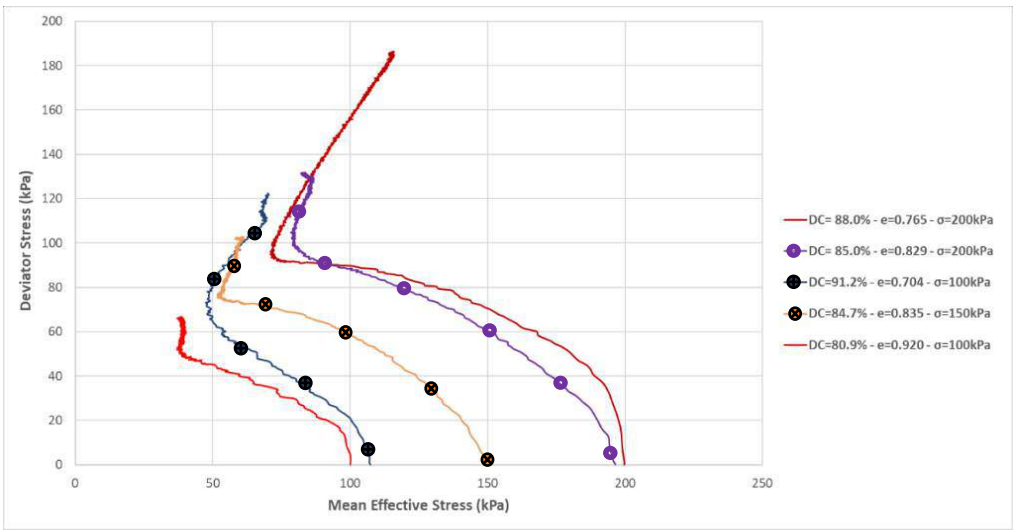

Figure 4.35 Effective Stress Path of Tests showing Dilative Behavior

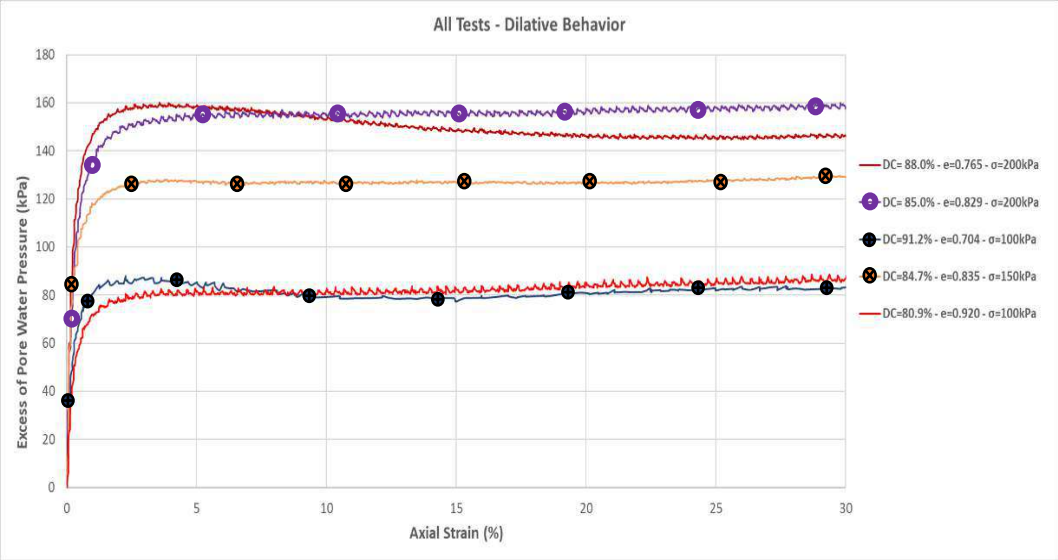

Figure 4.36 Excess Power Water Pressure of all tests showing Dilative behavior

As shown in Figure 4.34, neither peak deviator stress nor strain-softening occurs but purely strain-hardening which is more pronounced as density increases. The dilatant characteristics of the soils with densities of 88.0% of DC and 85% of DC at 200 kPa make their deviator stresses at residual stage (185.5 kPa and 131.2 kPa respectively) much higher than the deviator stress (52.9 kPa) of the test with 77.0% of DC at the same confining stress, but with contractive response.

The effective stress path in figure 4.35 shows that although the soils are dilatant, there is a considerable contractive behavior which induces a reduction in the effective confining stress until the Point of Phase Transformation. This is shown in table 4.6 where it is observed that the excess pore water pressure increases up to an average of 81% of the effective confining stress, being even higher than for the contractive soils at the peak state where collapse starts. At this point the effective confining stress is reduced to an average of 40% of its initial value, so despite not undergoing collapse (peak deviator stress and strain-softening) the stiffness of the soil is reduced, which in the case of real structures will generate lateral deformations. These confirms that the so-called cyclic mobility can be seen also in monotonic tests as suggested by Castro and Poulos (1977).

Table 4.6 Effective confining stress changes due to excess pore water pressure at PPT state for Dilative Samples

Type of Behavior	Final Degree of Compaction (DC_f) (%)	Final Void Ratio (e_f)	Effective Confining Stress (σ'_o) (kPa)	Point of Phase Transformation State			
				p'_{ppt} (kPa)	p'_{PPT}/σ'_o (%)	Excess PWP_{PPT}	Excess PWP_{ppt}/σ'_o (%)
Dilative	91.2	0.704	100	47.4	47.4	85.8	85.8
Dilative	88.0	0.765	200	71.0	35.5	158.0	79.0
Dilative	85.0	0.829	200	78.5	39.2	154.6	77.3
Dilative	84.7	0.835	150	51.8	34.5	127.5	85.0
Dilative	80.9	0.920	100	36.9	36.9	80.2	80.2

4.3.2.1 Summary of Tests

Table 4.7 shows the summary of the deviator stress, mean effective stress and the axial strain at peak, Point of Phase Transformation and Residual state of all tests. Since there is no strain-softening in the dilative specimens, no data for peak state was included.

Table 4.7 Summary of Peak, PPT and Residual Characteristics of Tests on Bauxite

Group	Type of Behavior	Final Degree of Compaction (DC_f) (%)	Final Void Ratio (e_f)	Effective Confining Stress (kPa)	Peak Characteristics			Point of Phase Transformation Characteristics			Residual Characteristics		
					q_{peak} (kPa)	p'_{peak} (kPa)	Axial Strain (%)	q_{ppt} (kPa)	p'_{ppt} (kPa)	Axial Strain (%)	q_{res} (kPa)	p'_{res} (kPa)	Axial Strain (%)
1	QSS	66.9	1.322	25	10.2	16.3	1.0	7.7	13.9	7.6	30.8	15.1	30.0
	QSS	72.5	1.143	100	42.6	42.6	1.5	40.9	38.6	2.4	52.9	30.6	30.0
	QSS	77.0	1.019	200	84.1	89.6	0.7	78.6	60.8	2.8	105.4	59.7	30.0
	QSS	79.7	0.950	400	141.7	184.2	0.7	131.9	118.6	2.8	180.6	114.1	30.0
2	QSS	80.4	0.934	600	208.9	235.9	1.1	193.2	149.5	4.9	249.5	165.8	30.0
	QSS	82.6	0.882	800	279.7	316.8	0.7	258.1	194.3	3.1	329.7	213.5	30.0
	QSS	84.8	0.833	1000	333.2	311.9	1.2	318.1	227.3	3.3	405.5	264.1	30.0
	QSS	88.9	0.748	1000	390.0	339.0	1.1	373.5	245.9	3.7	410.3	245.6	30.0
3	QSS	89.8	0.731	600	250.5	230.0	1.1	242.0	182.1	2.2	294.3	179.4	30.0
	QSS	92.7	0.676	800	341.9	349.3	0.9	313.8	205.9	4.8	351.9	222.4	30.0
	QSS	95.3	0.631	1000	436.8	412.8	1.1	413.2	266.9	4.3	429.0	279.8	30.0
4	Dilative	91.2	0.704	100	-	-	-	73.0	47.4	1.6	123.3	70.3	30.0
	Dilative	88.0	0.765	200	-	-	-	94.8	71.0	2.4	185.5	115.0	30.0
	Dilative	85.0	0.829	200	-	-	-	104.8	78.5	4.3	131.2	82.5	30.0
	Dilative	84.7	0.835	150	-	-	-	76.6	51.8	4.3	102.0	58.2	30.0
	Dilative	80.9	0.920	100	-	-	-	51.9	36.9	3.5	66.0	37.8	30.0

4.3.3 Steady State Line

In this thesis, it is believed the hypothesis of the existence of a unique Steady State Line (SSL) for soils. Then, the states at 30% of axial strain of all the tests were plotted on the plane e vs log (p'), differentiating those showing dilative behavior from contractive behavior. The results of the tests corresponding to 66.9% of DC (e=1.322) at 25kPa (contractive) and 85% of DC (e=0.829) at 200 kPa (dilative) allowed to narrow down the area where the SSL can be located. Within such narrow area, 3 ultimate states corresponding to 80.4% of DC (e = 0.934) at 600 kPa, 82.6% of DC (e = 0.882) at 800 kPa and 84.8% of DC (e = 0.833) at 1000 kPa are located. Further, the ultimate state of these 3 states fulfills the definition of definition of Steady State by Poulos (1981):

> "The Steady State is the state of deformation for any mass of particles is that stat in which the mass is continuously deforming at constant volume, constant normal effective stress, constant shear stress, and constant velocity"

Then, by joining these states, the SSL (solid blue line) was defined in Figure 4.36. This line was projected (dotted blue line) considering that in the plane e vs log (p ') the SSL is linear, although this is not totally correct since Verdugo (1992) obtained a curved line for Toyoura sand in the same plane.

It is worth mentioning that there are at least 3 additional tests that fulfill with the definition of Poulos (1981) for the Steady State. For the cases corresponding to 72.5% of DC (e=1.143) at 100 kPa, 77% of DC (e=1.019) at 200 kPa, and 79.7% of DC (e=0.950) at 400 kPa the Steady State conditions are fulfilled:

- ✓ Constant volume is maintained by the undrained condition of the test
- ✓ Constant effective stress is achieved as well. When analyzing the data of the effective stress path, the effective stress barely changes in the last 3% of axial strain
- ✓ Constant shear stress is complied by a constant deviator stress in the last 10% of axial strain as seen in figure 4.28
- ✓ Constant velocity is complied by the constant strain rate set at the beginning of the test

Then, the reason why the final states of these tests does not reach the proposed SSL might be due to the lack of accuracy in void ratio estimation

- ✓ Sladen and Handford (1987) reported that potential errors in void ratio calculation in undrained tests can be large, up to 0.15 for Syncrude Tailings in Canada. Jefferies (1991) stated that the main source of error arises when volume changes due to the saturation procedure are not measured accurately.
- ✓ According to Rahman et al (2010), void ratio (e) may not be a good parameter for characterizing sand with fines under Critical State Soil Mechanics suggesting the use of Granular Void Ratio (e*) where conventional void ratio (e) is modified by including only the amount of fines that actually contribute to the mechanical response of the soil.

Another reason may be the existence of non-unique Steady State Lines for soils with high content of fines. As stated by Yamamuro and Covert (2001), silty sands may possess properties that create non-unique steady-state lines. The reasons for this unusual behavior may be associated with the particle structures. Depending on the depositional and densification process that is used, silty sands may exhibit quite different patterns of behavior because they may possess different particle structures resulting in their being essentially different soils, although the reasoning of Yamamuro and Covert (2001) do not provide a clear difference between fabric and structure. This is important because Ishihara (1993) concluded that at the Steady State all the effects of initial fabric are erased.

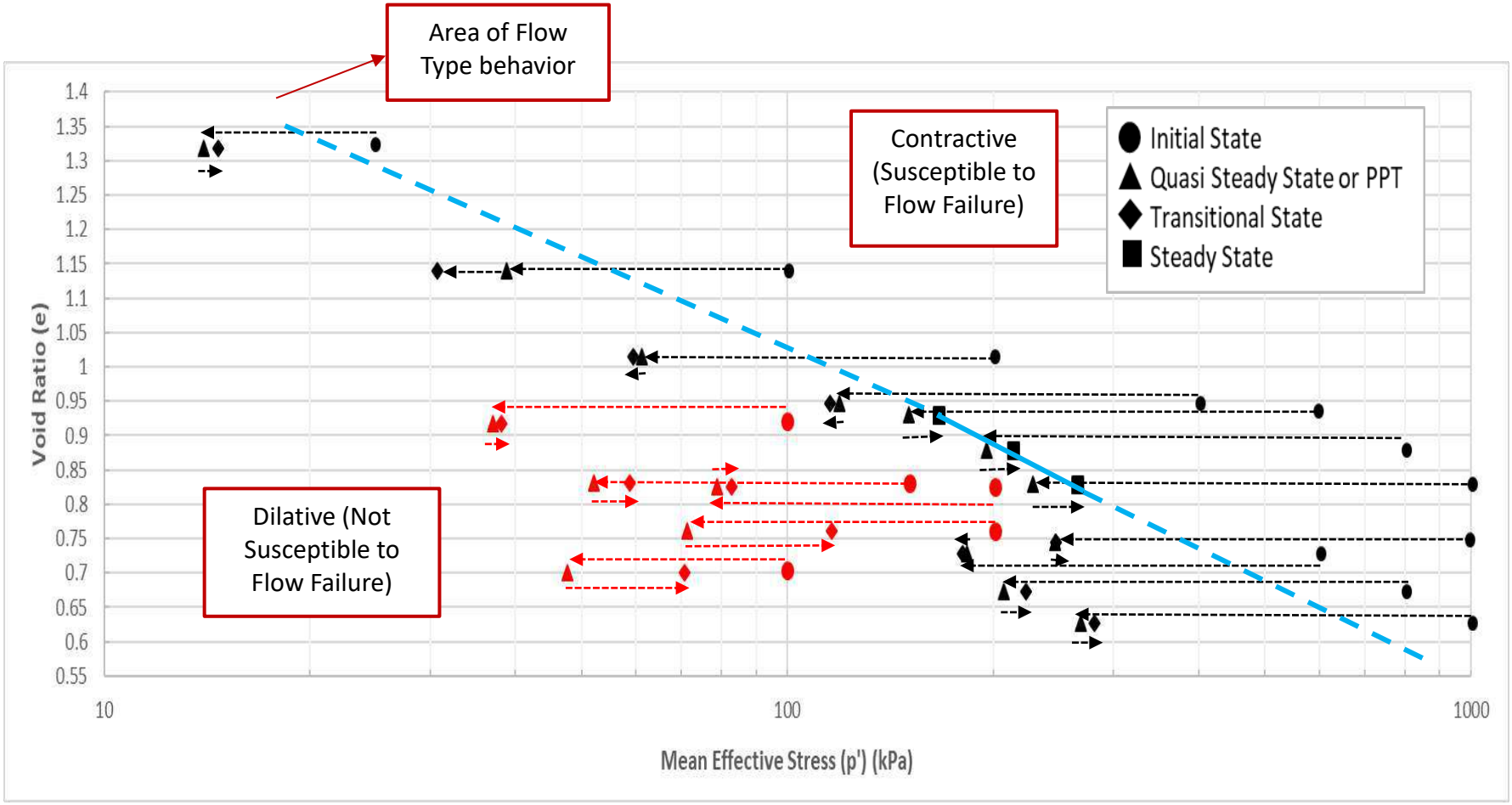

Figure 4.37 Steady State Line of Bauxite

4.3.4 Shear Strength Parameters

4.3.4.1 Evolution of Mobilized Friction Angle

Figure 4.38 shows the behavior of the mobilized friction angle with respect to axial strain for 3 tests performed at 100 kPa of effective confining stress, but with a different density. Figure 4.39 is similar, but for tests at 200 kPa of effective confining stress. This was done to study the effect of density on the behavior of the mobilized friction angle. The angles corresponding to the Point of Phase Transformation (PPT) are shown in inverted triangles.

Figure 4.38 shows that soils with higher density mobilized bigger friction angles at small, medium strain and large strain until 15% of axial strain for 100 kPa case including the angle at the PPT. At very large strain (30%) the loose soil tends to mobilize a bigger friction angle around 42°, while the denser soils reach a common value.

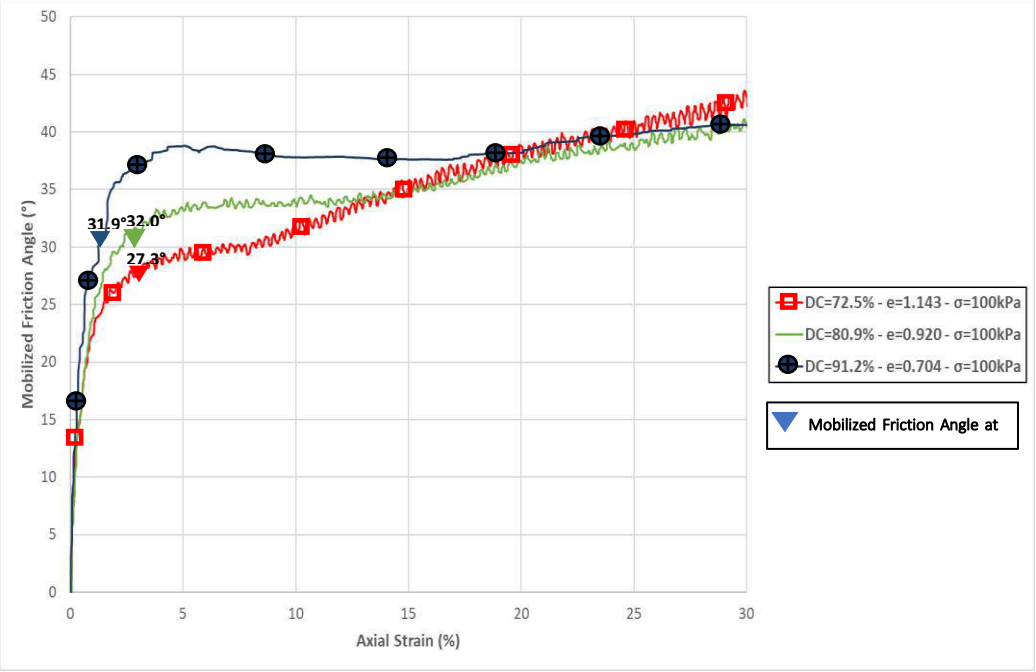

Figure 4.38 Effective Mobilized Friction Angle (°) VS Axial Strain (%) of specimens of different density at 100 kPa

Similarly, figure 4.39 shows that the soils with higher density mobilized bigger friction angles at small, medium strain and large strain until 12% of axial strain. However, for the mobilized friction angle at the PPT, the soil with 85.0% of DC shows bigger angle than the soil with 88.0% of DC. At very large strain (30%) the loose soil tends to mobilize a bigger friction angle around 40°, while the denser soils reach a common value.

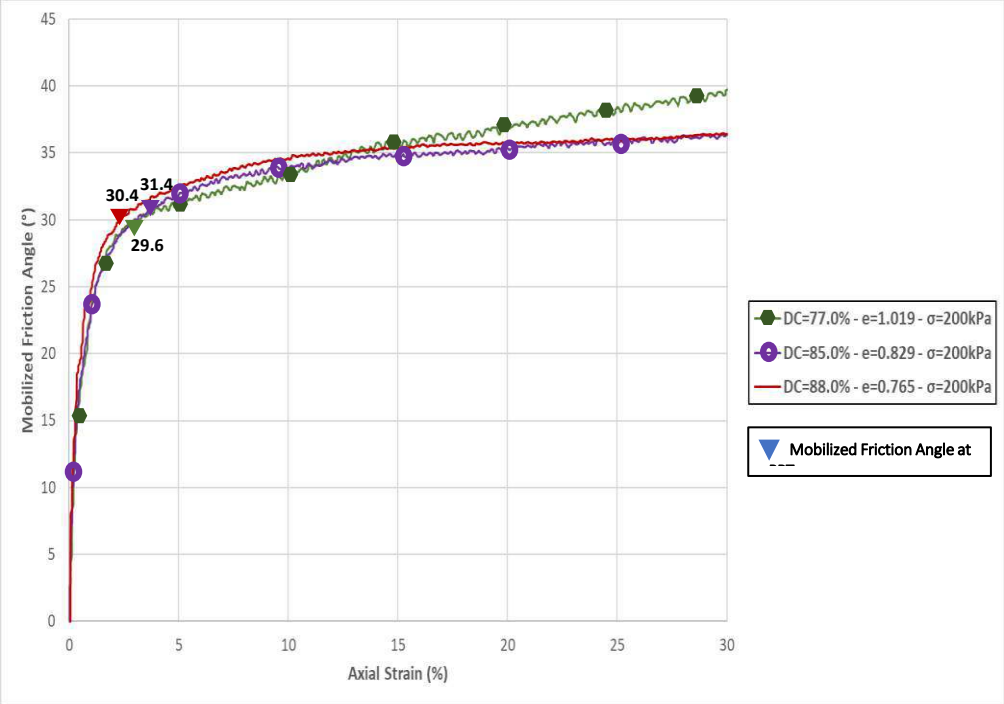

Figure 4.39 Effective Mobilized Friction Angle (°) VS Axial Strain (%) of specimens of different density at 200 kPa

In addition, the effects of effective confining stress on the mobilized friction angle will be analyzed. To do this, 3 tests with similar void ratios were grouped, but at different levels of confining stress. Figure 4.40 shows no clear effect of the effective confining stress on the mobilized friction angle, in fact the soil at 150 kPa presented higher angle of mobilized friction than the soil at 1000 kPa in almost all the test.

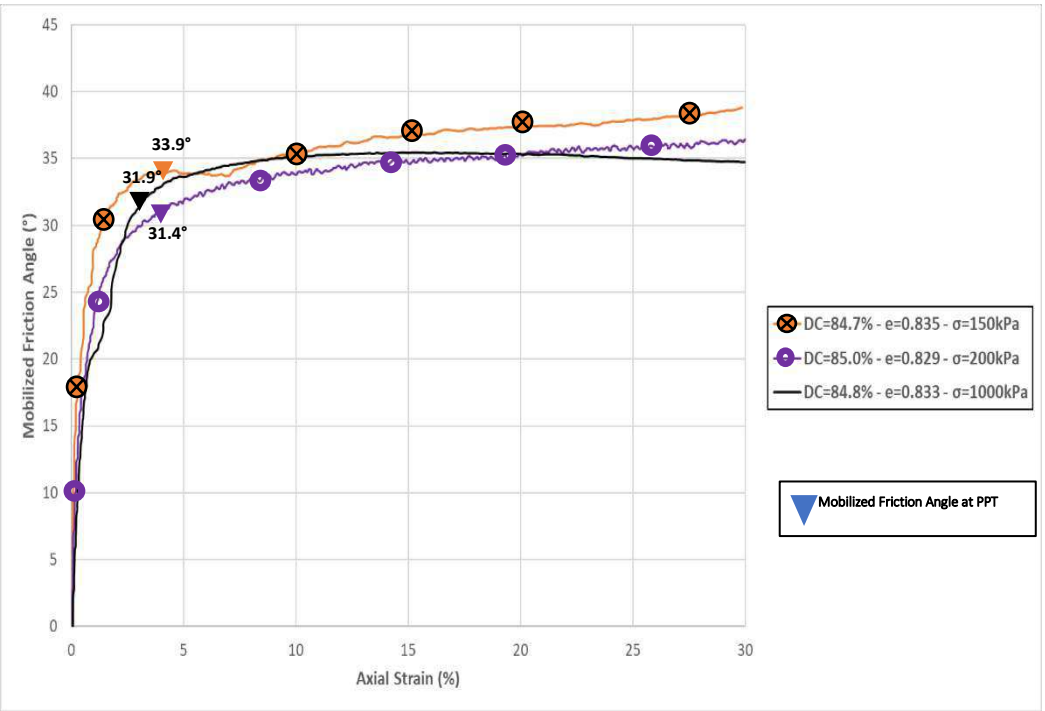

Figure 4.40 Effective Mobilized Friction Angle (°) VS Axial Strain (%) of specimens of similar density at different effective confining stress

Figure 4.41 shows the behavior of the mobilized friction angles for all the results obtained. There is a similar behavior in terms of shape and magnitude in almost all of them except for the 66.9% of DC at 25kPa test that shows low values compared to the rest, but reaches the other tests at 30% of strain

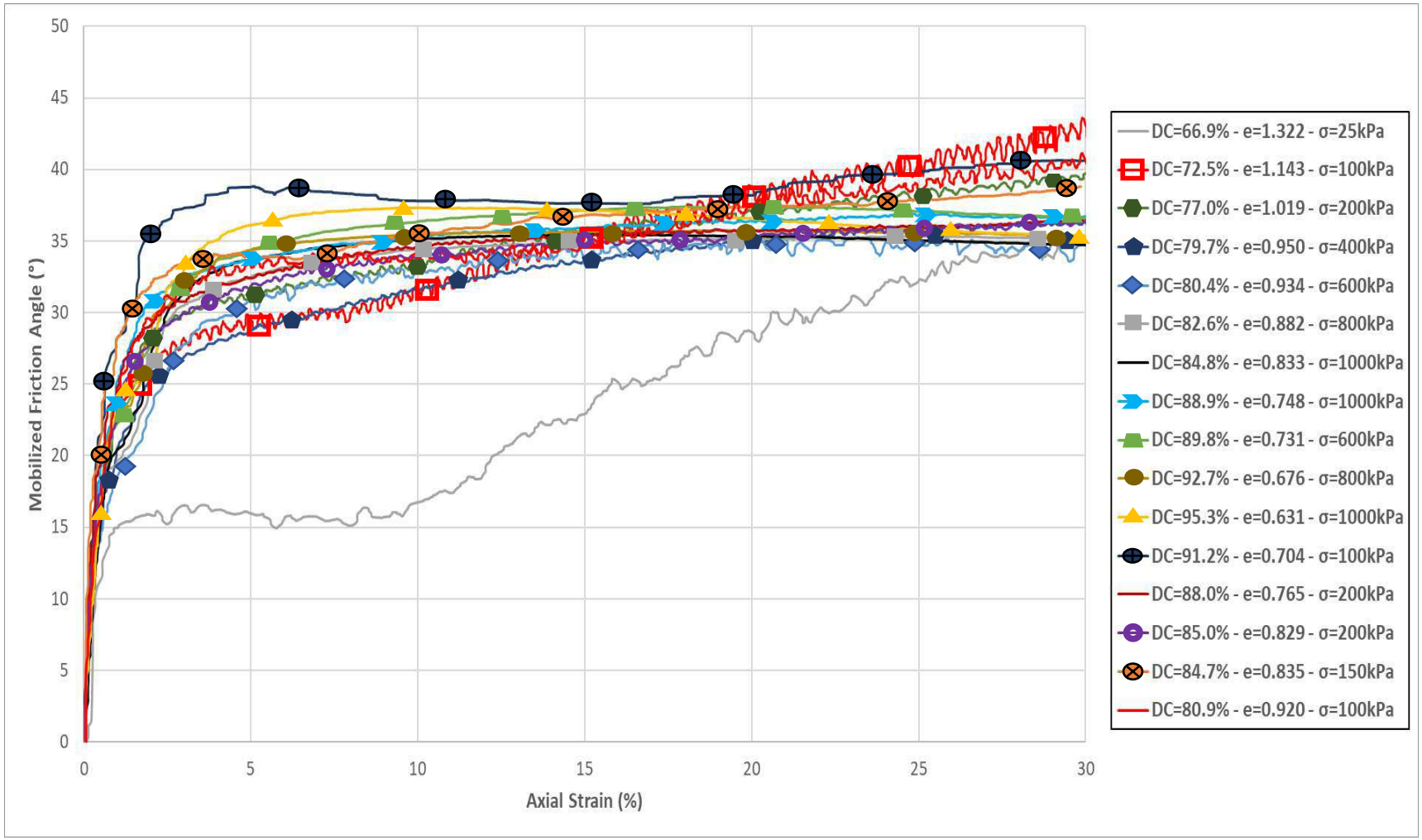

Figure 4.41 Effective Mobilized Friction Angle (°) of all tests

Table 4.8 Summary of Effective Mobilized friction angles at peak, point of phase transformation (PTT) and residual state

Group	Type of Behavior	Final Degree of Compaction (DC_f) (%)	Final Void Ratio (e_f)	Effective Confining Stress (kPa)	ϕ'_{mob} (Peak)	ϕ'_{mob} (PPT)	ϕ'_{mob} (Residual)
1	QSS	66.9	1.322	25	15.0°	15.6°	34.9°
	QSS	72.5	1.143	100	25.2°	27.2°	42.5°
	QSS	77.0	1.019	200	19.6°	29.6°	39.6°
	QSS	79.7	0.950	400	17.8°	26.7°	36.2°
2	QSS	80.4	0.934	600	18.9°	30.7°	34.5°
	QSS	82.6	0.882	800	19.0°	30.7°	35.2°
	QSS	84.8	0.833	1000	20.5°	31.9°	34.7°
	QSS	88.9	0.748	1000	25.8°	33.0°	36.7°
3	QSS	89.8	0.731	600	22.6°	29.2°	36.6°
	QSS	92.7	0.676	800	22.9°	34.2°	35.3°
	QSS	95.3	0.631	1000	24.1°	35.6°	35.4°
4	Dilative	91.2	0.704	100	40.7°	31.9°	40.7°
	Dilative	88.0	0.765	200	36.4°	30.4°	36.4°
	Dilative	85.0	0.829	200	36.3°	31.4°	36.3°
	Dilative	84.7	0.835	150	38.8°	33.9°	38.8°
	Dilative	80.9	0.920	100	40.6°	32.0°	40.6°

Except for the test of 72.5% of DC at 100 kPa, the average effective friction angle mobilized at the residual level (30% of axial strain) for tests showing QSS is 36.5°, while for dilative samples is 38.6° showing the effects of pure strain-hardening. On average the residual effective mobilized friction angle can be regarded as 37°.

4.3.4.2 Critical State Friction Angle

There are many failure criteria to estimate the effective friction angle (ϕ'). Brandon et al (2006) reviewed 6 types of failure criteria:

- ✓ Maximum deviator stress (q_{peak}),
- ✓ Maximum principal stress ratio $(\sigma'_1/\sigma'_3)_{max}$
- ✓ Maximum excess pore water pressure
- ✓ Reaching the K_f line
- ✓ Limiting strain at 15%
- ✓ Excess pore water pressure of 0 (u_e=0)

Wang and Luna (2012) applied all these criteria to Mississippi River Valley Silt, obtaining that the first 3 criteria provide similar values which are also close to the effective friction angle obtained using the concepts of critical soil mechanics.

Since it is more practical to obtain and provides reliable results, the critical state theory will be used for the calculation of shear strength parameters in this thesis. By plotting all the final states of the tests, the following graphic can be obtained.

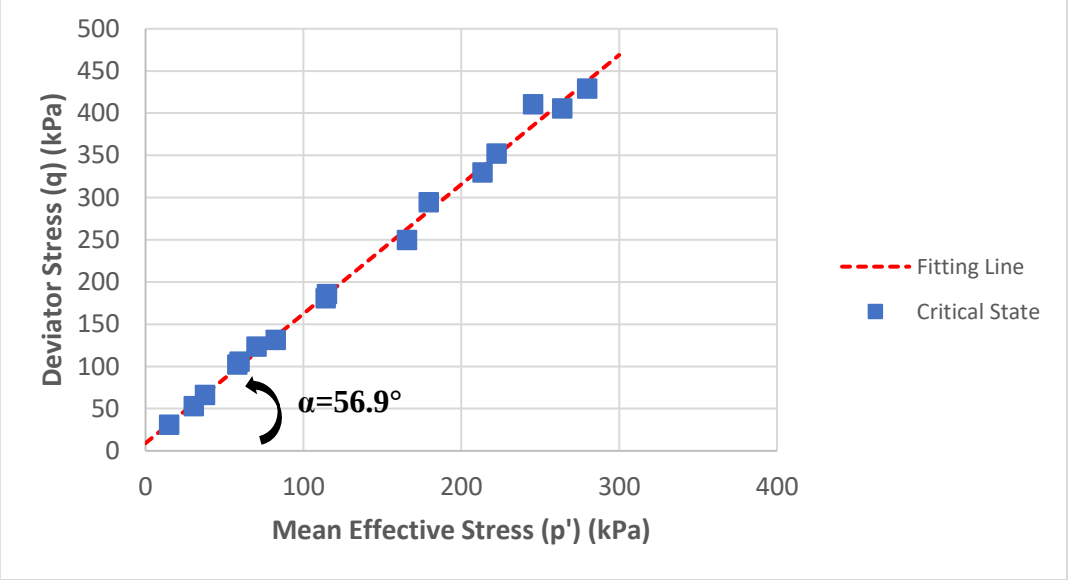

Figure 4.42 Critical State Line in q vs p' plane

By using the expressions of Critical State Soil Mechanics:

$$\tan 56.9° = \frac{6 \sin \emptyset'}{3 - \sin \emptyset'} \qquad 8.3\ kPa = \frac{6 \sin \emptyset'}{3 - \sin \emptyset'} * c'$$

$$\emptyset' = 37.6° \qquad c' = 5.4\ kPa$$

$$M_{CSL} = 1.533$$

Cohesion (5.4 kPa) is very small compared to the confining stress range of this study (up to 1000 kPa), so it will be assumed that the material is purely frictional. Figure 4.43 shows the ultimate states at 30% of all the tests in the plane q/2-p'.

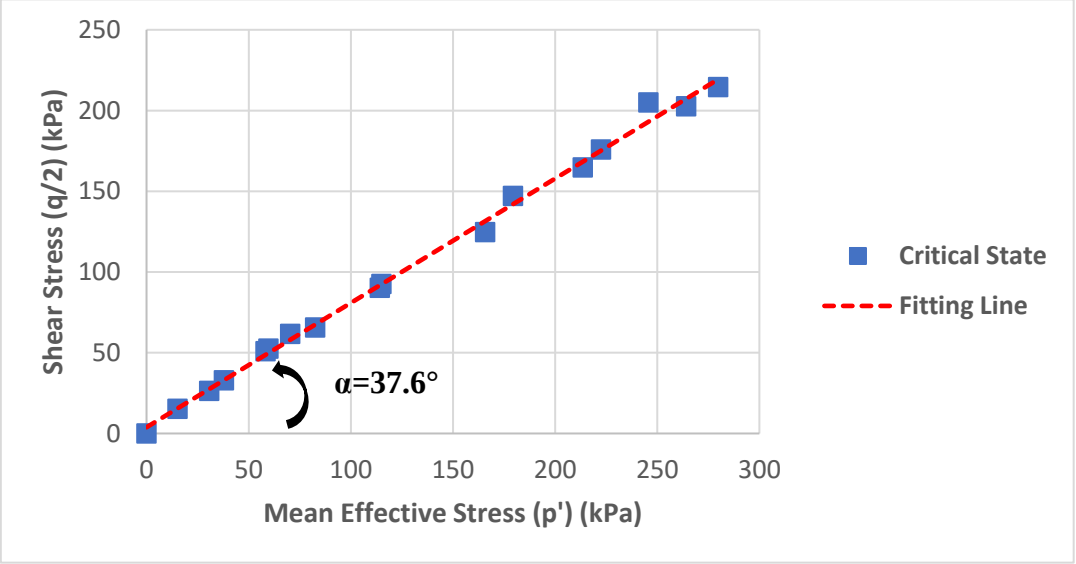

Figure 4.43 Critical State Line in q/2 vs p' plane

Figures 4.44 and 4.45 compare the critical state line (CSL) of Bauxite with the critical state line of other materials: Toyoura Sand (Verdugo, 1992), silty sands with 100%, 60%, 40%, 20% and 18% of fines (Kwa and Airey, 2017) and Iron Ore Fines (Wang et al, 2018) in the q vs p' and q/2 vs p' planes. Bauxite has greater ultimate resistance than Toyoura Sand evidenced by the bigger angle of friction. Bauxite's CSL is located between the CSL of silty sands found by Kwa and Airey (2017) with 100% and 60%, and 40% of fines. Bauxite used in this thesis has 38.6% of fines which means that feldspar silty sands can resemble accurately the behavior of Bauxite at large strain. However, Iron Ore Fines are much stronger (ϕ'=45°) even close to some rockfill materials probably because of its heavier metallic minerals. The metallic minerals of Bauxite, on the other hand, are not so heavy which can be seen in the large difference in specific gravity (4.444 of IOF against 2.642 of Bauxite). This leads to the conclusion that the effects of metallic mineralogy in Bauxite are not as pronounced as in IOF at least in terms of the critical state friction angle.

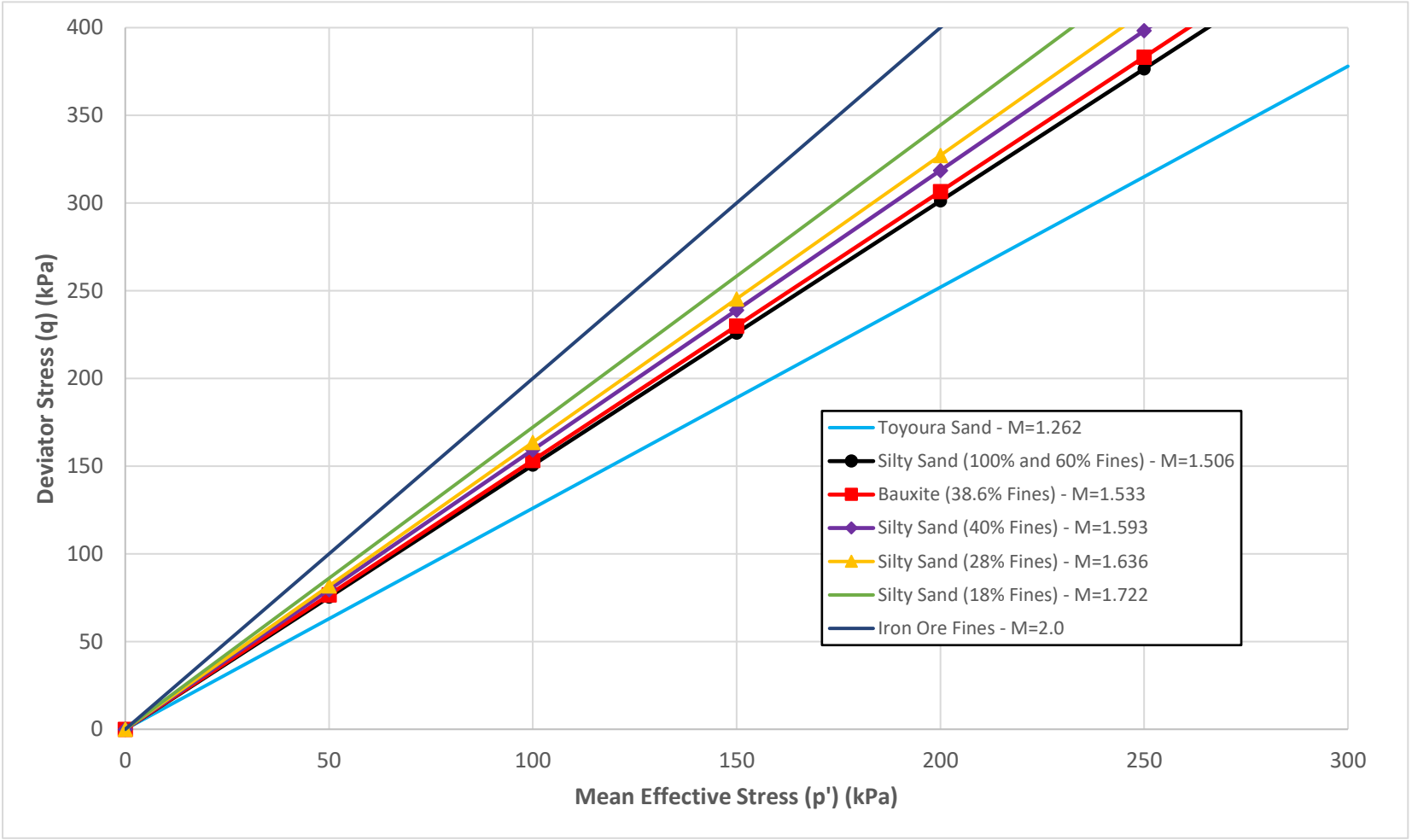

Figure 4.44 Critical State Line in q vs p' plane of Bauxite and other materials

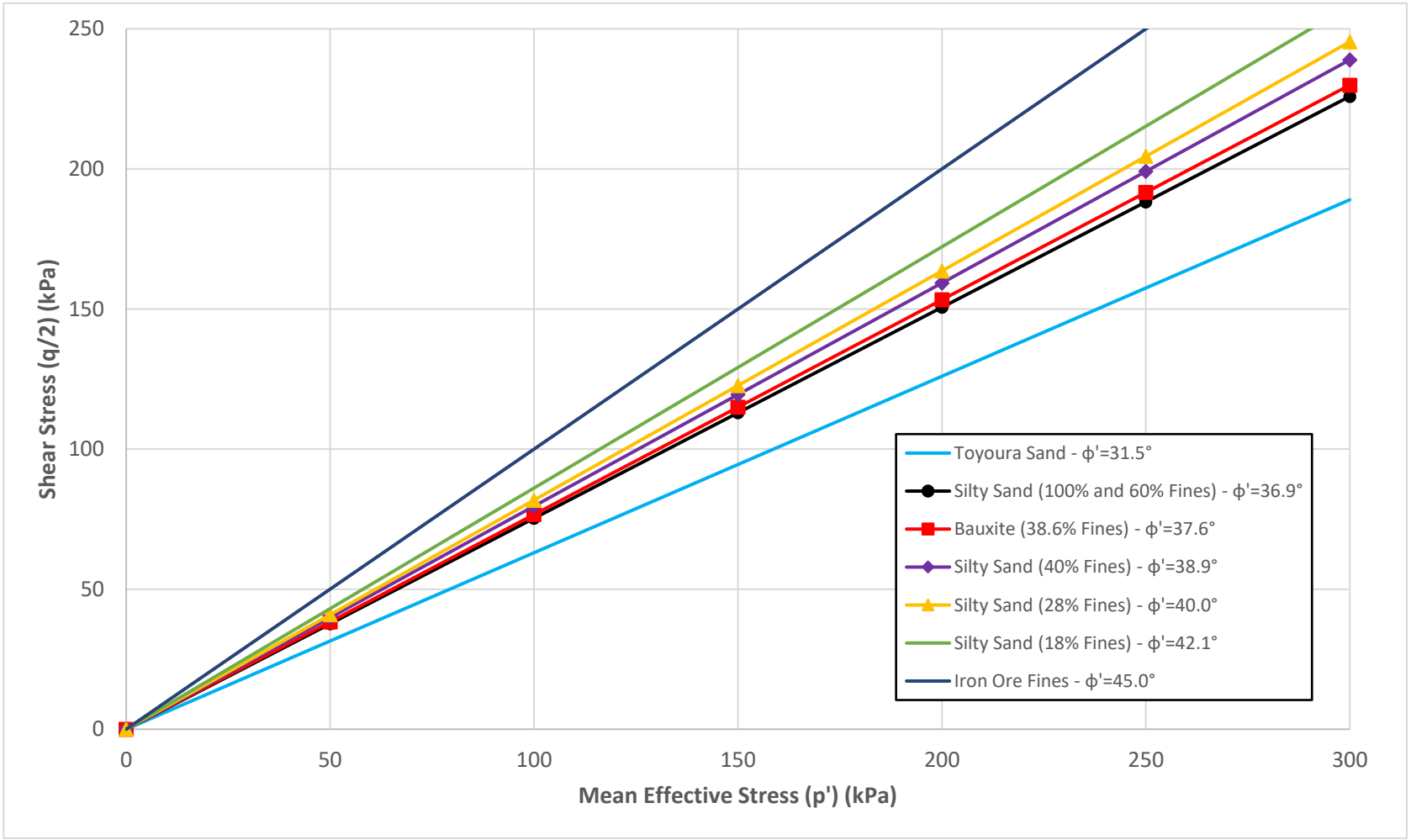

Figure 4.45 Critical State Line in q/2 vs p' plane of Bauxite and other materials

4.3.4.3 Shear Strength mobilized at the Quasi Steady State

As mentioned in chapter 2.3.3, the quasi-steady-state shear strength can be regarded as the post-liquefaction shear strength for stability analysis. For its calculation, Ishihara (1993) recommended the following expression:

$$\frac{S_{qss}}{\sigma'_o} = \frac{q_s}{2} * \frac{\cos \emptyset_s}{\sigma'_o}$$

Where $\emptyset_s$ and q_s are the mobilized friction angle and the deviator stress at the quasi steady state respectively. By applying this expression to the test results that showed Quasi Steady State behavior, it is possible to obtain the following results:

Table 4.9 Summary of Normalized Mobilized Shear Strength at Quasi Steady State

Group	Type of Behavior	Final Degree of Compaction (DC_f) (%)	Final Void Ratio (e_f)	q_{ppt} (kPa)	ϕ'_{mob} (PPT)	S_{qss} (kPa)	Effective Confining Stress (kPa)	Normalized $\frac{S_{qss}}{\sigma'_o}$
1	QSS	66.9	1.322	7.7	15.6°	3.7	25	0.15
	QSS	72.5	1.143	40.9	27.4°	18.2	100	0.18
	QSS	77.0	1.019	78.6	29.6°	34.1	200	0.17
	QSS	79.7	0.950	131.9	26.7°	58.9	400	0.15
2	QSS	80.4	0.934	193.2	30.7°	83.1	600	0.14
	QSS	82.6	0.882	258.1	30.7°	111.0	800	0.14
	QSS	84.8	0.833	318.1	31.9°	135.0	1000	0.13
	QSS	88.9	0.748	373.5	33.0°	156.6	1000	0.16
3	QSS	89.8	0.731	242.0	29.2°	105.6	600	0.18
	QSS	92.7	0.676	313.8	34.2°	129.7	800	0.16
	QSS	95.3	0.631	413.2	35.6°	167.9	1000	0.17

By plotting the undrained normalized shear strength at the quasi steady state and the void ratio, figure 4.46 is obtained:

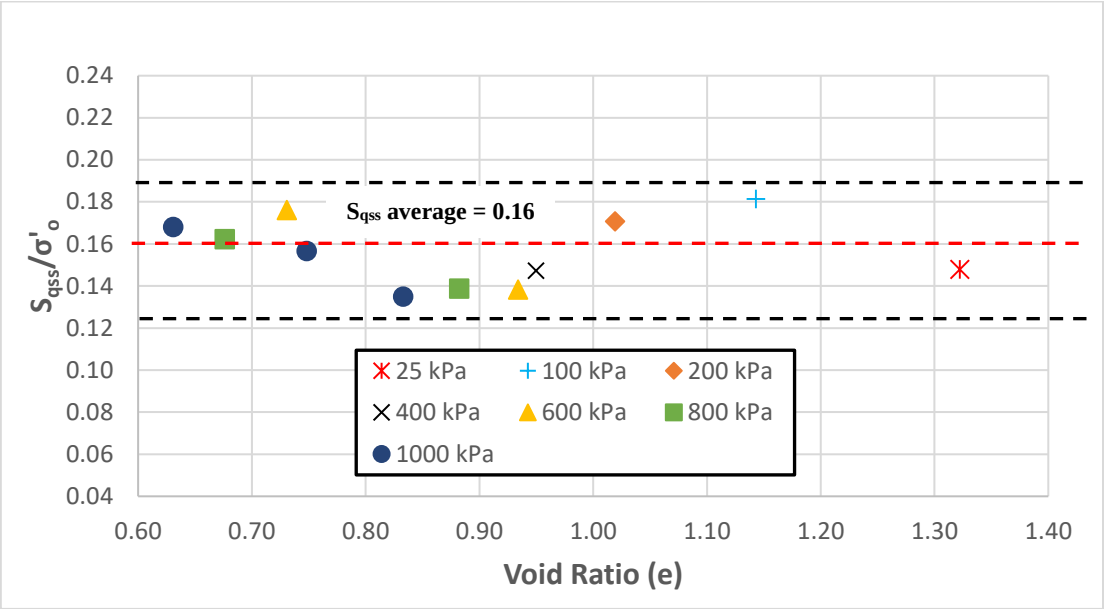

Figure 4.46 Normalized Quasi Steady State Shear Strength $\left(\frac{S_{qss}}{\sigma'_o}\right)$ *VS void ratio (e)*

Even though many soils do not have a unique ratio $\frac{S_{us}}{\sigma'_o}$ because they do not present a unique isotropic consolidation line (Kramer, 1996), the results for Bauxite show little scattering and therefore an average value can be established.

$$\frac{S_{qss}}{\sigma'_o} = \mathbf{0.16}\ (\boldsymbol{for\ Bauxite})$$

As mentioned in chapter 2.3.4, Olson and Stark (2003) conducted a survey on post-liquefaction shear strengths based on laboratory test results and back analysis of case studies concluding that laboratory-based strengths range from 0.02 to 0.22, while back analysis-based strengths range from 0.05 to 0.12. The value obtained for Bauxite lies within the first range, although it is higher than the ranges found using failure back-analysis which is expected as the undrained resistance from laboratory tests tend to be less conservative.

Table 4.10 shows the ratio obtained for Bauxite and similar materials. For Sand Fernando Dam silty sand (Baziar and Dobry, 1995), Duncan Dam silty sand (Pillai and Salgado, 1994) and Cooper Tailings Slimes (Castro and Troncoso, 1989), the post-liquefaction

shear strength was defined as the undrained shear strength at the Steady State because samples showed flow-type behavior. On the other hand, “Lagunillas” sandy silt and “Tía Juana” silty sand (Ishihara, 1993) showed Flow-type with limited deformation and therefore the shear strength at the quasi steady state was calculated. This is the reason why the shear strength depends on the sample preparation, as mentioned in chapter 2.2.4.2, at the quasi steady state the effects of fabric are still not erased.

Table 4.10 Normalized Undrained Shear Strength Ratios for similar materials

Type of Soil	S_{us}/σ'_o (at Steady State)	S_{qss}/σ'_o (at Quasi Steady State)
Bauxite – Moist-Tamping	-	0.16
San Fernando Dam Silty Sand [1]	0.12	-
Duncan Dam Silty sand[2]	0.21	-
Lagunillas Sandy Silt - Water Sedimentation[3]	-	0.134
Lagunillas Sandy Silt - Dry Deposition[3]	-	0.086
Tía Juana Silty Sand - Water Sedimentation[3]	-	0.181
Tía Juana Silty Sand - Dry Deposition[3]	-	0.146
Cooper Tailings Slimes[4]	0.07	-

1. Baziar and Dobry (1995)
2. Pillai and Salgado (1994)
3. Ishihara (1993)
4. Castro and Troncoso (1989)

In the author's professional experience in tailings dam design, the values of the ratio $\frac{S_{us}}{\sigma'_o}$ are generally chosen from correlations of back-analysis database and SPT number of blows, and subsequently reduced by a safety factor of 30%. According to the literature review, the resistance obtained from laboratory tend to be non-conservative. Furthermore, the value obtained for Bauxite is at the quasi steady state which is dependent of sample preparation, so this ratio is not definitive. Hence, it is suggested to apply a 50% of safety factor, defining the ratio as 0.08 for engineering applications.

4.3.5 Collapse Surface

The Steady State Line (SSL) gives information about whether a soil's state is susceptible to flow failure. But, it does not provide information on how far or close the soil is to flow failure. The concept of Collapse Surface (Sladen et al, 1985) solves this issue. By joining the collapse point (peak deviator stress) with the steady state point in the e vs p' plane is possible to obtain the collapse surface. Vaid and Chern (1983) stated alternatively that the collapse surface should pass through the origin of the plot. Figure 4.47 shows 2 soils A and B at different states in q vs p' plane. A is very close to the collapse surface and therefore a small disturbance is enough to trigger flow failure, whereas B is a long way away requiring very high excess pore water pressure for flow failure to occur.

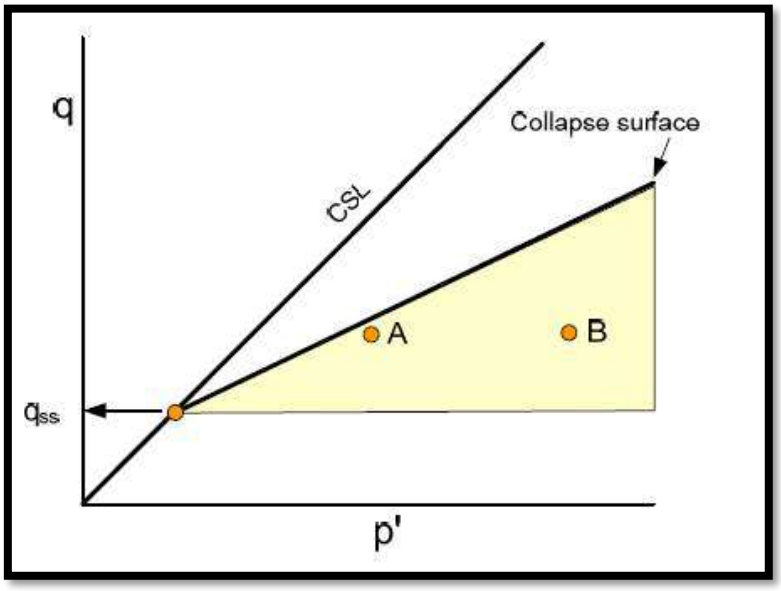

Figure 4.47 Illustration of the Collapse Surface (GEO-SLOPE International, 2007)

In this thesis, the steady state for flow-type was not found for any of the tests so the collapse surface will be obtained by joining the peak deviator stress point and the origin as suggested by Vaid and Chern (1983).

Table 4.11 shows all the values of the collapse surface slope (M_L) for the test results showing Quasi Steady State behavior.

Table 4.11 Summary of Slopes of Collapse Surfaces

Group	Type of Behavior	Final Degree of Compaction (DC_f) (%)	Final Void Ratio (e_f)	Effective Confining Stress (kPa)	Slope of the Collapse Surface (M_L)
1	QSS	66.9	1.322	25	0.628
	QSS	72.5	1.143	100	0.999
	QSS	77.0	1.019	200	0.934
	QSS	79.7	0.950	400	0.769
2	QSS	80.4	0.934	600	0.886
	QSS	82.6	0.882	800	0.883
	QSS	84.8	0.833	1000	1.068
	QSS	88.9	0.748	1000	1.151
3	QSS	89.8	0.731	600	1.089
	QSS	92.7	0.676	800	0.979
	QSS	95.3	0.631	1000	1.058

4.4 PARTICLE CRUSHING

Since the tests were conducted at high confining stress (up to 1000kPa), particle crushing effects are expected. This phenomenon can be studied by comparing the gradations of the materials before and after testing using the criterion of Hardin (1985):

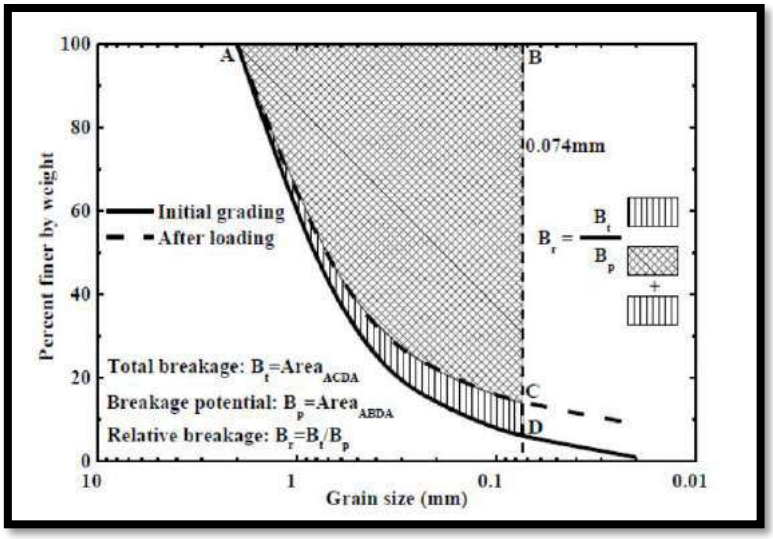

Figure 4.48 Definition of Particle Breakage (Hardin, 1985)

Particle size distribution was carried out after tests at 400 kPa, 600 kPa, 800 kPa and 1000 kPa. The results are shown in figure 4.49. It should be noted that the regular procedure after finishing the tests was to introduce the wet sample directly to the oven which reduced the content of fines. Only once, for a test at 1000 kPa, the sample was placed on the desiccator for 24 hours followed by drying in the environment, these results are indicated with (*).

4.4.1 Particle Size Distribution After Testing

Figure 4.49 shows important increments on the content of sands starting from 600 kPa of confining stress with an increase on average of 8% for coarse and medium sands. In the case of the test at 1000 kPa of confining stress there was a significant increase in the content of sands for the samples dried in the oven reaching up to 20% for particles greater than 0.425 mm and 17% for particles greater than 0.85 mm (coarse sands). For the sample not placed on the oven (an increase of 10% on average in fines and fine sands can be seen (particles less than 0.106 mm) with a similar increase in coarse sands than the oven-dried case for 1000 kPa.

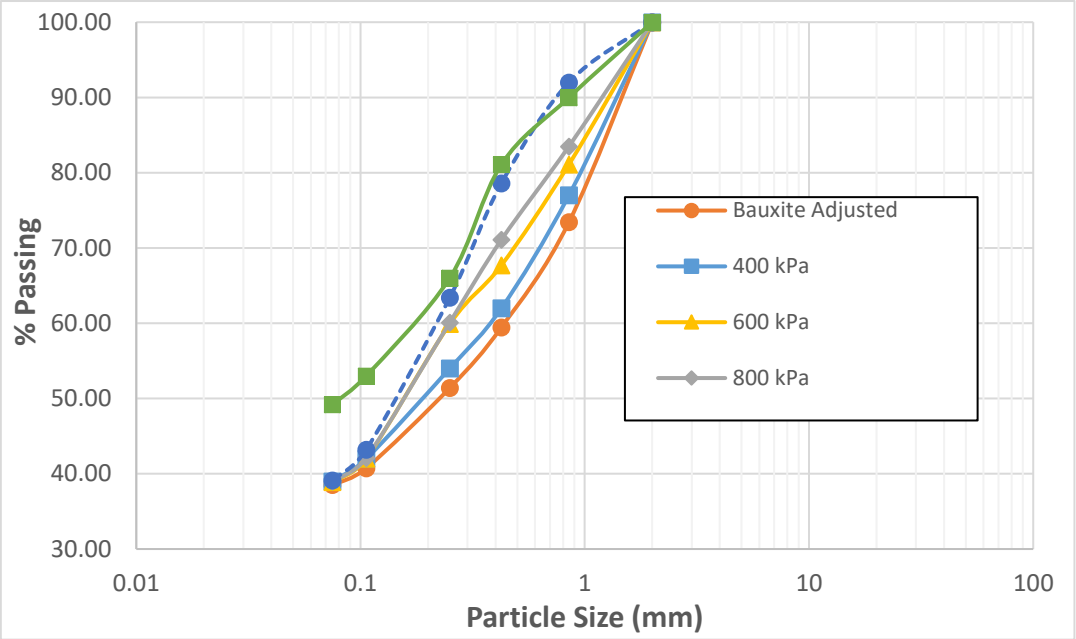

Figure 4.49 Particle Size Distribution of original Bauxite and after shearing at different effective confining stress

4.4.2 Microscopic Images

Figures 4.50 and 4.51 show microscopic photos were taken of the Bauxite before and after being subjected to monotonic loading at 1000 kPa of confining stress for the specimen dried on the desiccator and environment. The figures show a magnification of 25 times. The shape of the coarse particles (sub-angular) keeps similar after shearing, but the fine matrix that surrounds it is much greater.

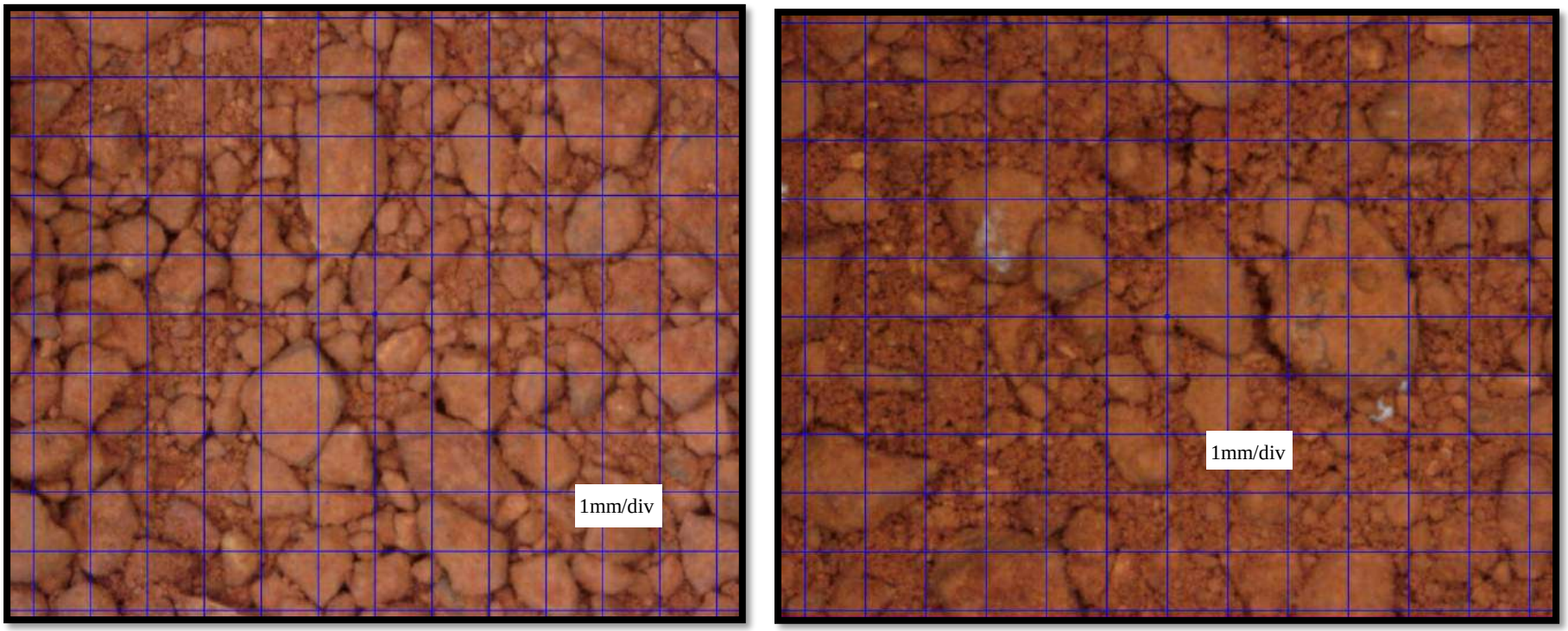

Figure 4.50 and Figure 4.51 Microscopic Image of Bauxite before and after testing at 1000 kPa of effective confining stress

5. EXPERIMENTAL RESULTS AND DISCUSSION ON SIMULATED BAUXITE

5.1 GENERAL REMARKS

A mixture of several Silica Sands with the same content of fines and with the same gradation of Bauxite's sandy fraction (Simulated BX) was prepared as described in chapter 3. A set of 4 undrained monotonic tests were conducted on fully saturated Simulated BX for comparison with the behavior of actual bauxite (BX)

The same method of preparation (moist-tamping) was used. Due to time constraints, it was decided to perform tests only on loose samples aiming to obtain contractive responses.

The void ratio after consolidation ranged from 0.781 to 0.718 corresponding to degrees of compaction of 75.6% and 78.5% of the maximum dry density obtained by the modified Proctor test respectively

On the other hand, the effective confining stress varied from 200 kPa to 800 kPa. The high-pressure compressor was used, initiating consolidation at an effective stress of 30 kPa.

The summary of all the tests performed considering the effective confining stress and the initial and final density and void ratio is shown in table 5.1.

Table 5.1 Summary of Tests Conducted on Simulated Bauxite

N° of test	Initial Degree of Compaction (DC_f) (%)	Initial Void Ratio (e_f)	Effective Confining Stress (kPa)	Final Degree of Compaction (DC_f) (%)	Final Void Ratio (e_f)
1	74.1	0.817	200	75.6	0.781
2	74.2	0.814	400	76.8	0.753
3	75.0	0.796	600	77.9	0.728
4	75.0	0.796	800	78.5	0.718

5.2 CONSOLIDATION

Consolidation was done under isotropic conditions; all tests results will be presented at the same time.

5.2.1 Effective Confining Stress vs Axial Strain

Figure 5.1 shows the behavior of axial strain with respect to the effective confining stress of all the tests conducted.

Despite similar initial degrees of compaction (DC), the 4 tests present different behaviors showing anomalies as in the case of Bauxite. Although in the case of soils at 75.0% of DC, the initial behavior is different, but the level of axial strain at 600 kPa is similar for both.

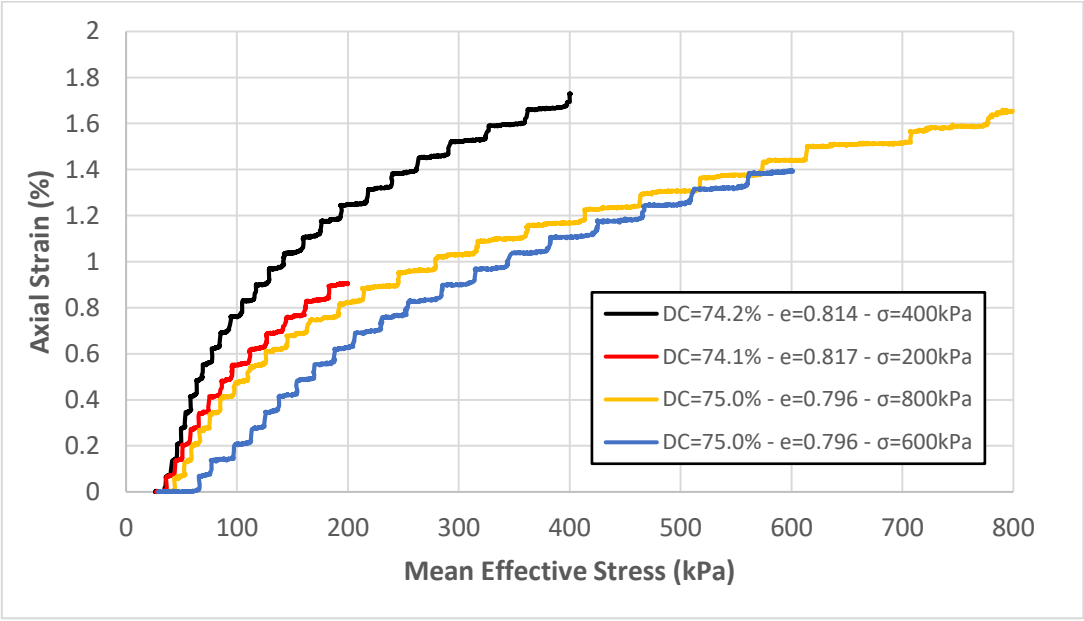

Figure 5.1 Mean Effective Stress (kPa) vs Axial Strain (%)

5.2.2 Axial Strain vs Volumetric Strain

Figure 5.2 shows the results of all tests. In the case of the 2 soils at initial density of 75% of DC (tests N°3 and N°4), different behaviors are observed again. For Test N°3, volumetric strains are observed without axial deformations indicating possible leakage at the beginning of the consolidation process.

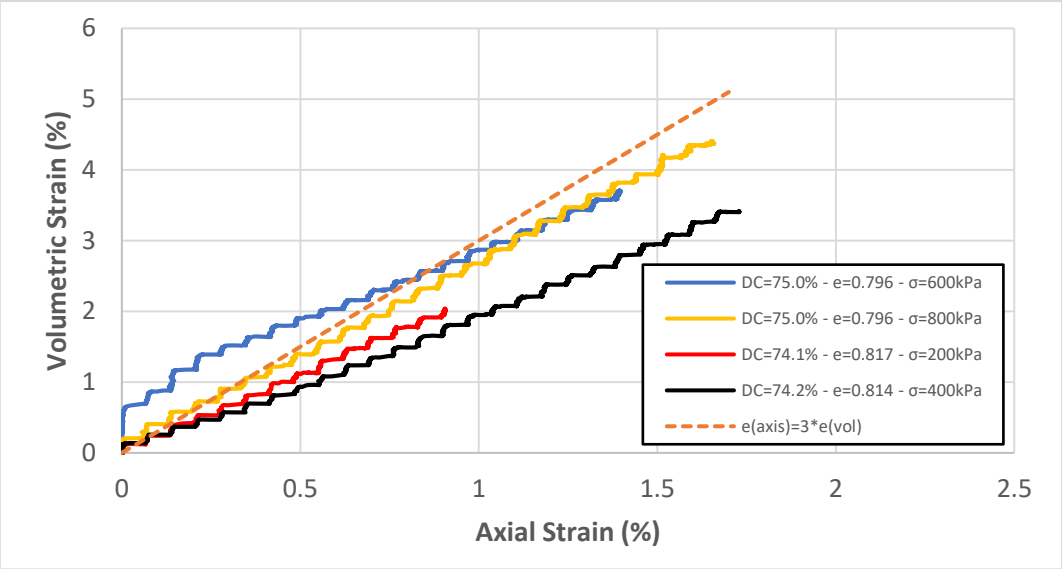

Figure 5.2 Axial Strain (%) vs Volumetric Strain (%)

5.2.3 Effective Confining Stress vs Volumetric Strain

Figure 5.3 shows that Simulated BX is less compressible than actual BX (see figure 4.16). In tests conducted in BX, even dense soils (more than 80% of DC) undergo on average 10% of volumetric strain when subjected to confining stress up to 800 kPa, whereas Simulated BX only undergoes 4.5% of volumetric strain at 800 kPa of confining stress.

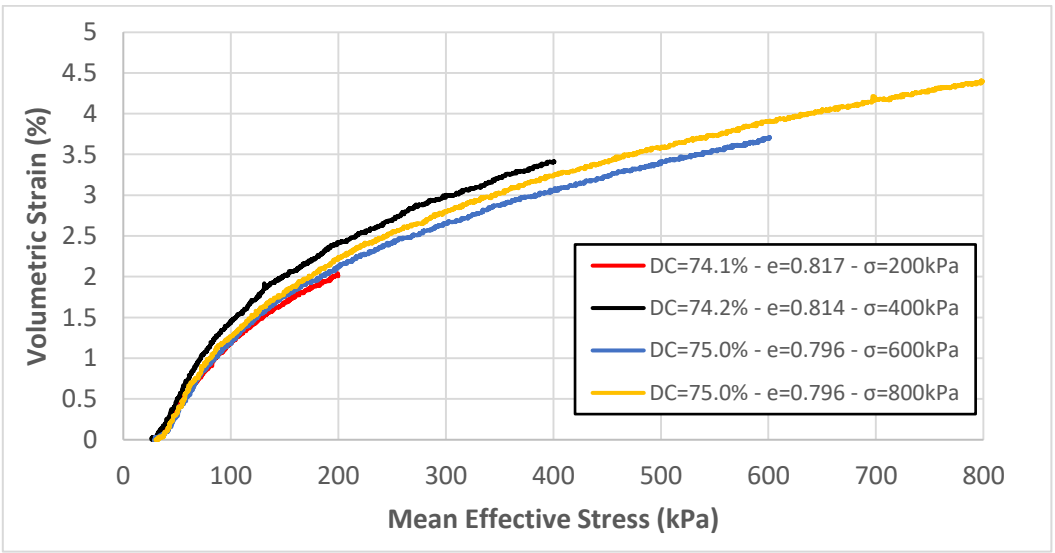

Figure 5.3 Mean Effective Stress (kPa) vs Volumetric Strain (%)

5.2.4 Isotropic Consolidation Lines

Like in BX, a unique ICL was not found, but the 2 soils at 75% of DC presented very similar behavior until 200 kPa.

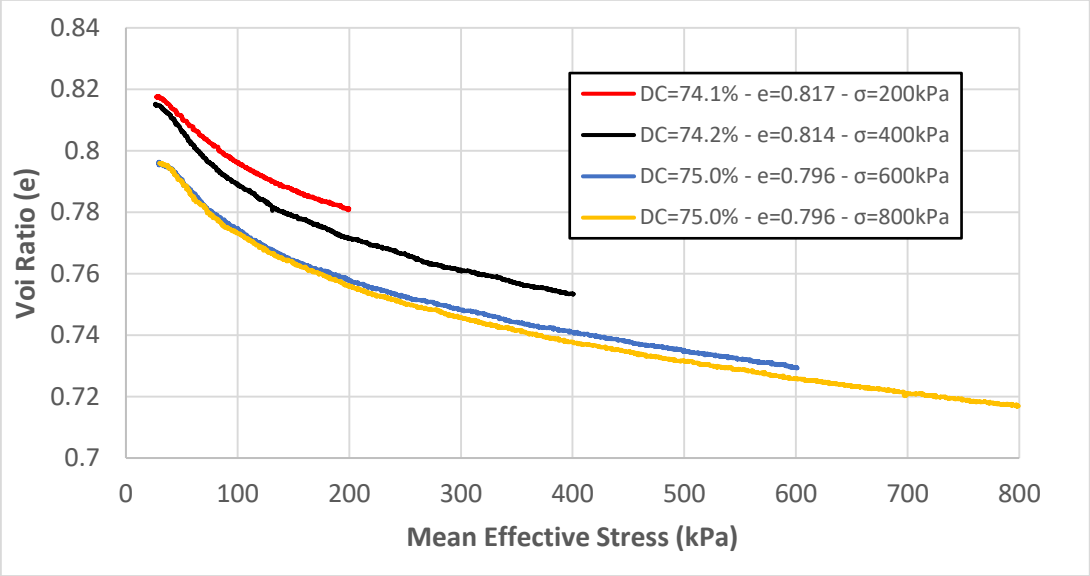

Figure 5.4 Isotropic Consolidation Lines

5.3 UNDRAINED MONOTONIC BEHAVIOR OF SIMULATED BAUXITE

For Simulated BX, it was possible to obtain flow type behavior (Steady State) in 2 tests on loose samples. The other 2 tests showed flow type with limited deformation (Quasi Steady State). The presentation of test results will be divided between those showing flow type behavior (SS) and those showing Quasi Steady State (QSS) behavior. Table 5.2 describes the initial and final degree and compaction and void ratio of all tests and their type of behavior.

Table 5.2 Summary of Tests including final Degree of Compaction and Void Ratio

N° of test	Type of Behavior	Initial Degree of Compaction (DC_f) (%)	Initial Void Ratio (e_f)	Effective Confining Stress (kPa)	Final Degree of Compaction (DC_f) (%)	Final Void Ratio (e_f)
1	Flow Type	74.1	0.817	200	75.6	0.781
2	Flow Type	74.2	0.814	400	76.8	0.753
3	QSS	75.0	0.796	600	77.9	0.728
4	QSS	75.0	0.796	800	78.5	0.718

5.3.1 Flow type behavior

Figures 5.5, 5.6 and 5.7 show the plots of stress-strain, effective stress path and excess pore water pressure of the 2 tests showing flow type behavior. Table 5.3 describes the changes in confining stress due to excess pore water pressure at peak and residual state.

The 2 tests show a peak stress state around 1.0% of axial strain, after which they undergo strain-softening until a minimum deviator stress of approximately 40 kPa for test N°1 and 140kPa for test N°2. However, there is no subsequent strain-hardening as occurred in all the contractive tests conducted on BX (see figure 4.29) and therefore the deviator stress keeps constant until the end of the test. This behavior is consistent with the flow type response described in Ishihara (1993). Soils showing this type of behavior reach the steady state directly after the strain-softening.

The effective stress path of test N°2 shown in figure 5.6 moves slightly to the right at the beginning evidencing a small positive dilatancy, but this does not occur for test N°1 which is totally contractive.

According to table 5.3, the excess pore water pressure at the peak state is on average 62.7% of the initial effective confining stress. Despite the flow-type behavior, the excess pore water pressure still does not reach 100% for the phenomena to be considered as liquefaction. After the strain-softening, the soil reaches the so-called Steady State which keeps constant until the end of the test at 30% of axial strain. At this state, the pore water pressure increment becomes 88.6% of the initial confining stress reducing it until only 20.2% of its initial value for the test N° 1, and 24.9% for the test N°2.

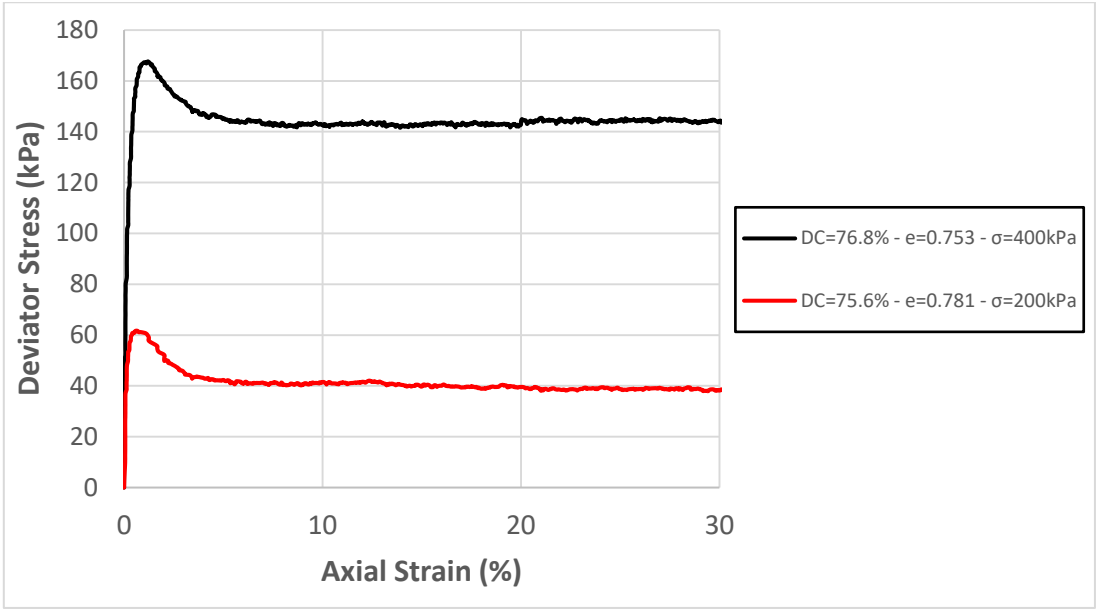

Figure 5.5 Deviator Stress (kPa) vs Axial Strain (%) of tests showing Flow Type behavior

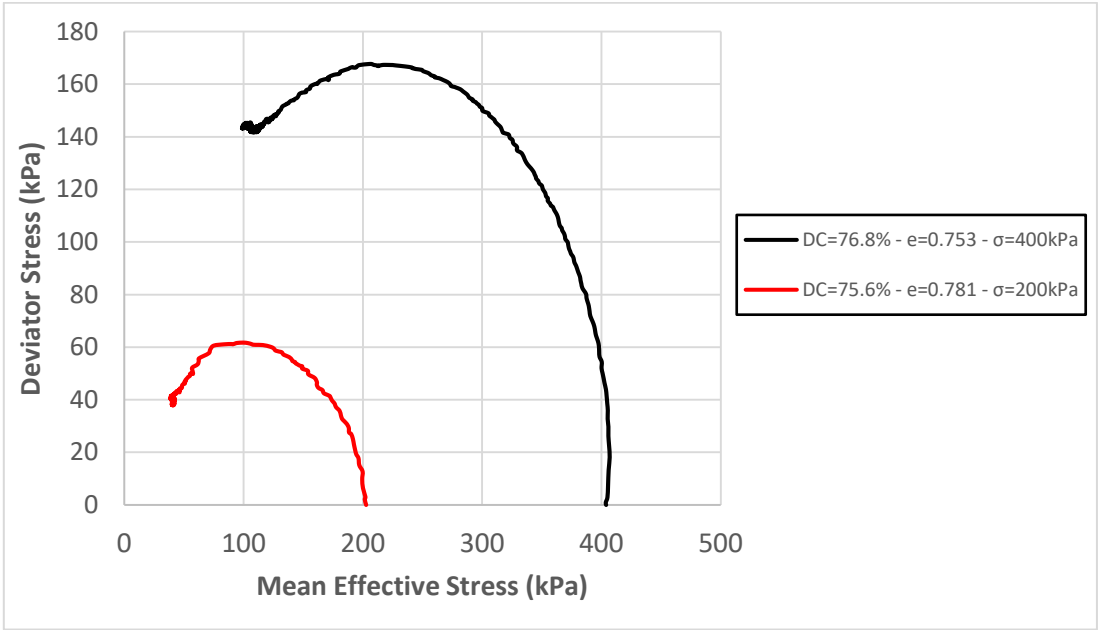

Figure 5.6 Effective Stress Path of tests showing Flow Type behavior

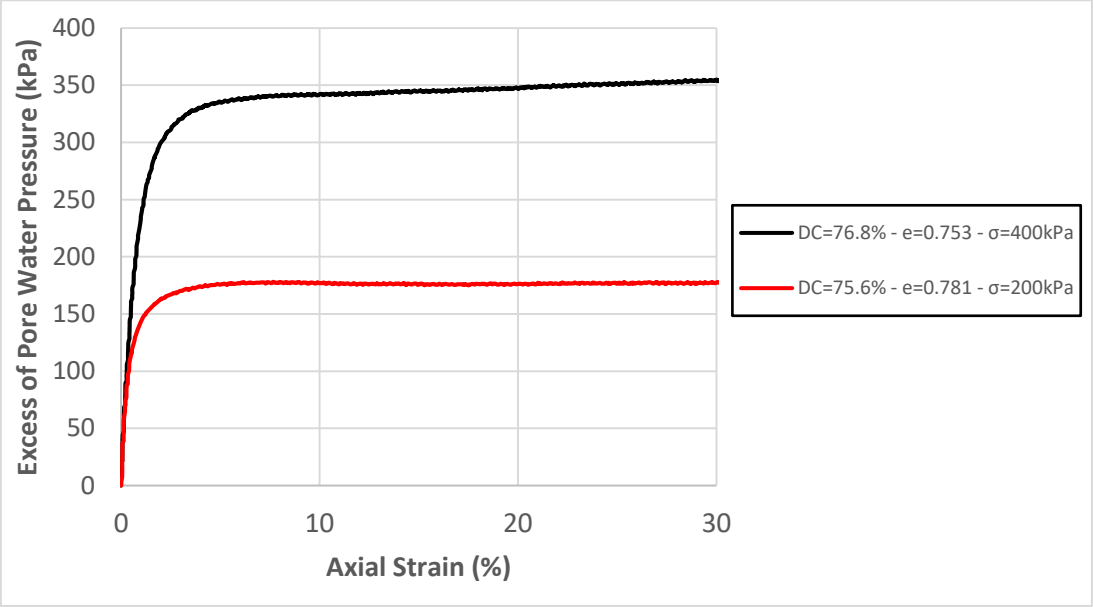

Figure 5.7 Excess Pore Water Pressure of tests showing Flow Type behavior

Table 5.3 Effective confining stress changes due to excess pore water pressure at peak and residual state for soils showing Flow Type behavior

N° of test	Type of Behavior	Final Degree of Compaction (DC_f) (%)	Final Void Ratio (e_f)	Effective Confining Stress (σ'_o) (kPa)	Peak State				Residual State			
					p'_{peak} (kPa)	p'_{peak}/σ'_o (%)	Excess PWP_{peak} (kPa)	Excess PWP_{peak}/σ'_o (%)	p'_{res} (kPa)	p'_{res}/σ'_o (%)	Excess PWP_{res} (kPa)	Excess PWP_{res}/σ'_o (%)
1	Flow Type	75.6	0.781	200	99.7	49.9	123.5	61.8	40.4	20.2	177.3	88.7
2	Flow Type	76.8	0.753	400	205.3	51.3	254.4	63.6	99.4	24.9	354.2	88.6

5.3.2 Flow type with limited deformation or Quasi Steady State Behavior

Quasi Steady State behavior was seen in the other 2 tests. Figures 5.8, 5.11 and 5.12 shows the test results and table 5.4 indicates the changes in the effective confining stress due to excess pore water pressure at peak and quasi steady state.

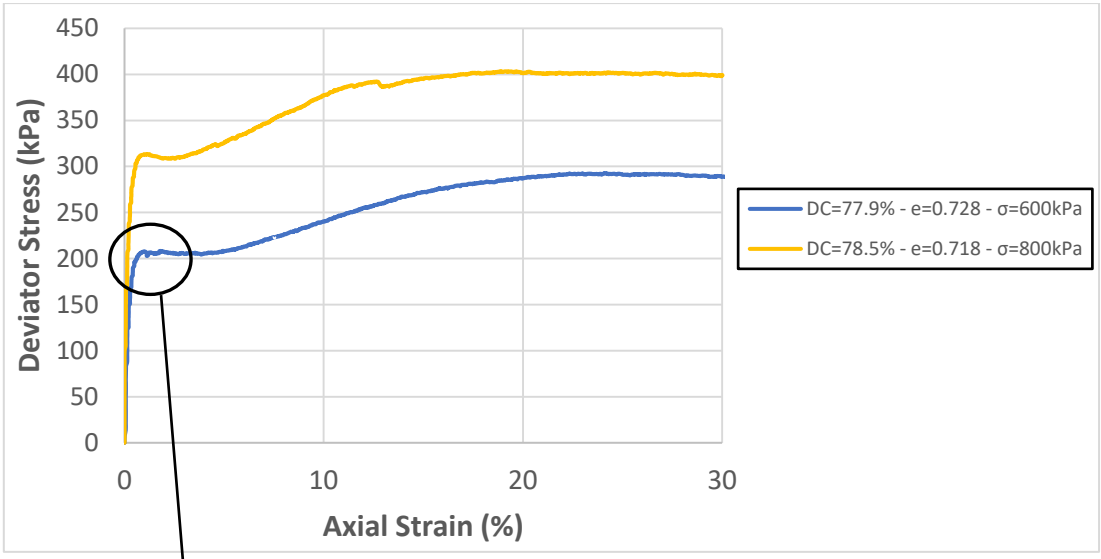

Figure 5.8 Deviator Stress (kPa) vs Axial Strain (%) of tests showing Quasi Steady State behavior

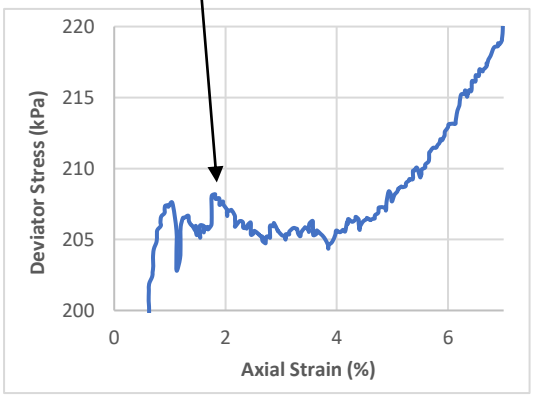

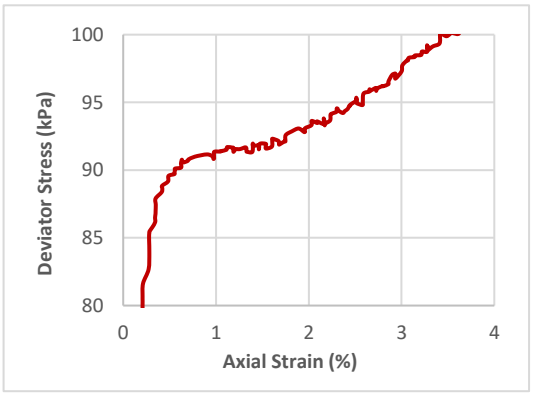

Figure 5.9 and Figure 5.10 Zoom in of Test 3 and comparison with dilative response obtained in actual Bauxite (88.0% of DC at 200 kPa of effective confining stress)

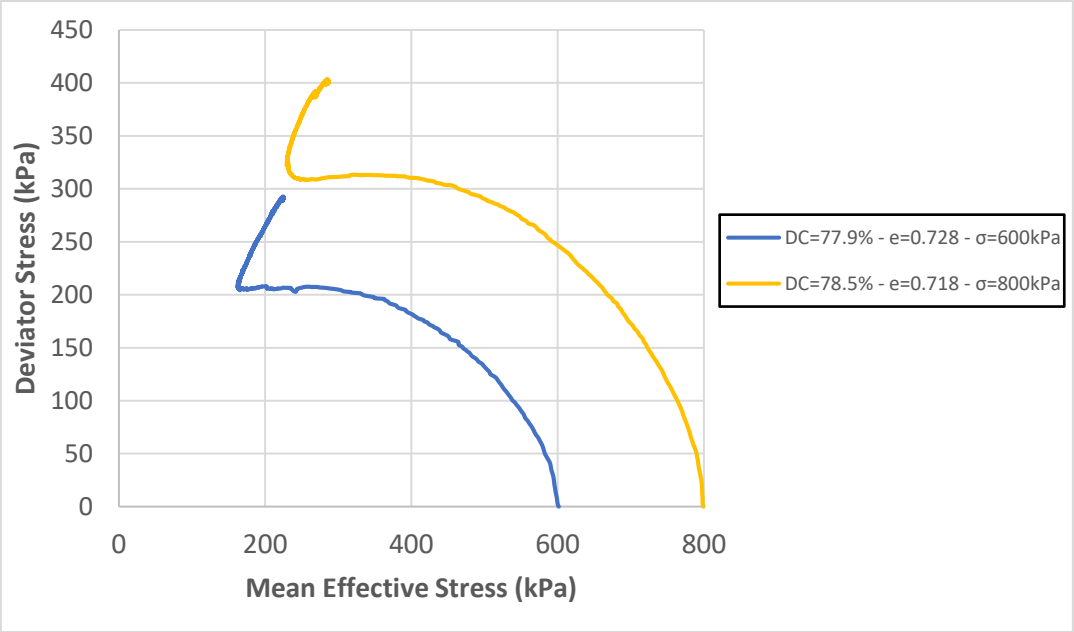

Figure 5.11 Effective Stress Path of Tests showing tests showing Quasi Steady State behavior

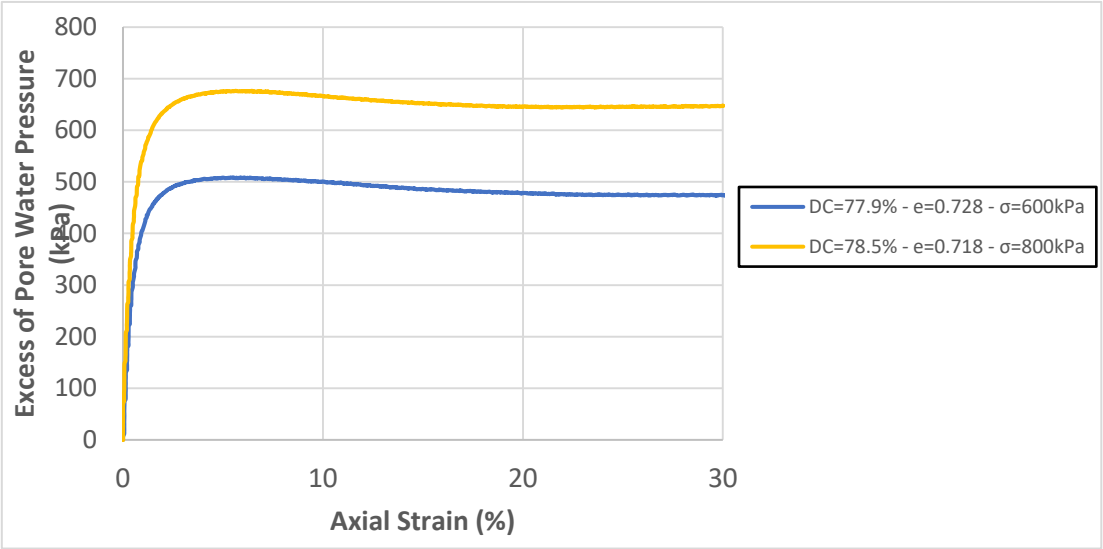

Figure 5.12 Excess Power Water Pressure of Tests showing tests showing Quasi Steady State behavior

As shown in Figure 5.8, tests N°3 and N°4 show a peak in the deviator stress at approximately 1.0% of axial strain. Although in the case of test N°3 test, the post-peak strain-softening is not easy to see at first sight and may even seem like a dilative behavior, but when zooming in (figure 5.9), an abrupt drop after the Peak can be seen, then the deviator stress recovers a little and subsequently it is reduced again to a minimum value after which strain-hardening begins. This behavior is opposed to a dilative response

(figure 5.10) where the deviator stress never drops. Finally, both tests reach a deviator stress of 1.5 times the peak deviator stress at 30% of axial strain.

Table 5.4 shows the effects of pore water pressure increments on the effective confining stress at Peak and Quasi Steady State. On average, the excess pore water pressure reaches more than 70% of the initial confining stress with a maximum of 78.4% for test N°3 at the peak state. At the Quasi Steady State, the excess pore water pressure reaches more than 80% of the initial confining stress.

Table 5.4 Effective confining stress changes due to excess pore water pressure at peak and quasi steady state for soils showing Quasi Steady State behavior

N° of Test	Type of Behavior	Final Degree of Compaction (DC_f) (%)	Final Void Ratio (e_f)	Effective Confining Stress (σ'_o) (kPa)	Peak State				Quasi Steady State			
					p'_{peak} (kPa)	p'_{peak}/σ'_o (%)	Excess PWP_{peak} (kPa)	Excess PWP_{peak}/σ'_o (%)	p'_{qss} (kPa)	p'_{qss}/σ'_o (%)	Excess PWP_{qss} (kPa)	Excess PWP_{qss}/σ'_o (%)
3	QSS	77.9	0.728	600	200.5	33.4	470.1	78.4	165.2	27.5	503.9	84.0
4	QSS	78.5	0.718	800	321.1	40.1	582.1	72.8	259.0	32.4	641.4	80.2

5.3.3 Summary of All Tests

Figures 5.13, 5.14 and 5.15 show all the tests conducted in Simulated BX. Table 5.5 shows the summary of the deviator stress, mean effective stress and the axial strain at peak, Quasi Steady State and Residual state of all tests.

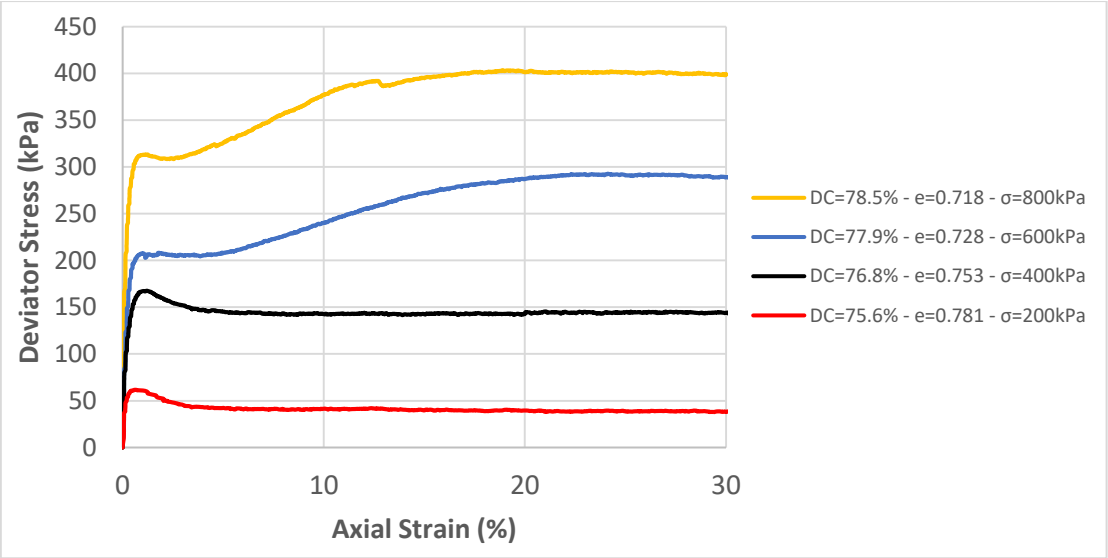

Figure 5.13 Deviator Stress (kPa) vs Axial Strain (%) of all tests

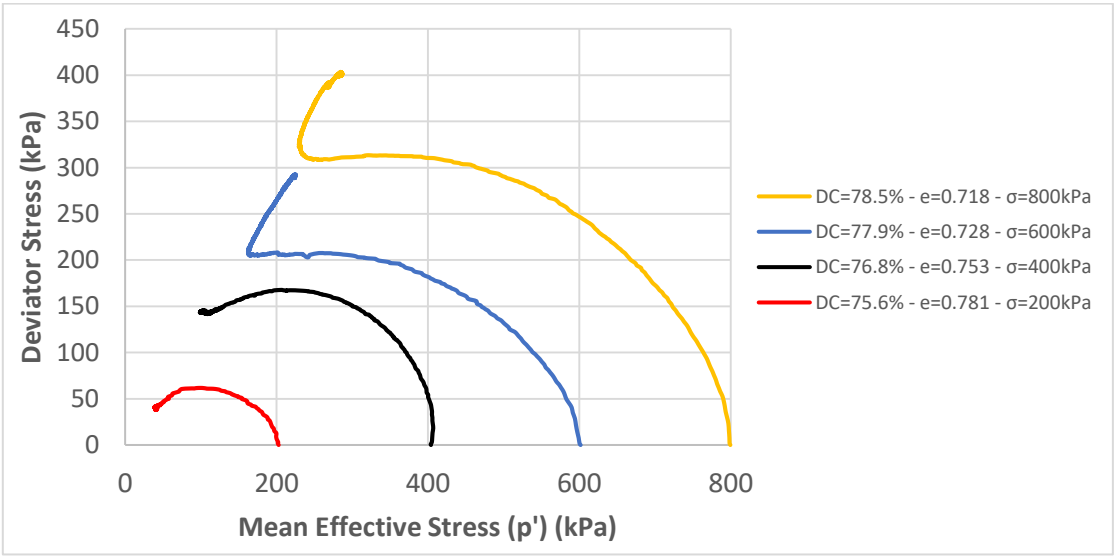

Figure 5.14 Effective Stress Path of all tests

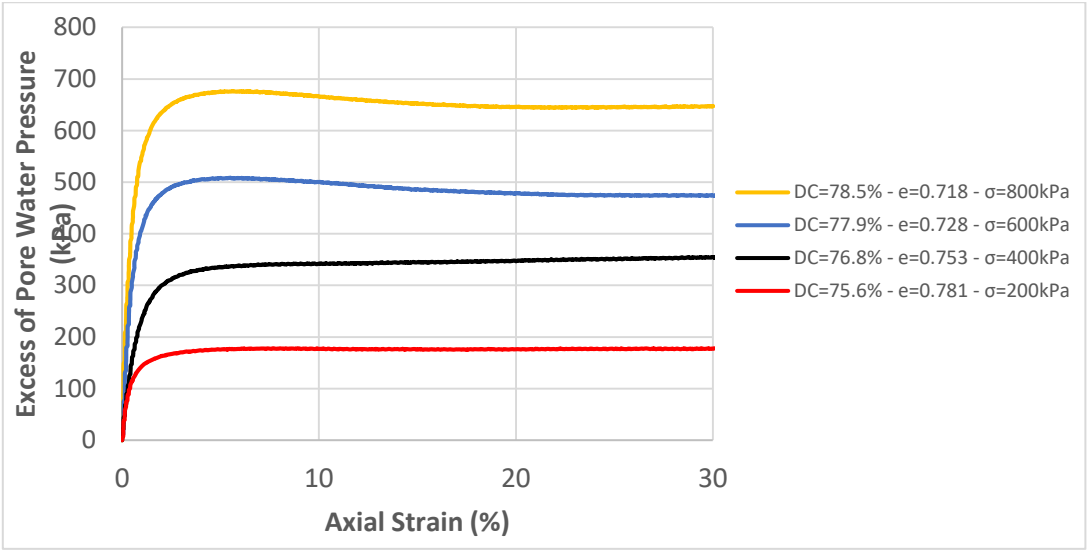

Figure 5.15 Excess Power Water Pressure of all tests

Table 5.5 Summary of Peak, Quasi Steady State and Residual Characteristics of Tests on Simulated Bauxite

N° of test	Type of Behavior	Effective Confining Stress (kPa)	Final Degree of Compaction (DC_f) (%)	Final Void Ratio (e_f)	Peak Characteristics			Quasi Steady State Characteristics			Residual Characteristics		
					q_{peak} (kPa)	p'_{peak} (kPa)	Axial Strain (%)	q_{qss} (kPa)	p'_{qss} (kPa)	Axial Strain (%)	q_{res} (kPa)	p'_{res} (kPa)	Axial Strain (%)
1	Flow Type	200	75.6	0.781	61.7	99.7	0.6	-	-	-	38.4	40.4	30.0
2	Flow Type	400	77.1	0.746	167.7	205.3	1.2	-	-	-	143.4	99.4	30.0
3	QSS	600	77.90	0.729	208.2	200.5	1.8	204.3	165.2	3.8	288.9	223.4	30.0
4	QSS	800	78.5	0.717	313.4	321.1	1.2	308.4	259.0	2.2	399.0	281.0	30.0

5.3.4 Comparison of Simulated BX and actual BX

To compare Simulated BX and actual BX, 2 tests with similar confining stress and void ratio will be used:

- ✓ Test on BX with 89.8% of DC (e=0.731) at 600 kPa of confining stress showing Quasi Steady State behavior from chapter 4
- ✓ Test on Simulated BX with 77.9% of DC (e=0.728) at 600 kPa of confining stress showing Quasi Steady State behavior

The responses of stress strain, effective stress path and pore water pressure increments of both tests are observed in figures 5.16, 5.17 and 5.18 respectively.

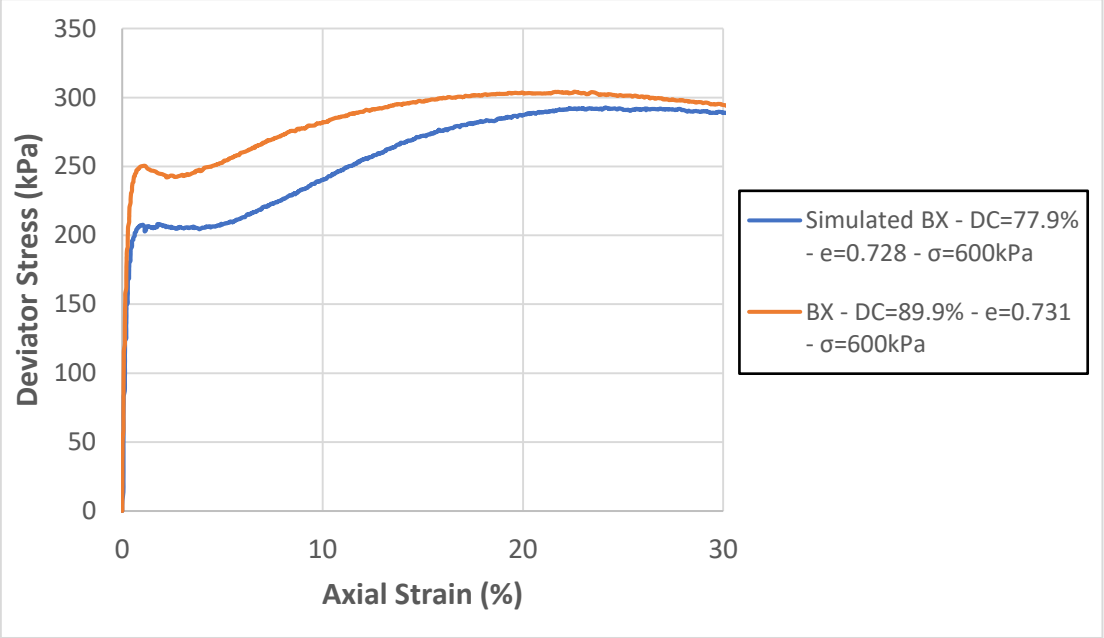

Figure 5.16 Stress Strain of tests on BX and Simulated BX for comparison

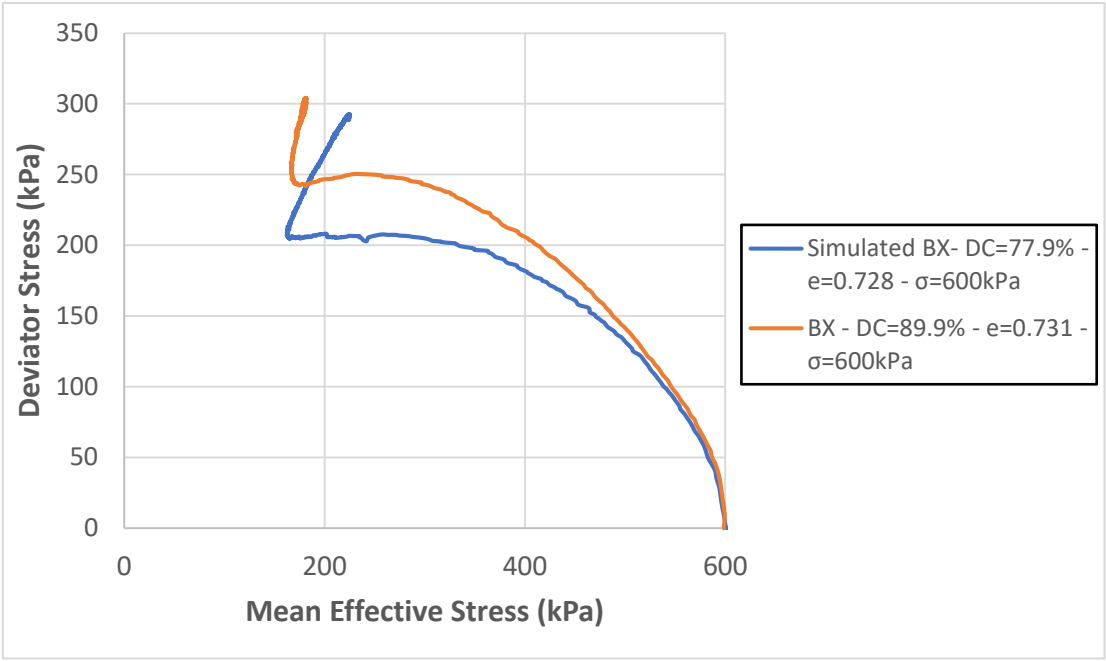

Figure 5.17 Effective Stress Path of tests on Bx and Simulated BX for comparison

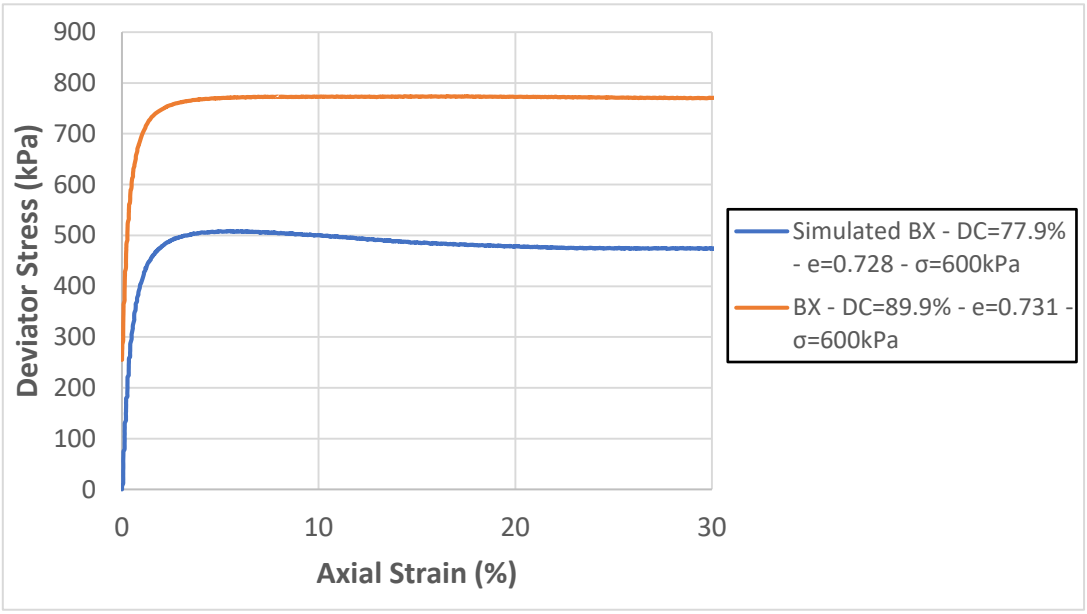

Figure 5.18 Excess Pore Water Pressure of tests on Bauxite and Simulated Bauxite for comparison

Figure 5.16 shows that both materials reach the peak at similar levels of axial strain, but actual BX has a higher peak deviator stress (250 kPa against 208 kPa). The strain-softening in BX is more pronounced and the Quasi Steady State occurs at a lower level of axial strain than in Simulated BX (2.5% against 3.8% of axial strain). However, at the residual level both display very similar deviator stress.

From figure 5.17, it can be noted that the initial effective confining stress (600 kPa) of both tests are reduced in a very similar way, reaching an almost identical minimum value (162kPa of Simulated BX against 167kPa of BX); however, BX requires greater excess pore water pressure to reach such state (780kPa), while Simulated BX only requires 500 kPa as shown in Figure 5.18. This means that the negative dilatancy developed by BX is lower than Simulated BX under similar conditions which can be interpreted as BX showing bigger resistance to pore water pressure increments and therefore a bigger resistance to liquefaction.

5.3.5 Steady State Line

As mentioned in the literature review, the final state of soils presenting Flow Type behavior belongs directly to the Steady State Line (SSL), so the residual states of tests N°1 and N°2 form a line which can be regarded as the SSL. Then, this line was projected linearly in the plane e vs Log (p ') and it was observed that the final states of tests N°3 and N°4 are very close to such line. In addition, observing Figure 5.13, tests N°3 and N°4 present a constant deviator stress after 20% of axial strain. The confining stress is also constant in the last 5% of axial strain of both tests and together with the undrained condition of the test and the fixed strain rate fulfills the requirements proposed by Poulos (1981) for a soil to be considered at the Steady State. Thus, it can be concluded that tests N°3 and N°4 have also reached the SSL. Figure 5.19 shows the Steady State Line (SSL) proposed for Simulated BX.

Figure 5.20 shows the SSL obtained for Simulated BX (blue color with square dots) along with the SSL of BX shown in chapter 4 (red color), and other materials: Toyoura Sand (Verdugo, 1992), Iron Ore Fines (Wang et al, 2018) and silty sands with different content of fines (Kwa and Airey, 2017). It is worth mentioning that Kwa and Airey (2017) obtained different SSL for a same soil but prepared in dense and loose conditions.

The SSL of Simulated BX is very similar to the SSL of Iron Ore Fines (black line) and the Silty Sand with 100% fines (yellow line), but it is below the SSL of actual BX, which indicates that there are states of density and confining stress for which BX is not susceptible to Flow Failure (dilative response), but at which Simulated BX is susceptible (contractive response). This is a second indication that BX has greater resistance to liquefaction than Simulated BX.

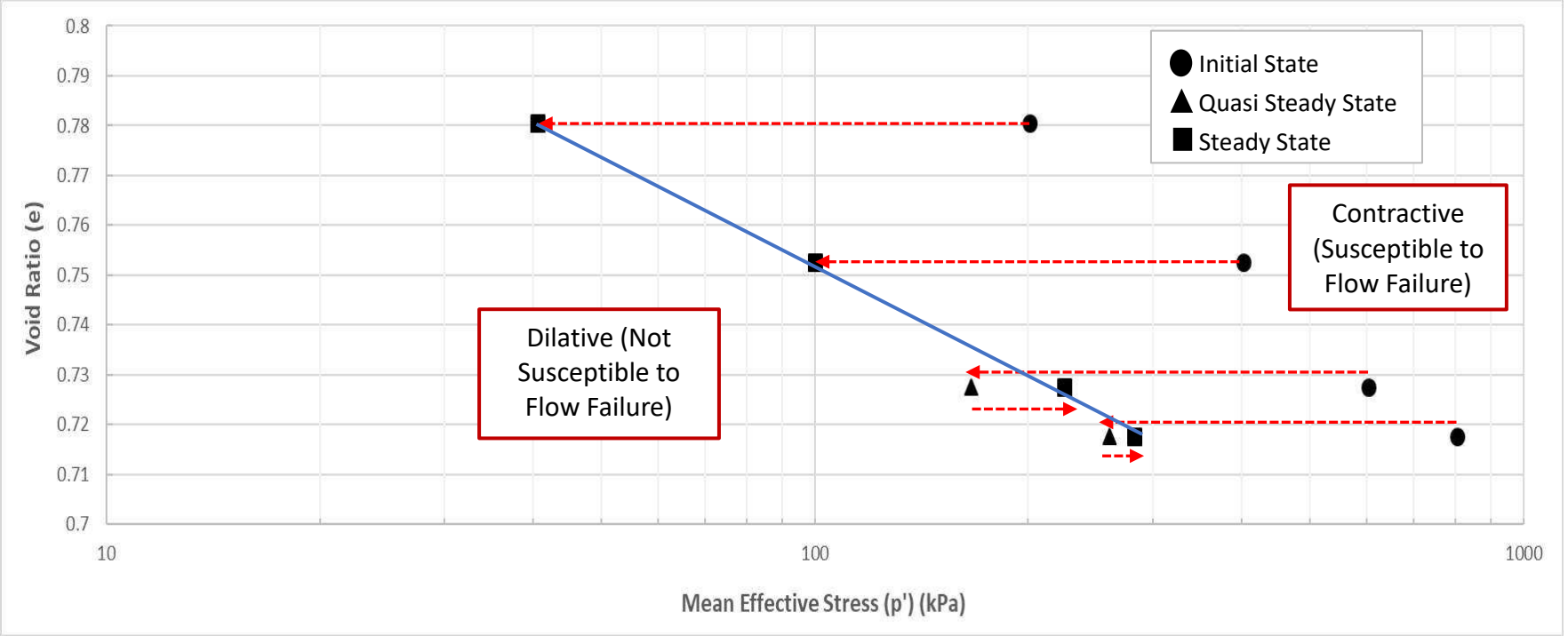

Figure 5.19 Steady State Line of Simulated Bauxite

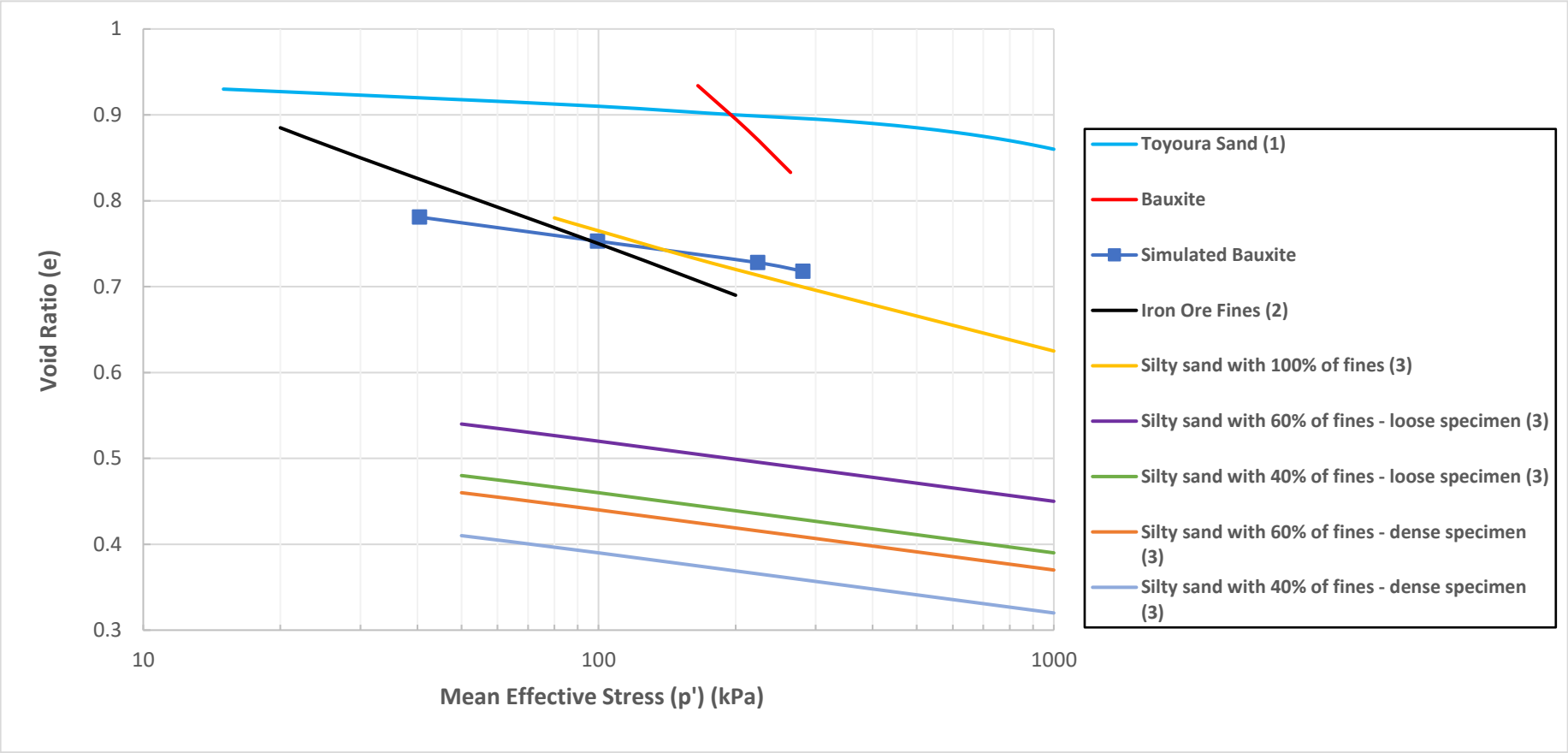

1. Verdugo (1992)
2. Wang et al (2018)
3. Kwa and Airey (2017)

Figure 5.20 Steady State Line of Bauxite, Simulated Bauxite and other materials

5.3.6 Shear Strength Parameters

5.3.6.1 Critical State Friction Angle

By plotting all the final states of the tests, the figure 5.21 can be obtained. It is assumed that cohesion is zero since Simulated BX showed no plasticity and cement was not included in the mixture.

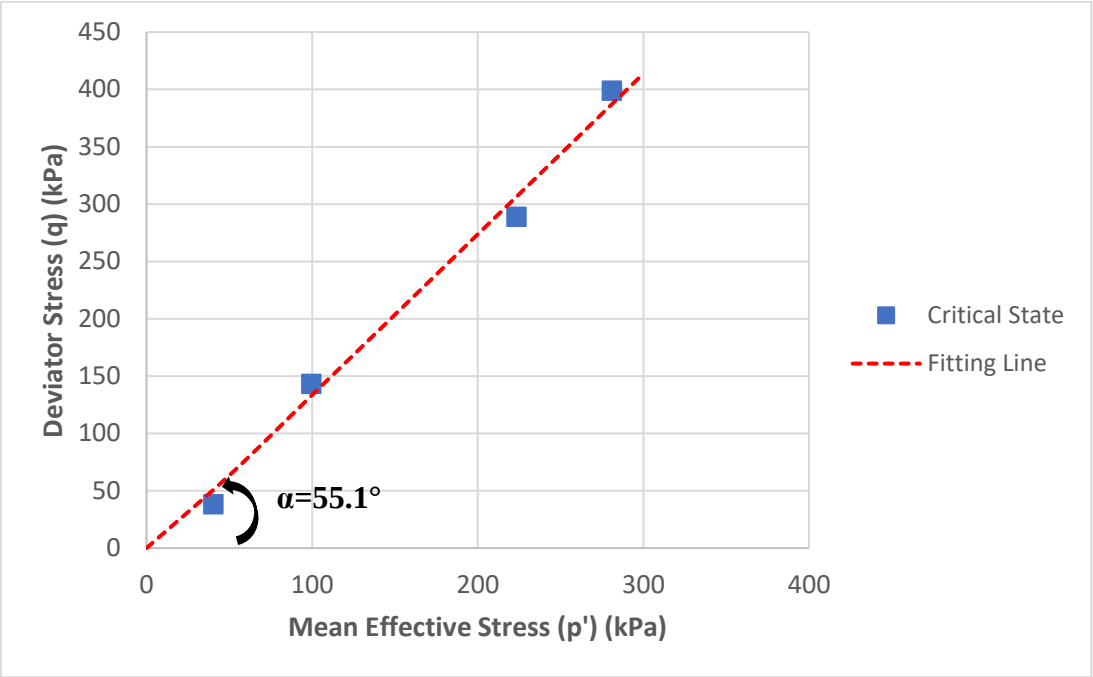

Figure 5.21 Critical State Line in q vs p' plane

Then, using the expressions of Critical State Soil Mechanics:

$$\tan 55.1° = \frac{6 \sin \emptyset'}{3 - \sin \emptyset'}$$

$$\emptyset' = 35.3°$$

$$M_{CSL} = 1.433$$

Figure 5.22 shows the ultimate states at 30% of all the tests in the plane q/2-p'.

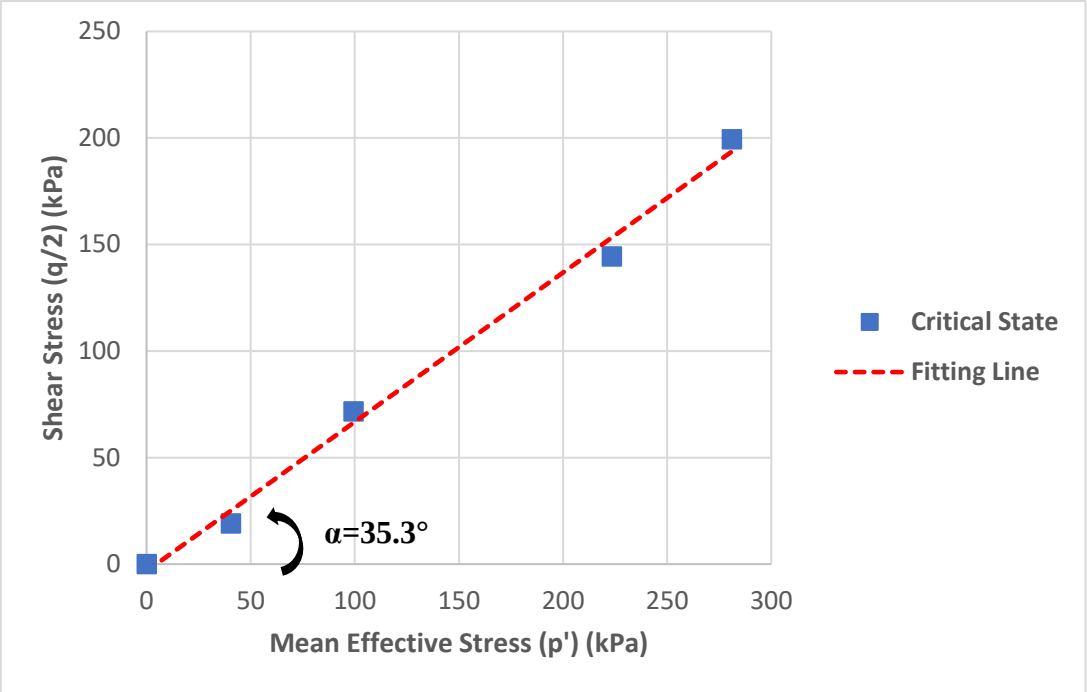

Figure 5.22 Critical State Line in q/2 vs p' plane

Figures 5.23 and 5.24 compare the critical state line (CSL) in the q vs p' and q/2 vs p' planes of Simulated BX with the results of actual BX showed in chapter 4 and with other materials: Toyoura Sand (Verdugo, 1992), silty sands with 100%, 60%, 40%, 20% and 18% of fines (Kwa and Airey, 2017) and Iron Ore Fines (Wang et al, 2018). Simulated BX has bigger critical state friction angle than Toyoura sand, but lower than actual BX (35.3° against 37.6°) and all the silty sands.

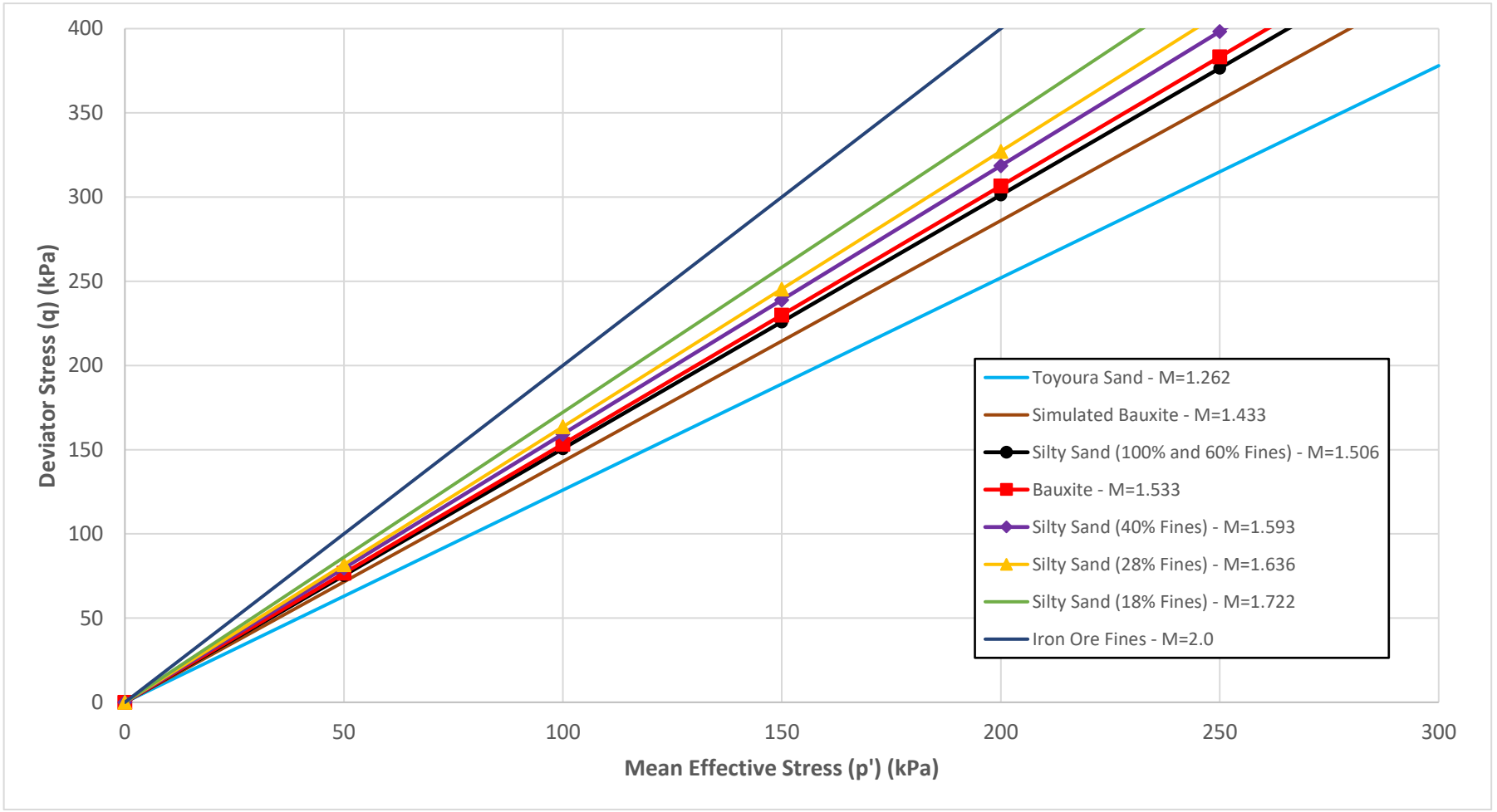

Figure 5.23 Critical State Line in q vs p’ plane of Simulated BX and other materials

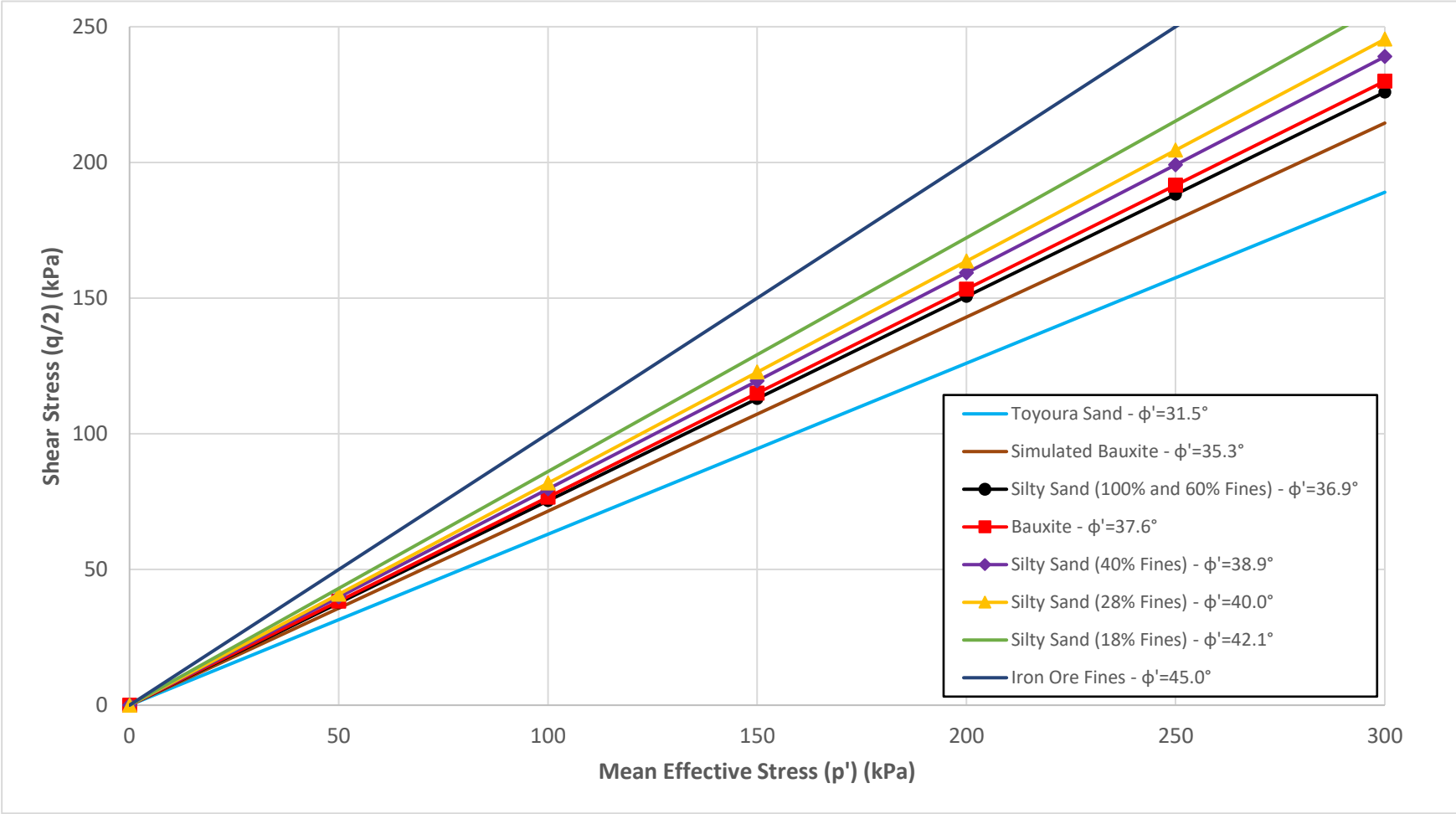

Figure 5.24 Critical State Line in q/2 vs p' plane of Simulated BX and other materials

5.3.6.2 Post-liquefaction Shear Strength

Since both Flow type and Flow with limited deformation (Quasi Steady State) behaviors were obtained, the post-liquefaction shear strength will be estimated in both states using the following expressions:

- ✓ Undrained Shear Strength Mobilized at the Steady State:

$$S_{us} = \frac{q_{ss}}{2} \text{ (Castro et al, 1992)}$$

Where q_{ss} is the deviator stress at the Steady State

- ✓ Undrained Shear Strength Mobilized at the Quasi Steady State:

$$S_{qss} = \frac{q_s}{2} * \cos \emptyset_s \text{ (Ishihara, 1993)}$$

Where $\emptyset_s$ and q_s are the mobilized friction angle and the deviator stress at the quasi steady state respectively.

The results of applying the two expressions are shown in table 5.7. There is not enough data to propose a ratio $\frac{S_{us}}{\sigma'_o}$ as it was done for BX in chapter 4, but the post-liquefaction shear strength of tests with similar void ratio and confining stress can be compared as in section 5.3.4 (Table 5.6), noting that Bauxite has greater resistance.

Table 5.6 Comparison of Post-Liquefaction Shear Strengths of BX and Simulated BX

Material	Final Degree of Compaction (DC_f) (%)	Final Void Ratio (e_f)	S_{qss} (kPa)	Effective Confining Stress (kPa)	Normalized S_{qss}/σ'_0
BX	89.8	0.731	105.6	600	0.18
Simulated BX	77.9	0.728	90.8	600	0.15

Table 5.7 Summary of Normalized Mobilized Shear Strength at Steady State and Quasi Steady State

Type of Behavior	Final Degree of Compaction (DC_f) (%)	Final Void Ratio (e_f)	q_{ss} (kPa)	S_{us} (kPa)	q_{qss} (kPa)	ϕ'_{qss} (PPT)	S_{qss} (kPa)	Effective Confining Stress (kPa)	Normalized S_{us}/σ'_0	Normalized S_{qss}/σ'_0
Flow Type	75.6	0.781	38.4	19.2	-	-	-	200	0.10	-
Flow Type	76.8	0.753	143.4	71.7	-	-	-	400	0.18	-
QSS	77.9	0.728	-	-	204.3	27.3°	90.8	600	-	0.15
QSS	78.5	0.718	-	-	308.4	27.7°	136.6	800	-	0.17

5.3.7 Collapse Surface

Figure 5.25 shows the collapse surfaces obtained for the 4 tests in simulated BX and the Critical State Line. As in Chapter 4, it was decided that the collapse surface pass through the origin of coordinates.

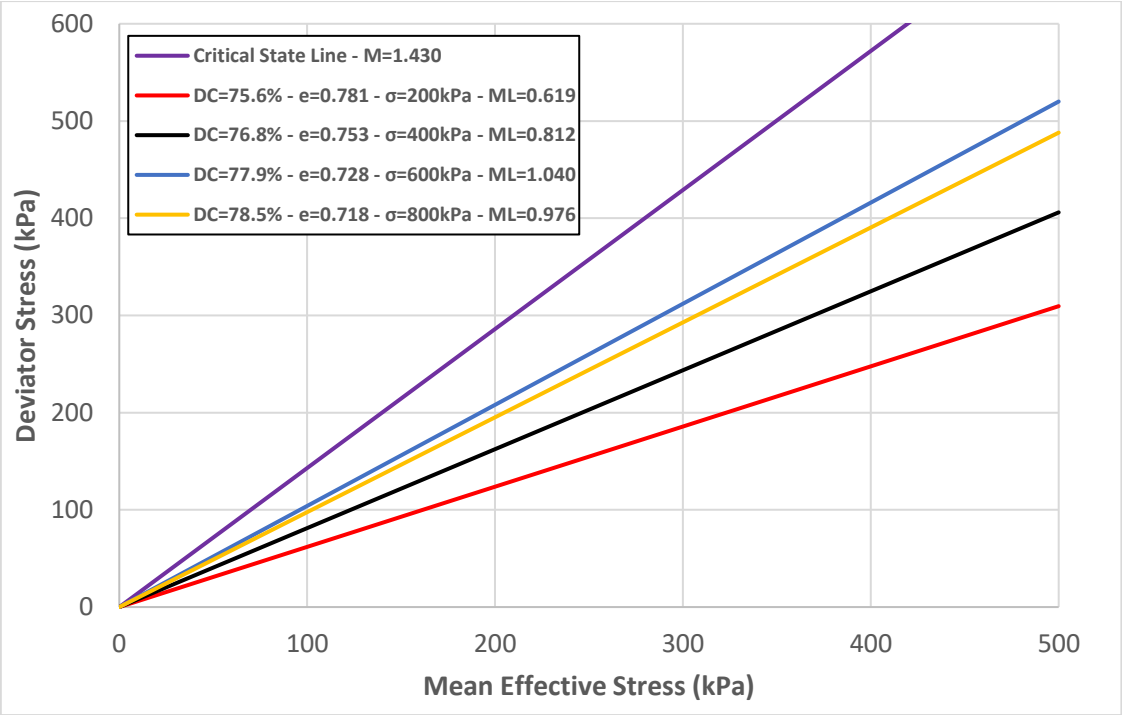

Figure 5.25 Collapse Surface for all tests on Simulated Bauxite

The closeness of a soil's state to the collapse surface in the p' vs q plane is a good indicator of the susceptibility to Flow Failure. According to Sladen et al (1985), if a state of a soil reaches the Collapse Surface, it will inevitably undergo Flow Failure. Then, in the same way as in 5.3.4, the collapse surface of BX and Simulated BX with similar void ratio and confining stress will be compared. As can be seen in figure 5.26, actual BX has a collapse surface with a steeper slope (M_L = 1.089) than Simulated BX (M_L = 1.040), which indicates that, although slightly, it is less susceptible to Flow failure requiring higher loads to reach the collapse surface. This is a third indication that BX has greater resistance to liquefaction than the Simulated BX, probably due to its higher level of plasticity and clay content (IP = 10.9).

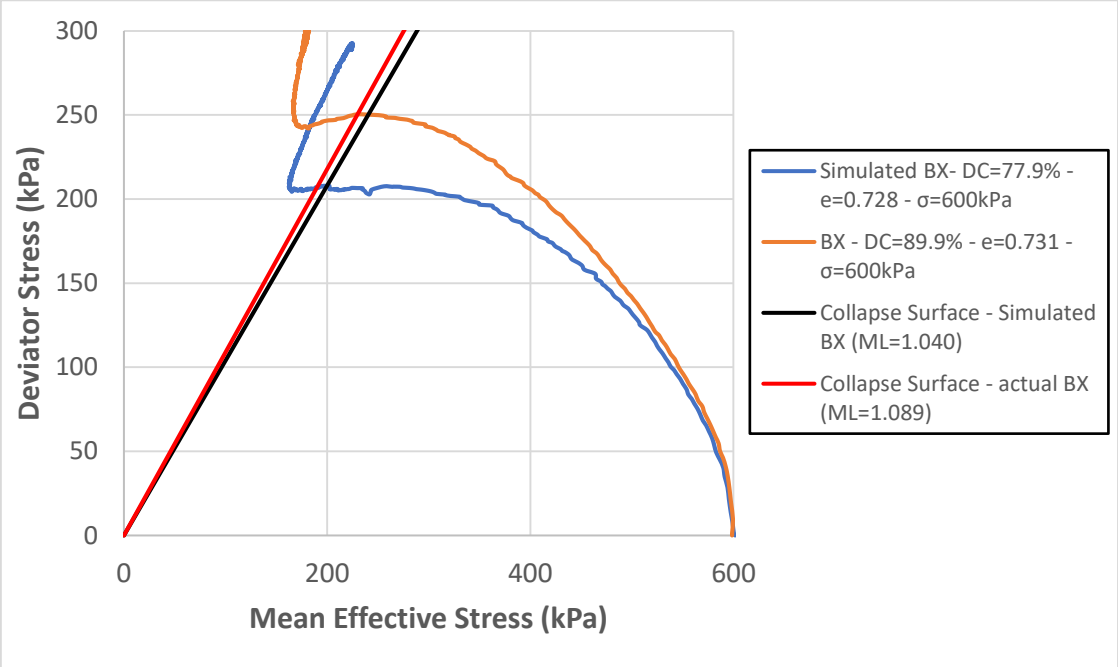

Figure 5.26 Comparison of Collapse Surfaces of Simulated BX and Actual BX

6. CONCLUSIONS AND RECOMENDATIONS

6.1 CONCLUSIONS

This thesis studied the undrained monotonic behavior of saturated Bauxite with the objective of identifying the state conditions (density and effective confinement pressure) that favor the susceptibility of Bauxite to liquefaction. This will help to prevent Flow failure in Aluminum Ore Heaps in Bulk Cargoes that has caused capsizing of vessels. The report of the conclusions will be made according to the general objective and the specific objectives.

General Objective: To study the undrained monotonic behavior at large deformations of Bauxite under several conditions of density and effective confining stress

Specific Objectives:

- ✓ To verify the applicability of the Steady State theory to this type of soil
- ✓ To estimate undrained residual shear strength for the post-seismic stability analysis of bauxite heaps
- ✓ To compare the behavior of Bauxite with a mixture of Silica Sands of similar particle size distribution

6.1.1 General Conclusions

a) Bauxite possess a high level of compressibility as noted from consolidation test results where it can be seen than even dense specimens (more than 80% of DC) undergo more than 10% of volumetric strain.

b) As most sandy soils, Bauxite does not present a unique Isotropic Consolidation Line (ICL). For loose soils (70% of DC), a single ICL showed a fair level of fitting until 300 kPa of confining pressure. However, for denser samples many ICL were seen.

c) Bauxite shows only two types of undrained response: flow with limited deformation and dilation. Even for the loosest density condition achieved by using moist-tamping and a very small effective confining stress (e=1.322 and 25 kPa), it was not possible to obtain flow type behavior.

d) The post-peak local minimum deviator stress (Quasi Steady State) can be better seen at higher confining stress (starting from 400kPa) and occurs in levels of axial strain within 2.2% to 7.6%.
e) All soils showing Quasi Steady State present a residual deviator stress much higher than the peak deviator stress. In samples starting from 600 kPa of confining stress, a second small strain-softening occurs at large deformations evidencing the onset of particle crushing.
f) On average, the excess pore water pressure for all tests showing Quasi Steady State behavior reaches 73% of the initial confining stress with a maximum of 80.5% for the case of 84.8% of DC at 1000 kPa. However, none of the tests fulfills the criteria to define initial liquefaction which requires the water pressure excess to build up to a value of 100%. Hence, for all these cases the mechanism occurring at the peak state due to pore water pressure increments was regarded not as liquefaction, but as collapse of granular soils.
g) No shear banding was observed in the tests after the monotonic loading
h) Even soils with dilative response showed a considerable contractive behavior which induces a reduction in the effective confining pressure until the Point of Phase Transformation. The excess pore water pressure in dilative samples increases up to an average of 81% of the effective confining stress, being even higher than for the contractive soils at the peak state where collapse starts. At this point the effective confining stress is reduced to an average of 40% of its initial value, so despite not undergoing collapse (peak deviator stress and strain-softening) the stiffness of the soil is greatly reduced.
i) Critical State Theory was used to obtain the effective friction angles at large strains. Cohesion existed (5.4 kPa) but was not considered as it is very small.
j) The effective friction angle at the critical state was 37.6° which is larger than Toyoura Sand (31.5°) and a feldspar silty sand with 100% and 60% of fines (36.9°). However, Bauxite's critical friction angle is lower than feldspar silty sands with 40% of fines (38.9°), 28% of fines (40.0°), 18% of fines (42.1°) and Iron Ore Fines (45°).
k) Particle Crushing effects were studied by analyzing changes in gradation. Changes were seen since 400 kPa of confining stress, but only since 600 kPa of confining stress there was an important increment of medium and fine sands (10% on average)

l) In the case of the test at 1000 kPa of confining stress there was a significant increase in the content of sands reaching up to 20% for particles greater than 0.425 mm and 17% for particles greater than 0.85 mm (coarse sands). For the sample not placed on the oven an increase of 10% on average in fines and fine was observed (particles less than 0.106 mm). The increment in the fine matrix was later confirmed by using microscopic images.

6.1.2 Specific Objective 1

a) An area separating dilative than contractive responses was narrow down which probes the applicability of the Steady State Theory for Bauxite, although only 3 tests reach the Steady State Line.
b) Besides the 3 tests mentioned above, 3 additional tests fulfill with the rigorous definition of the Steady State as are the cases of 72.5% of DC (e=1.143) at 100 kPa, 77% of DC (e=1.019) at 200 kPa, and 79.7% of DC (e=0.950) at 400 kPa. Nevertheless, these 3 tests did not reach the proposed SSL probably because a lack of accuracy in void ratio estimation.

6.1.3 Specific Objective 2

a) The undrained shear strength mobilized at the Quasi Steady State was obtained for 11 tests showing values ranging from 3.7 kPa to 167.9 kPa. These values were established as post-liquefaction shear strength for stability analysis.
b) The aforementioned values were normalized with respect to the effective confining stress and plotted against their void ratio showing little scattering which means that, unlike other sandy soils, Bauxite has a unique ratio $\frac{S_{qss}}{\sigma'_o}$
c) The average ratio $\frac{S_{qss}}{\sigma'_o}$ was defined as 0.16 which lies within the database of ratios obtained from laboratory tests (0.02-0.22) although it is a bit higher than ratios obtained from back analysis of failures (0.05-0.12)
d) The average ratio $\frac{S_{qss}}{\sigma'_o}$ corresponds to the Quasi Steady State at which the effects of initial fabric are still not completely erased. Hence, this value may be different if triaxial testing of Bauxite is conducted using other methods of sample preparation.

e) Since laboratory-based post-liquefaction shear strengths are not conservative, it is suggested to apply a safety factor of 50% for engineering applications establishing the ratio as 0.08.

6.1.4 Specific Objective 3

a) A mixture of Silica Sands N° 3, 5, 7, 8 and 9 was used to prepared (Simulated BX) a soil with the same content of fines and gradation of Bauxite (BX).
b) Simulated BX showed a lower specific gravity (2.613) than actual BX (2.642)
c) Some key differences between the two are:
    - Fines gradation: The fines content is the same, but the fines of BX have better gradation and higher clay content (15.4% against 0.35%).
    - Plasticity: Bauxite has a certain level of plasticity (IP = 10.9), but Simulated BX does not have any plasticity at all
    - Mineralogy: BX have predominantly metallic minerals and in smaller proportion clayey minerals (Montmorillonite). Simulated BX is mainly composed of Quartz.
    - Particle shape: Coarse sands included in the Simulated BX possess predominantly angular particles, while BX has sub-angular particles
d) Simulated BX presented both flow type behavior and flow with limited deformation (Quasi Steady State) and it was possible to draw the Steady State Line for it
e) Simulated BX is less compressible than actual BX. In tests conducted in BX, even dense soils (more than 80% of DC) undergo on average 10% of volumetric strain when subjected to confining stress up to 800 kPa, whereas Simulated BX only undergoes 4.5% of volumetric strain at 800 kPa of confining pressure.
f) To compare Simulated BX and actual BX, two tests of similar final void ratio and effective confining stress were used:
    - Test on BX with 89.8% of DC (e=0.731) at 600 kPa of confining stress showing Quasi Steady State behavior
    - Test on Simulated BX with 77.9% of DC (e=0.728) at 600 kPa of confining stress showing Quasi Steady State behavior

g) Actual BX has a higher peak deviator stress (250 kPa against 208 kPa) than Simulated BX. The strain-softening in BX is more pronounced and the Quasi Steady State occurs at a lower level of axial strain than in Simulated BX (2.5% against 3.8% of axial strain). However, at the residual level both display very similar deviator stress.

h) The effective stress path that both tests follow until the critical state is very similar reaching an almost identical minimum value of effective confining pressure (162kPa of Simulated BX against 167kPa of BX). Nevertheless, actual BX required a higher excess pore water pressure to reach such value (780kPa approximately), whereas Simulated BX only required 500 kPa of excess pore water pressure indicating that negative dilatancy developed by BX is lower than Simulated BX under similar conditions. This is a first sign that actual BX has greater resistance to liquefaction than simulated BX.

i) Actual BX has greater post-liquefaction shear strength than Simulated Bauxite when the two similar tests are compared (105.6 kPa against 90.8 kPa).

j) The SSL of Simulated BX is below the SSL of actual BX. Therefore, there are states of density and confining pressure for which actual BX is not susceptible to Flow Failure (dilative response), but at which Simulated BX is susceptible (contractive response). This also implies that actual BX possess greater resistance to liquefaction than simulated BX.

k) Actual BX has a steeper collapse surface (M_L = 1.089) than Simulated BX (M_L = 1.040) which allows to conclude that actual BX requires greater reduction in effective confining stress to undergo Flow Failure. This is a third sign that BX has greater resistance to liquefaction than the Simulated BX

l) From the 3 signs mentioned above, it is possible to conclude that actual BX shows more resistance to the development of excess pore water pressure and therefore it is more resistant to liquefaction than Simulated BX. This is probably due to the higher level of plasticity and clay content (IP = 10.9) of BX.

m) Despite being prepared by almost purely Quartz sands and silts, the critical state friction angle of Simulated BX (ϕ'=35.3°) is smaller than actual BX (ϕ'=37.6°). This is probably because of Bauxite's stronger mineralogy and particle shape (sub-angular).

6.2 RECOMMENDATIONS

a) It is suggested to test Bauxite with different sample preparation methods and different equipment (Shear Ring, Torsional Shear) aiming to find whether is possible or not to obtain in laboratory the flow type behavior.
b) It is recommended to conduct tests at higher confining stress to establish the threshold at which the Steady State Line changes its slope due to particle crushing.
c) The application of the concepts of granular void ratio is highly encouraged for soils with high content of non-plastic fines like Bauxite in subsequent studies.
d) Further research is needed to improve the accuracy in measuring the void ratio after consolidation since the Steady State Line is very sensitive to it
e) The data of this thesis can be used to calibrate a constitutive model for simulating the collapse of Bauxite under shipping loads. The constitutive models developed by Lade (1992) and “Nor-Sand” by Jefferies (1993) are suggested.

REFERENCES

- Ahmed, B. (2016) “Flow Failure of Saturated Iron Ore Fines under Undrained Monotonic Loading”, The University of Tokyo - Master of Engineering Thesis
- Alarcon-Guzman, A.; Leonards, G. A. and Chameau, J. L. (1988) “Undrained Monotonic and Cyclic Strength of Sands”, *Journal of Geotechnical Engineering*, Vol. 114, n° 10, pp. 1089-1109
- Alberto Hernández, Y. (2014), “Undrained Behavior of Sand with Non-plastic Silts and its Application to Ground Deformation Analysis”, PhD Thesis, The University of Tokyo
- Ampadu, S. K. and Tatsuoka, F. (1993) “Effect of Setting Method on the Behavior of Clays in Triaxial Compression from Saturation to Undrained Shear” *Soils and Foundations*, vol. 33, nº 2, pp. 14-34
- Atkinson, J. H. and Bransby, P. L. (1978) “The Mechanics of Soils: An Introduction to Critical State Soil Mechanics”, London - McGraw-Hill
- Baziar, M. H. and Dobry, R. (1995) “Residual Strength and Large Deformation Potential of Loose Silty Sands” *Journal of Geotechnical Engineering*, vol. 121, nº 12, pp. 896-906
- Black, D. K. and Lee, K. L. (1973) “Saturating Laboratory Samples by Back Pressure” *Journal of the Soil Mechanics and Foundations Division*, vol. 99, nº 1, pp. 75-93
- Bowles, J. E. (2012) “Engineering Properties of Soils and their Measurements” 4th edition, McGraw Hill Education
- Brandon, T. L.; Rose, A. T. and Duncan, J. M. (2006) “Drained and Undrained Strength Interpretation for Low-plasticity Silts” *Journal of Geotechnical and Geoenvironmental Engineering*, vol. 2, nº 132, pp. 250-257
- Casagrande, A. (1936) “Characteristics of Cohesionless Soils Affecting the Stability of Slopes and Earth Fills”, *Journal of the Boston Society of Civil Engineers*
- Casagrande, A. (1975) “Liquefaction and Cyclic Deformations of Sands - A Critical Review”, Proceedings of the 5th Pan-American Conference on Soil Mechanics and Foundation Engineering, Buenos Aires, Argentina
- Castro, G. (1969) “Liquefaction of Sands” PhD Thesis, Harvard University

- Castro, G. and Poulos, S. (1977) “Factors Affecting Liquefaction and Cyclic Mobility”, *Journal of the Geotechnical Engineering Division*, vol. 103, nº 6, pp. 501-506
- Castro, G. and Troncoso, J. (1989) “Effects of 1989 Chilean earthquake on three tailings dams” Proceedings of the 5th Chilean Conference on Seismology and Earthquake Engineering - Santiago, Chile
- Castro, G.; Seed, R. B.; Keller, T. O. and Seed, H. B. (1992) “Steady State Strength Analysis of Lower San Fernando Dam Slide” *Journal of Geotechnical Engineering*, vol. 118, nº 3
- Consolidation and shear stage of triaxial compression test (from Web-site). Available in http://www.soilmanagementindia.com (Visited on April 2018)
- Corps of Engineers, U.S. Dept. of the Army (1939) “Report on the Slide of a Portion of the Upstream face at Fort Peck Dam” U.S. Government Printing Office, Washington, D.C.
- Finn, L. W. (1998) “Estimating Post-Liquefaction Displacements in Embankments Dams and Prioritizing Remediation Measures”, Proceedings of the Fourth International Conference on Case Histories in Geotechnical Engineering. St. Louis, Missouri
- GEO-SLOPE International (2007) “Procedures and Methods for a Liquefaction Assessment using Geostudio 2007”, Alberta, Canada
- Ghafghazi, M.; Shuttle, D. A. and DeJong, J. T. (2014) “Particle Breakage and the Critical Sate of Sand”, *Soils and Foundations*, vol. 54, nº 3, pp. 451-461
- Global Bauxite Working Group (2017) “Report on Research into the Behavior of Bauxite during Shipping” – Technical Report. Available in http://tmltesting.com/w/images/e/e7/Global_Bauxite_WG_report_CCC_4-INF.10-Annexes.pdf
- Gu, J.; Huang, Z.; Fan, H.; Jin, Z.; Yan, Z. and Zhang, J. (2013) “Mineralogy, geochemistry, and genesis of lateritic bauxite deposits in the Wuchuan–Zheng'an–Daozhen area, Northern Guizhou Province, China” *Journal of Geochemical Exploration*, vol. 130, pp. 44-59
- Hardin, B. O. (1985) “Crushing of Soil Particles” *Journal of Geotechnical Engineering*, vol. 111, nº 10

- Idriss, I. M. and Boulanger, R. (2008) Soil Liquefaction during Earthquakes, Earthquake Engineering Research Institute, California
- Ishihara, K. (1984) "Post-Earthquake Failure of a Tailings Dam due to Liquefaction Pond Deposit", First International Conference on Case Histories in Geotechnical Engineering, St. Louis, Missouri
- Ishihara, K. (1993) "Liquefaction and Flow Failure During Earthquakes", *Geotechnique*, vol. 43, nº 3, pp. 351-415
- Ishihara, K. (1996) "Soil Behavior in Earthquake Geotechnics", Oxford Science Publications
- Ishihara, K. (2008), "Flow Slides of Underwater Sands Deposits in Jamuna River Bed" Qian Jiahuan Lecture of the Geotechnical Engineering for Disaster Mitigation and Rehabilitation Conference, Nanjing, China
- Ishihara, K. and Koseki, J. (1989) Discussion on Cyclic Shear Strength of fines containing sand, Earthquake Geotechnical Engineering Conference, Proceedings of the 12th International Conference of Soil Mechanics, Río de Janeiro, pp.101-106
- Ishihara, K.; Tatsuoka, F. and Yasuda, S. (1975), "Undrained Deformation and Liquefaction of Sand Under Cyclic Stresses", *Soils and Foundations*, vol. 15, nº 1
- Japanese Geotechnical Society (2015) "Laboratory Testing Standards of Geomaterials Vol I, II and III" (English version), Tokyo, Japan
- Jefferies, M. (1991) "The Critical State of Sand" *Geotechnique*, vol. 41, nº 3, pp. 365-381
- Jefferies, M. and Been, K. (2000) "Implications for Critical State Theory from Isotropic Compression of Sand" *Geotechnique*, vol. 50, pp. 419-429
- Jefferies, M. and Been, K. (2006) "Soil Liquefaction - A Critical State Approach", London: Taylor and Francis
- Jefferies, M. G. (1993) "Nor-Sand: A Simple Critical State Model for Sand" *Geotechnique*, vol. 43, N°1, pp. 91-103
- Kramer, S. (1996) Geotechnical Earthquake Engineering, Washington University - Prentice Hall
- Kwa, K. and Airey, D. W. (2017) "Effects of Fines on Liquefaction Behavior in well-graded Materials", *Canadian Geotechnical Journal*, vol. 54, pp. 1460-1471

- Lade, P. (1992) “Static Instability and Liquefaction of Loose Fine Sandy Slopes” *Journal of Geotechnical Engineering*, ASCE vol. 118, nº 1, pp. 51-72
- Lade, P. (2016) “Triaxial Testing of Soils” John Wiley and sons, Ltd. Oxford, United Kingdom
- Lade, P. and Yamamuro, J. (1997) “Effects of Non-plastic Fines on Static Liquefaction of Sands”, *Canadian Geotechnical Journal*, vol. 34, pp. 918-928
- Lateritic Deposits of Bauxite, “Britannica” (from web-site). Available in: https://www.britannica.com/science/laterite (Visited on March 2018)
- Leroueil, S.; Tavenas, F.; La Rochelle, P. and Tremblay, M. (1988) “Influence of Filter Paper and Leakage on Triaxial Testing” Advanced Triaxial Testing of Soil and Rock ASTM STP 977, pp. 189-201
- Mele, L.; Tan Tian, J.; Lirer, S.; Flora, A. and Koseki, J. (2018) "Liquefaction Resistance of Unsaturated Sands: Experimental Evidences and Theoretical Interpretation," Geotechnique (In Press).
- Mikawa Keiseki, (from web Site). Available at http://www.mikawakeiseki.co.jp/fuhi (visited in June 2018)
- Munro, M. and Mohajerani, A. (2016) "Liquefaction Incidents of Mineral Cargoes on Board Bulk Carriers," Advances in Materials Science and Engineering, vol. 2016, pp. 20-45.
- Murthy, T. G.; Loukidis, D.; Carraro, J. A.; Prezzi, M. and Salgado, R. (2007) “Undrained Monotonic Response of Clean and Silty Sands” *Geotechnique*, vol. 57, nº 3, pp. 273-288
- Nguyen, L. (2017) “Mechanical characteristics of cement-mixed sand in triaxial compression tests”, The University of Tokyo - Master of Engineering Thesis
- Olson, S. (2001) “Liquefaction Analysis of Level and Sloping Ground using Field Case Histories and Penetration Resistance” PhD Thesis, University of Illinois
- Olson, S. M. and Stark, T. D. (2003) “Use of Laboratory Data to Confirm Yield and Liquefied Strength Ratio Concepts” *Canadian Geotechnical Journal*, vol. 40, p. 1164–1184
- Pillai, V. S. and Salgado, F. M. (1994) “Post-liquefaction Stability and Deformation analysis of Duncan Dam” *Canadian Geotechnical Journal*, vol. 31, nº 6, pp. 967-978

- Poulos, S. (1981) “The Steady State of Deformation”, *Journal of the Geotechnical Engineering Division*, vol. 107, nº 5, pp. 553-562
- Rahman, M.; Robert, S. and Cubrinovski, M. (2010) “Equivalent Granular Void Ratio and Behavior of Loose Sand with Fines”, Proceedings of the 5th International Conference on Recent Advances on Geotechnical Earthquake Engineering and Soil Dynamics - San Diego, California
- Reid, D. and Fourie, A. (2014) “Estimating Post-liquefaction Strength in the Design Stage - A Review and Update”, Proceedings of Paste 2014 Conference, Vancouver
- Sadrekarimi, A. and Olson, S. M. (2012) “Effect of Sample-Preparation Method on Critical-state Behavior of Sands” *Geotechnical Testing Journal*, vol. 35, nº 4
- Sand Atlas (from web-site). Available in: http://www.sandatlas.org/bauxite. (Visited on March 2018).
- Santos Ossandon, E. F. and Verdugo, R. (2011) “Comportamiento Monotónico y Cíclico de Relaves Integrales” (in spanish), Universidad de Chile - Tesis de Maestría
- Sasaki, T. (2017) “Effect of layers of specimen by wet tamping on the liquefaction strength” Lab Seminar Presentation of the Geotechnical Engineering Laboratory, The University of Tokyo
- Seed, H. B. and Idriss, I. (1971) "Simplified Procedure for Evaluating Soil Liquefaction Potential," Journal of the Soil Mechanics and Foundations Division, ASCE, vol. 97, no. 9, pp. 1249-1273.
- Seed, H. B. and Lee, K. (1966) "Liquefaction of Saturated Sands During Cyclic Loading," Journal of the Soil Mechanics and Foundations Division, ASCE, vol. 92, no. 6, pp. 105-134.
- Seed, R. B. and Harder, L. F., Jr. (1990) “SPT-Based Analysis of Cyclic Pore Pressure Generation and Undrained Residual Strength”, Proceedings of H. B. Seed Memorial Symposium, Bi-tech publishing Ltd., Vol. 2, pp. 351-376
- Shrivastava P. K.; Asthana R.; Roy S. K. Swain, A; Dharwadkar, A. (2012) “Provenance and depositional environment of epi-shelf lake sediment from Schirmacher Oasis - scanning electron microscopy of quartz grain, size distribution and chemical parameters”. *Polar Science Journal*, Vol. 6, pp. 165-182.

- Skempton, A. W. (1954) “The Pore-Pressures Coefficients A and B” Geotechnique, vol. 4, pp. 143-147
- Sladen, J. A. and Handford, G. (1987) “A potential Systematic Error in Laboratory Testing of Very Loose Sands” *Canadian Geotechnical Journal*, vol. 24, nº 3, pp. 462-466
- Sladen, J. A; D'Hollander, R. D. and Krahn, J. (1985) “The Liquefaction of Sands, a Collapse Surface Approach” *Canadian Geotechnical Journal*, vol. 22, nº 4, pp. 564-578
- Stark, T. D and Mesri, G. (1992) “Undrained Shear Strength of Liquefied Sands for Stability Analysis” *Journal of Geotechnical Engineering*, vol. 118, pp. 1727-1747
- Sze, H. Y. and Yang, J. (2013) “Failure Modes of Sand in Undrained Cyclic Loading: Impact of Sample Preparation” *Journal of Geotechnical and Geoenvironmental Engineering*, vol. 140, nº 1, pp. 152-169
- Tan Tian, J.; Hailong, W and Koseki, J. (2018) "Evaluation of Liquefaction Resistance of Unsaturated Soils Using Volumetric Strain Ratio Index," Japanese Geotechnical Society Conference, Hokkaido, Japan.
- Tatsuoka, F.; Frans, M.; Torii, T. and Huno, T. (1984) “Behavior of Lubrication Layers of Platens in Element Tests” *Soils and Foundations*, vol. 24, nº 1, pp. 113-128
- Terzaghi, K.; Peck, R. B. and Mesri, G. (1996) Soil Mechanics in Engineering Practice, 3rd ed. John Wiley-Interscience Publication, New York
- Thomson, P. R. and Wong, R. C. (2008) “Specimen Nonuniformities in Water-Pluviated and Moist-tamped Sands Under Undrained Triaxial Compression and Extension” *Canadian Geotechnical Journal*, vol. 45, pp. 939-956
- To-Anh, P.; Darn-Horng, H. and Nguyen, P. (2016) “Critical State Line and State Parameter of Sand-Fines Mixtures” Proceedings of Sustainable Development of Civil, Urban and Transportation Engineering Conference, Vietnam
- Towhata, I. (2008) Geotechnical Earthquake Engineering, Springer, 2008.
- Vaid, Y. P and Chern, J. C. (1983) “Effect of Static Shear on Resistance to Liquefaction” *Soils and Foundations*, vol. 23, nº 1, pp. 47-60
- Vaid, Y. P. and Sivathayalan, S. (1996) “Post Liquefaction Behavior of Saturated Sand Under Simple Shear Loading”, Proceedings of the 14th ICSMFE, Hamburg

- Verdugo, R. (1992), “Characterization of Sandy Soils Under Large Deformations”, PhD Thesis, The University of Tokyo
- Vesic, A. S and Clough, W. (1968) “Behavior of Granular Materials Under High Stresses” *Journal of the Soil Mechanics and Foundations Division*, vol. 94, nº 3, pp. 661-688
- Wang, H.; Koseki, J.; Cai, F. and Nishimura, T. (2018) “Undrained monotonic triaxial loading behaviors of a type of Iron Ore Fines” *Canadian Geotechnical Journal*, vol. 55, nº 4, 2018.
- Wang, S. and Luna, R. (2012) “Monotonic Behavior of Mississippi River Valley Silt in Triaxial Compression” *Journal of Geotechnical and Geoenvironmental Engineering*, vol. 138, nº 4, pp. 516-525
- World Bank Mining Department (2015), "The Contribution of the Mining Sector to Socioeconomic and Human Development," The World Bank Group. Washington DC. Available in http://documents.worldbank.org
- Yamamuro, J. and Covert, K. M. (2001) “Monotonic and Cyclic Liquefaction of Very Loose Sands with High Silt Content”, *Journal of Geotechnical and Geoenvironmental Engineering*, vol. 127, N°4, pp. 314-324
- Yamamuro, J. and Lade, P. (1998) “Steady State Concepts and Static Liquefaction of Sands” *Journal of Geotechnical and Geo-environmental Engineering*, vol. 124, nº 9, pp. 868-877
- Yang, S.; Sandven, R. and Grande, L. (2006) “Steady State Line of Sand-silt mixtures” *Canadian Geotechnical Journal*, vol. 43, pp. 1213-1219
- Yoshimine, M. and Ishihara, K. (1998) “Flow Potential of Sand During Liquefaction”, *Soils and Foundations*, vol. 38, nº 3, pp. 189-198
- Youd, L. (1973) “Liquefaction, Flow, and Associated Ground Failure”, Geological Survey Circular
- Yu, F. (2014) “Experimental Study on Particle Breakage under High Pressures” The University of Tokyo - PhD Thesis
- Yu, F. W. (2017) “Particle Breakage and the Critical State of Sands” *Geotechnique*, vol. 67, nº 8, pp. 713-719
- Zhang, H. and Garga, V. K. (1997) “Quasi-steady state: a real behavior?” *Canadian Geotechnical Journal*, vol. 34, pp. 749-761